UNIVERSIDADE DE SÃO PAULO
INSTITUTO DE GEOCIÊNCIAS

FROM OROGEN TO RIFTED PASSIVE MARGIN FORMATION IN BRAZIL: GEODYNAMIC NUMERICAL MODELING CONSIDERING THE EFFECTS OF STRUCTURAL INHERITANCE AND RHEOLOGY

Claudio Alejandro Salazar Mora

Orientador: Prof. Dr. Marcos Egydio da Silva
Co-orientador: Ritske S. Huismans

TESE DE DOUTORAMENTO

Programa de Pós-Graduação em Mineralogia e Petrologia

São Paulo
2017

UNIVERSIDADE DE SÃO PAULO
INSTITUTO DE GEOCIÊNCIAS

FROM OROGEN TO RIFTED PASSIVE MARGIN FORMATION IN BRAZIL: GEODYNAMIC NUMERICAL MODELING CONSIDERING THE EFFECTS OF STRUCTURAL INHERITANCE AND RHEOLOGY

CLAUDIO ALEJANDRO SALAZAR MORA

Orientador: Prof. Dr. Marcos Egydio da Silva
Co-orientador: Prof. Dr. Ritske S. Huismans (UiB)

Tese de Doutorado

Nº 570

COMISSÃO JULGADORA

Prof. Dr. Marcos Egydio da Silva (IGc-USP)

Prof. Dr. Victor Sacek (IAG-USP)

Prof. Dr. Ginaldo Ademar da Cruz Campanha (IGc-USP)

Prof. Dr. Renato Paes de Almeida (IGc-USP)

Prof. Dr. Alexandre Uhlein (IGc-UFMG)

SÃO PAULO
2017

Ficha catalográfica preparada pelo Serviço de Biblioteca e Documentação
do Instituto de Geociências da Universidade de São Paulo

Salazar-Mora, Claudio Alejandro
From orogen to rifted passive margin formation in Brazil: geodynamic numerical modeling considering the effects of structural inheritance and rheology/ Claudio Alejandro Salazar-Mora. – São Paulo, 2017.
93 p. : il

Tese (Doutorado) : IGc/USP
Orient.: Silva, Marcos Egydio da
Coorient.: Huismans, Ritske S.

1. Geodinâmica 2.Modelagem Numérica 3. Herança estrutural 4. Rifteamento 5. Margens conjugadas I. Título

Popular *myths* among geologists:

"*Numerical modeling is very complicated; it is too difficult for people with traditional geological background and should be performed by mathematicians.*"

Answer to "popular myth" by Taras Gerya in "Introduction to geodynamic numerical modeling":

"***Golden Rule 1: Numerical modeling is simple and is based on simple mathematics.***

All you need to know is:

- *Linear algebra,*
- *Derivatives.*

[…] I often say to my students that all is needed is:

- *Strong motivation,*
- *Usual maths,*
- *Clear explanations,*
- *Regular exercises.*

Motivation is most important, indeed…

Golden Rule 2: When numerical modeling looks complicated, see Rule 1."

Dedico este trabalho à minha amada família: mãe, pai, minha irmã Ka e minha irmã Pam.

Agradecimentos

Meus sinceros agradecimentos ao meu orientador Prof. Dr. Marcos Egydio da Silva pela grande oportunidade e incentivo que me deu de abraçar esse doutorado com um tema completamente novo e desafiador para mim. Obrigado também pela sua orientação, amizade e belas risadas. Espero que ainda tenhamos muitos desafios (geológicos) pela frente!

I also want to thank my co-supervisor Prof. Ritske Huismans, who received me in Bergen, who showed me how to perform numerical simulations and how to use the results of these simulations. Thanks for all the knowledge shared. Thanks for the great opportunity of living in Bergen for a whole year. It was amazing. I cannot forget about my colleagues at the University of Bergen (UiB), also supervised by Ritske and also part of the Geodynamics Group in Bergen, Arjan Grool, Sebastian Wolf, Thomas Theunissen and Romain Beucher. Hadn't you guys shared your patience and knowledge with me, this thesis wouldn't have been the same. Tusentusen takk! Many thanks to Rosa Polanco, my next-door office friend in Bergen. Thanks for the many laughs, many cup of teas, beer and wine. You are an amazing friend! Savner deg! Professor Haakon Fossen. I would also like to dedicate him many thanks. Thanks for all the geological conversations, all the coffees in Bergen and Brazil, and for the amazing fieldtrip in Norway. Min første glaciar og min første eklogitt frembrudd ble begge vist til meg av deg. Jeg vil aldri glemme! Mange takk!

Minhas grandes amigas, Alice (Kenga) e Adriana (Bisteka). Já são muitos anos juntos aqui no nosso corridor B, do Petrologia e Mineralogia. Duas grandes mulheres, geólogas e amigas que, além de amizade e amor, trouxeram duas bebês lindas para eu mimar e amar, a Amora e a Flora. Obrigado, vocês duas, por sempre me ajudarem e por sempre me amarem, como eu amo vocês. Falando no corredor B do Petrologia e Mineralogia, não posso jamais esquecer da invasão (no melhor dos sentidos) colombiana. Astrid, Maria Isabel, Daniel, Santiago e Andres. Vocês fizeram, e alguns poucos que restaram, ainda fazem esse corredor ser tão legal de se trabalhar. Obrigado pelas risadas, pelos cafés, pelas festa e pelas trocas geológicas. Colômbia, obrigado por trazer o amor da minha vida, quem eu amo, admiro e respeito. A gente é pra sempre! A Melina, que além de uma ótima companhia, é uma super amiga pra tudo e pra sempre. Valeu, Me! O Pedro (Porra) e a Rafaela (Bilóba), que são da "minha época" e são ótimos geólogos, amigos e companhias nesse nosso corredor B. Bilis, obrigado por indicar aquela fesioterapia da lombar no CEPE, foi genial! Aos meus irmãos Fares e Átila Pessoa, obrigado por serem meus irmãos escolhidos e meus melhores amigos. Amo vocês demais.

Às minhas grandes amigas, Tainá, Mari (e Teresa), Camila, Clarissa, de infância, de vida e de fora da Geo: o suporte, a torcida, o amor e a amizade de vocês também foram importantíssimos para mim, nas horas deprê e nas horas boas desse doutorado.

Agradeço à CAPES, pelo meu sanduíche na Noruega, ao Programa de Formação de Recursos Humanos em Geologia do Petróleo e Meio Ambiente da Petrobrás pela minha bolsa de Doutorado e à FUSP.

Por fim, agradeço a todos aqueles que, não por mal, esqueci. ☺

Abstract

The parallelism between older collisional belts and younger rift systems is widely known and particularly portrayed along the Atlantic Ocean. In what follows, the relationship between lithospheric inherited structures and nucleation of rift systems has been focus of many studies. Nevertheless, it is still poorly understood how inherited tectonic and new-formed structures (i.e. during extension) affect the final architecture of rifted conjugate passive margins. In this thesis we use a modified highly efficient version of the Arbitrary Lagrangian-Eulerian finite–element code FANTOM to model thermal-mechanical coupled, plane-strain, viscous-plastic creeping flows to understand the geodynamics of the rifting process considering the effects of tectonic structural inheritance and rheology on the final architecture of rifted conjugate margins. The models consider different amounts of previous extension and contraction to produce the structural inheritance that is reactivated or not during rifting. Our results show that: 1) first reactivations occur along the lithospheric former suture zone; 2) upper crustal thick skinned basement thrusts are partially or fully reactivated depending on the amount of prior contraction and size of the orogen; 3) with a small amount of contraction, thick skinned thrusts are efficiently reactivated in extension and provide the template for rifted margin formation; 4) with larger amounts of precursor contraction, thick skinned thrusts distal to the lithospheric suture zone do not reactivate in extension; 5) reactivation of prior contractional shears dominates during the early stages of rifting, whereas during the final stage of rifted passive margin formation new-formed extensional shears dominate. Models with less precursor extension and more contraction resulted in a rifted conjugate passive margin similar to the Espírito Santo–Kwanza conjugate in the Central South Atlantic, whereas more precursor extension and less contraction, develops into margin showing similar behavior of fault reactivations in the Norwegian margin, North Atlantic. Our models also show that rheological differences between upper and lower continental crusts cause them to decouple both during subduction and subsequent eduction. The latter process, associated to thermal necking of the upwelling asthenosphere, is responsible to leave slivers of previously subducted lower continental crust within the eduction channel in the mantle lithosphere, as it is seismically evidenced under the Newfoundland-Iberia rifted conjugate margins. In what follows, lower continental crust of the former subducting plate can be removed long before depth-dependent extension during magma-poor rifted margin development.

Keywords: Numerical modeling; Structural inheritance; Rifting; Conjugate margins; Rheology; Geodynamics.

Resumo

O paralelismo entre antigos cinturões colisionais e sistemas de riftes mais jovens é amplamente reconhecido e especialmente observado ao longo do Oceano Atlântico. A relação entre estruturas litosféricas herdadas e a nucleação de sistemas de riftes tem sido o foco de muitos estudos. Entretanto, a relação entre estruturas herdadas e estruturas neo-formadas (i.e. durante a extensão) e a estruturação de margens passivas conjugadas ainda é pouco entendida. Na presente tese, usamos uma versão muito eficiente do código computacional Lagrangiano-Euleriano de elementos finitos FANTOM para modelar fluxos termo-mecânicos acoplados visco-plásticos de forma a entender a geodinâmica do processo de rifteamento considerando os efeitos das estruturas tectônicas herdadas e da estrutura reológica na litosfera continental. Os modelos consideram quantias variadas de extensão e contração prévios para desenvolver a herança tectônico-estrutural, a qual é ou não reativada durante o desenvolvimento da margem passiva. Nossos resultados mostram que: 1) as primeiras reativações da cunha orogênica ocorrem seguindo zona de cisalhamento principal de escala litosférica (antiga sutura); 2) zonas de cisalhamento crustais (antigos cavalgamentos) são parcial ou totalmente reativadas dependendo da quantia de contração anterior; 3) com pouca contração anterior, os cavalgamentos *thick-skin* são eficientemente reativados e controlam a formação da margem passiva; 4) maiores quantias de contração prévia permitem que zonas de cisalhamento afastadas da sutura não dão reativadas e preservam a estrutura orogênica; 5) a reativação de zonas de cisalhamento compressivas dominam durante os estágios iniciais do rifteamento, enquanto que em estágios finais e de afinamento crustal, dominam estruturas neo-formadas. Nossos modelos ajudaram a explicar algumas características das margens passivas conjugadas do Espírito Santo – Kwanza no Atlântico Central Sul, e da margem passiva norueguesa no Mar do Norte. Nossos modelos também mostraram que diferenças reológicas entre a crosta superior e a crosta inferior causam um desacoplamento durante subducção e posterior educção. Este último processo, associado ao *necking* termal da astenosfera ascendente, é responsável por deixar lascas de crosta inferior no canal de subducção-educção no manto litosférico, como é evidenciado por antigas zonas de subdução fósseis associadas à margem conjugada Newfoundland-Iberia. Dessa forma, a remoção de crosta inferior em margens passivas conjugadas pode ocorrer muito antes do processo de rifteamento.

Palavras-chave: Modelagem numérica; Herança estrutural; Rifteamento; Margens conjugadas; Reologia; Geodinâmica

Table of Contents

List of tables

List of figures

Chapter 1 - Introduction

In the last decades, computational numerical models have proven to be an essential tool for geodynamic studies once the direct observation of tectonic processes is naturally limited – mainly because they are too slow and too deep on Earth. Computational numerical modelling is capable to simulate tens of millions of years in a short period of a few days, thus letting scientists go back in time, accompany a geodynamic process throughout its evolution or even predict future behavior or phenomena. Geodynamic numerical modelling is different from other common types of computational science (e.g. engineering community) because of the *time* problem attached to geological processes, that is, the geological timescale dependence of rock deformation. For instance, the Earth's mantle, which is elastic on a human timescale, is viscous on geological timescales (> 10000 years). This has led to much effort on adapting classical mathematical equations to geodynamics, that is, adapting equations to model long-term tectonic processes, and these are nowadays well-understood (Kaus *et al*., 2008).

Many geodynamic problems can be described by mathematical models, that is, by a set of partial differential equations and boundary and/or initial conditions defined in a specific model domain. Geodynamic models describe *quantitatively* what happens to the mantle and crust in a very slowly deforming process, often with the complications of simultaneous heat transport (e.g. thermal convection in the mantle or magma transport within the crust), complex rheology (e.g. non-Newtoninan flow, elasticity and plasticity), chemical reactions, lateral forces, etc (Ismail-Zaden & Tackley, 2010). Ultimately, the goal of geodynamic numerical modelling is to advance our understanding of the physics of geodynamic processes and to identify the key controlling parameters (Kaus *et al*., 2008).

In this thesis we use a modified highly efficient version of the Arbitrary Lagrangian-Eulerian finite–element code FANTOM (Thieulot, 2011; Erdős *et al*., 2014) to model thermal-mechanical coupled, plane-strain, viscous-plastic creeping flows to understand the geodynamics of the rifting process considering the effects of tectonic structural inheritance and rheology on the final architecture of rifted conjugate margins. Even though the link between continental inherited structures and nucleation of rift systems is widely known (e.g.

Misra and Mukherjee, 2015), it is still poorly understood how inherited and newly-formed structures control rift development.

Two sections along the Central South Atlantic conjugate margin in Brazil and Africa were chosen to enrich the discussion of the experimental numerical models in comparison to natural present-day rifted margin architecture. Because tectonic structural inheritance is a key-testing variable in this thesis, a complete bibliographic review is also presented, from the orogenic history of the Araçuaí-Congo Belt to the opening of the Central South Atlantic.

1.1 Goals

- Create geodynamic numerical models that describe features of Atlantic-type rifted conjugate margins formation;
- Assess the effects of tectonic structural inheritance during rifted conjugate margins formation;
- Assess the development and effects of newly-formed structures during rifting;
- Try establishing a relationship of inherited and newly-formed structures during rifting and the final rifted conjugate margin architecture;
- Assess rheological differences between upper and lower crust during subduction and rifting;
- Integrate geological and geophysical data to construct sections along the Central South Atlantic margin to constrain rifted margin lithospheric architecture connecting offshore and onshore structures;
- Discuss the numerical models in terms of present-day rifted margin architecture in the Central South Atlantic and their relationship to Brasiliano – Pan-African structural inheritance.

1.2 Structure of this thesis

In *Chapter 1*, I present the main subject and goals of this thesis. *Chapter 2* follows with a review and the rationale of geodynamic numerical modelling and a review on state-of-the-art geodynamic numerical modelling on rifting. *Chapter 3* is dedicated to a concise review on structural inheritance and rheology, which are important factors we investigated during the

numerical simulations. In *Chapter 4*, a thorough bibliographic review of the Araçuaí-West Congo Belt orogenesis is presented, being followed by a review on the Central South Atlantic rifting history. In this chapter I also include estimations of the crustal orogenic paleo-thicknesses and orogenic structure as well as present-day regional sections from the passive margin to the onshore orogenic structure. *Chapter 5* follows with the methods used in this thesis, that it, the numerical set-up used with all its parameters and design. In *Chapter 6* I present the main results concerning tectonic structural inheritance on rifted passive margin formation in the form of an article submitted to the journal *Earth and Planetary Science Letters*. *Chapter 7* is also in the form of an article (to be submitted to *Geology*), but now focusing in the rheological discrepancies within our modelled layered lithosphere that permit lower continental crust removal before continental rifting. Finally, *Chapter 8* comprises the main discussion and integration of data as well as the conclusions of this thesis.

Chapter 2 - Geodynamic Numerical Modelling

Numerical modelling in Geodynamics developed after the 1960's, when the theory of Plate Tectonics was well accepted and established. According to Gerya (2010), during this time, Geology became a more predictive, quantitative and physical science, evolving from a fully descriptive and qualitative past. When describing a geodynamic process, for example rifting, one must understand all the physical forces acting on a lithospheric plate that permits it to stretch, thin and ultimately break up. Divergent forces on either sides of a lithospheric plate (if we think in 2-D) can represent what is called *boundary conditions*. These are the conditions acting on the boundaries of your numerical model domain, but how the plate's properties respond to this stretching strongly depends on mathematical equations that describe the behaviour of specific physical parameters through the geological time.

Physical parameters are the main inputs for numerical modelling, and for geological problems they are related to upper, middle and lower continental crust, sediments, upper and lower oceanic crust, lithosphere, asthenosphere, etc. In Table 2.1, Thieulot (2011) summarizes the main physical parameters used in geological problems. The choice of parameters is based mainly on widely accepted literature that in turn is based on laboratorial experiments (e.g. Ranalli, 1995; Turcotte & Schubert, 2002). By incorporating rock properties not accessible in analogue or descriptive models (i.e. temperature- and stress-dependent viscosities, composite rheology, heat conduction and production), geodynamic numerical models allow us to isolate controlling factors or parameters in shaping mountains, oceanic basins, continental margin architecture and so on (Brune *et al*., 2017).

As exemplified by Kaus et al. (2008), a typical 2-D numerical model has around 20 to 30 parameters as inputs, each of which with uncertainties of around two factors, and if all of them are to be tested, 2^{20} to 2^{30} tests are needed, which implies in about 10^6 to 10^9 numerical simulations. Simple 2-D deformational numerical simulations take one day to compute in high performance computation, and this can be a drawback once numerical simulations are too expensive. Geodynamic modelers usually solve this drawback either by choosing end-member combinations of parameters (Kaus *et al*., 2008) or using *parallel* computing. Parallel processing is the use of multiple processors to execute different parts of the same computation simultaneously (Ismail-Zaden & Tackley, 2010), solving memory and time restrictions.

Table 2.1 – Main physical parameters used for geological problems in numerical simulations. Extracted from Thieulot (2011).

Symbol	Meaning and dimension
$\mathbf{A}, \mathbf{A_{qt}}, \mathbf{A_{ol}}$	Power-law initial constant ($Pa^{-n}\ s^{-1}$)
Cp	Heat capacity ($J\ kg^{-1}\ k^{-1}$)
g	Gravity acceleration vector ($m\ s^{-2}$)
H	Heat production ($W\ m^{-3}$)
k	Heat conductivity ($W\ m^{-1}\ K^{-1}$)
$\mathbf{L_x}, \mathbf{L_y}, \mathbf{L_z}$	Domain size (m)
n	Power-law creep exponent
p	Pressure (Pa)
R	Gas constant ($J\ K^{-1}\ mol^{-1}$)
s	Deviatoric stress vector (Pa)
$\mathbf{T}, \mathbf{T_o}$	Temperature (K)
v = (u,v,w)	Velocity ($m\ s^{-1}$)
$\mathbf{V}, \mathbf{V_{qt}}, \mathbf{V_{ol}}$	Power-law activation volume ($m^3\ mol^{-1}$)
α	Thermal expansion coefficient (K^{-1})
dt	Time step (s)
$\dot{\epsilon}$	Strain-rate tensor (s^{-1})
$\epsilon, \epsilon_1, \epsilon_2$	Strain
λ	Penalty coefficient (Pa s)
$\mu, \mu_{min}, \mu_{max}, \mu_{eff}$	Viscosity (Pa s)
ϕ, ϕ^{sw}	Angle of internal friction
ρ, ρ_0	Mass density ($kg\ m^{-3}$)
$\sigma_y, \sigma^{sw}_c, \mathbf{C}, \mathbf{C^{sw}}$	Cohesion (Pa)

The big set of mathematical equations that is thought to represent a certain geodynamic reality is nearly impossible to be solved analytically. Numerical solutions are then used as an approximation to the real solution of a set of mathematical equations. These equations are partial differential equations and the main methods used to numerically solve them are: finite differences method, finite volume method, finite element method and spectral

methods (Gerya, 2010). Different methods have been used in different codes, depending on the user's goal.

As well-summarized by Thieulot (2014), numerical codes in geodynamics have been used in 2-D to constrain lithospheric extension, subduction, underplating, normal faulting, burial and exhumation of UHP rocks, among others. In 3-D, they have been applied to the evolution of basins, indentation problems, subduction, oblique orogen convergence, transform faults at mid-ocean ridges, etc.

2.1 Rationale of Numerical Modelling, its components and properties

A few textbooks (e.g. Gerya, 2011; Ismail-Zadeh & Tckley 2010) present the main steps for successful numerical modelling. During the initial stage, a geodynamical model must be chosen and studied such that all forces acting in that system are described and all physical parameters are known. A physical model must be written trying to describe the complex reality (Figure 2.1). Models, as well-stated by Stüwe (2007), are tools designed to describe the world around us in a way we can really understand.

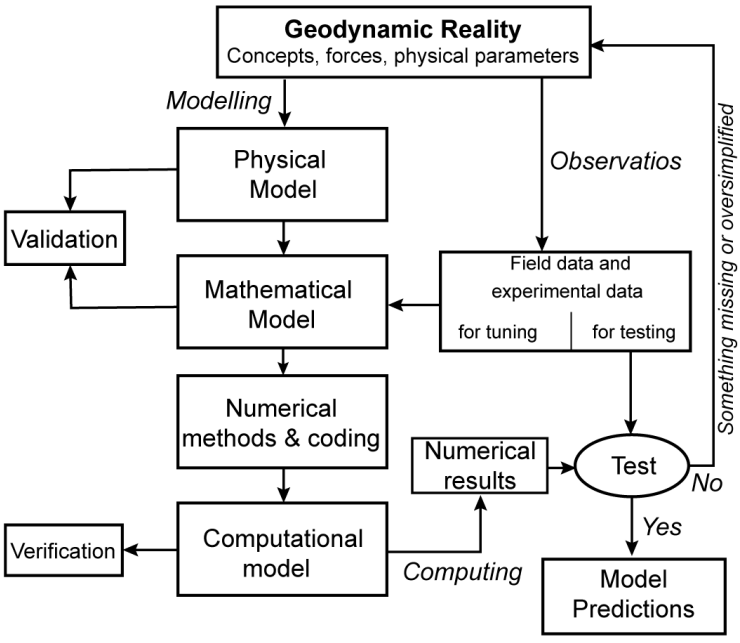

Figure 2.1 – Flowchart of geodynamic numerical modelling proposed by Ismail-Zaden & Tackley (2010).

Once the physical model is well understood, then it must be written mathematically, and the mathematical model is determined or tuned when at least one unknown parameter is successfully obtained. After the complete developing of the mathematical method, numerical resolutions must be chosen and relevant numerical codes must be constructed or obtained[1]. Nevertheless, before numerical resolutions are done, discretization methods are used to translate partial differential equations (PDE) to algebraic equations that can be understood by a computer. A system of algebraic equations can be conveniently expressed as a matrix, and this is how the computer solves the problem and presents an approximate solution to the PDE. This approximation is applied to small domains in space and/or time within the *numerical grid*, and these domains are named *nodal points* (large number nodal points increase the model's accuracy). In what follows, a continuous differential equation is going to be solved for each nodal point within the numerical grid. In Figure 2.2 is shown a simple discretization method using finite differences to solve the first-order derivative of the gravity potential in a nodal point.

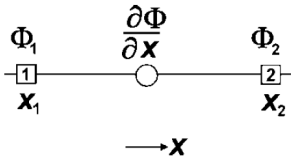

Figure 2.2 – 1D numerical grid used for computing the first-order derivative of the gravity potential Φ in a nodal point (centre).

The finite *difference* method for calculating the values of gravity potential in points 1 and 2 (Figure 2.2) can be expressed as follows

$$\frac{\partial \Phi}{\partial x} = \frac{\Delta \Phi}{\Delta x} = \frac{\Phi_2 - \Phi_1}{x_2 - x_1}, \tag{2.1}$$

where $\Delta\Phi$ is the difference in gravity potential between points 1 and 2 (Δx). One crucial point is that the smaller Δx is, the more accurate the computed derivative is. The mentioned example works for a 1-dimensional environment (just x-axis) and for a first-order differential equation. Real geodynamic numerical grids (or meshes) are likely to be at least 2-dimensional and most of the governing equations in geodynamics are second-order differential equations.

[1] Free codes can be found at the Computational Infrastructure for Geodynamics (CIG) website: www.geodynamics.org

In what follows, the one-step discretization showed in equation 2.1 should be multiplied by two (in the case of second-order PDE's) and the number of nodes used in a numerical grid are normally in the range of thousands. Thousands of nodes yield millions or even billions of linear equations for most 2D and 3D geodynamic models, and this is why we need supercomputers with no memory and processing drawbacks.

It is beyond the scope of this thesis to discuss the discretization methods of the partial differential equations, but it is worth mentioning that finite difference (FD) and finite element (FE) methods are preferentially used in geodynamic numerical models. For simplicity, a 1-D example of finite difference was described in the previous paragraph. Nevertheless, in terms of *pros* and *cons* (Becker & Kaus, 2016), FE is far better. For instance, FD is conceptually simpler, whereas FE implementation and coding is far more complicated. Unlike FD, FE is very good to simulate sharp boundaries and complex geometries, besides allowing for easier regional mesh refinement. FE is relatively more adaptable to new problems, while FD coding usually needs to be re-written from scratch to new problems adaptation.

After mathematical modelling, numerical methods and coding, verification must be done, that is, the assessment of the accuracy of the solution to the computational model by comparison with known solutions (analytic or numerical). After verification, numerical results are tested against observations and benchmarks, and if there is good agreement with field or experimental data, then the model can be considered a final geodynamic numerical model, which can prove some models or predictions or even brig forth new models.

In summary, Ismail-Zadeh & Tackley (2010) described the main components of numerical modelling as: (1) a physical and mathematical model that describe geodynamics; (2) a discretisation methods to convert mathematical equations into discrete equations to be solved numerically; (3) numerical methods to solve the equations; (4) computational codes to be developed or obtained that solve numerically the discrete equations; (5) supercomputers that perform calculations; (6) results of numerical modelling to be visualized, analysed and interpreted by a (7) geoscientist.

As one can see in Figure 2.1, *testing* is a main concern during numerical simulations because if the test goes negative, something is missed or oversimplified, and you simply go back to stage zero. These tests are done by checking numerical sensitivity and by comparing the model with benchmarks (sec. 2.3) and/or natural observations. Numerical sensitivity can be tested through some properties of the numerical methods (Ismail-Zaden & Tackley, 2010).

The first property is *consistency*, which is checked with the *truncation error*. The latter describes the difference between the discretized and the differential equations, so a

model is said to be consistent when the truncation error tends to zero at the same time as the grid spacing tends to zero. Consistency does not run alone, so it also depends on a property named *stability*, that is, a model that does not magnify its errors during the course of simulations. Stability is usually estimated with constant coefficients, that is, with no boundary conditions and with successively refined grids. If consistency is assessed as well as stability, the model is said to converge to a grid-independent solution, so it is also *convergent*. Because numerical solutions of geodynamic problems are approximate solutions, *accuracy* is one of the key properties that must be always remarked. Accuracy is mainly represented by modelling errors (e.g. simplifying too much the model equations, model geometry, boundary conditions), discretisation errors and iterations errors.

2.2 Governing Equations

One interesting assumption in Geodynamics is that it considers all geological media as *continuous*. This implies that the rocks under consideration do not contain any gap or void without mass. This behaviour is comparable to that of water, being then described in the realm of continuum fluid mechanics (e.g. Gerya, 2010; Thieulot, 2011 and references therein). If a rock or magma is displaced from one place to another, it is not supposed to create any gap. This can be true in Geodynamics if we consider the *geological time*, for example, in the dozens of millions of years a *nappe* system needs to migrate. If lower *nappes* are displaced to shallower crustal levels, other rocks (be it even lower *nappes* or magma) are supposed to come into this area and substitute the displaced fragment. In what follows, considering the geological time, rocks do behave like a fluid either in the crust or mantle.

The continuous realm is described by *field variables*, which are of three main types: scalars (e.g. pressure, temperature, density); vectors (e.g. velocity, mass flux, heat flux); and tensors (e.g. stress, strain, strain rate). For a relatively broad spectrum of geodynamic processes, there are three main governing equations that follow conservation laws: the equation of continuity (conservation of mass), the equation of motion (conservation of momentum) and the equation of temperature (conservation of heat). There are also other equations that refine even more geodynamic processes, like equations of stress, rheology, elasticity and plasticity. In the next paragraphs I will briefly summarize the main governing equations and the reader is referred to more specialized literature (e.g. Fletcher, 1988;

Ferziger and Perić, 2002; Gerya, 2010; Ismail-Zaden and Tackley, 2010) for details on stress, rheology and visco-plasticity numerical handling.

2.2.1 The Continuity Equation: conservation of mass

The continuity equation is a quantitative way to describe the qualitative understanding of mass conservation during the displacement of a continuous medium. As aforementioned, governing equations are solved for specific nodal points in a numerical grid, and these points can be either immobile or mobile. Mobile nodes are named Lagrangian points, and they are strictly connected to a single material point (i.e. a specific part of the model domain), so, in respect to time, it moves together with the material point. Alternatively, Eulerian points are immobile, so different Lagrangian material points are passing through the same Eulerian observational point with time (Gerya, 2010). Choosing either an Eulerian or a Lagrangian point will depend on the model's intention, particularly if one is trying to describe the movement of material *with* a flow.

In what follows, the continuity equation can be expressed both in the Lagrangian and the Eulerian forms. The Eulerian form is

$$\frac{\partial \rho}{\partial t} + \nabla.(\rho\, \vec{v}) = 0, \tag{2.2}$$

where the first term is the Eulerian time derivative, ρ is the local density (i.e. the amount of mass per unit volume kg/m^3), v is the local velocity (m/s) and ($\nabla.$) is a divergence operator. Divergence operators indicate whether the flux is going to or from a nodal point, so if divergence is positive, flux diverges and if divergence is negative, flux converges to the nodal point. Another interesting property of the Eulerian equation is the fact that ($\rho\, \vec{v}$) indicates the local mass flux vector, and this implies that if mass is leaving our observational point (i.e. $\nabla.(\rho\, \vec{v}) > 0$), then the local density decreases with time (i.e. $\frac{\partial \rho}{\partial t} < 0$).

To the other hand, the Lagrangian equation for continuity is not supposed to describe variations in density, once the nodal point is connected to the same material point as it moves. As a consequence, the equation takes the form of

$$\frac{D\rho}{Dt} + \rho \nabla.\vec{v} = 0, \tag{2.3}$$

where $\frac{D\rho}{Dt}$ is the Lagrangian time derivative and local density is kept as a constant.

There are interesting studies on geological problems that used coupled Lagrangian-Eulerian models (Fullsack, 1995; Allken *et al*., 2011, 2013; Huismans & Beaumont, 2011; Thieulot, 2011, 2014), and an interesting relationship of the two equations is presented below (see transformations in Gerya (2010)):

$$\frac{D\rho}{Dt} = \frac{\partial \rho}{\partial t} + \vec{v}\text{grad}(\rho), \tag{2.4}$$

where the extra term in the right-hand side of equation 2.4 is called *advective transport*. This term describes the variation of density in an immobile point due to the existing density gradient relative to this point (i.e. a moving grid). As density is not supposed to change in the Lagrangian realm, then $\frac{D\rho}{Dt} = 0$, so the Eulerian equation of continuity reduces to the advective transport equation

$$\frac{\partial \rho}{\partial t} = -\vec{v}\text{grad}(\rho). \tag{2.5}$$

What the Eulerian advective transport equation remarkably describes is the movement of a medium in relation to density. If a medium is moving towards decreasing density domains (i.e. $\vec{v}\text{grad}(\rho) < 0$), than density *increases* in an immobile observational point (i.e. $\frac{\partial \rho}{\partial t} > 0$).

In what follows, the advection equation (eq. 2.5) can be written to any scalar function that describes rock properties. This equation is used because deformation of a continuum media causes rock properties to change their spatial distribution within the model domain. Thereby, Eulerian-Lagrangian advection algorithms are often used, so properties are initially distributed on a large amount of Lagrangian points that are advected according to a given computed velocity field. The advected material properties are then interpolated from the displaced Lagrangian point to the Eulerian observational point by using a weighted-distance averaging formula.

2.2.2 The Equation of Motion: conservation of momentum

In order to describe motion with conservative laws, the momentum equation is firstly advocated to describe the conservation of momentum for a continuous media in the gravity field (Gerya, 2010). The Lagrangian form of this equation is as follows:

$$\frac{\partial \sigma_{ij}}{\partial x_j} + \rho g_i = \rho \frac{Dv_i}{Dt}, \tag{2.6}$$

which is basically a differential equivalent for Newton's second law $f = ma$. Because motion results from the balance of internal and external forces acting on the medium, *pressure* is introduced into the momentum equation considering the relation between total (σ_{ij}) and deviatoric (σ'_{ij}) stresses. The resulting equation is the Navier-Stokes equation, which describes the motion of a viscous fluid as

$$\frac{\partial \sigma'_{ij}}{\partial x_j} - \frac{\partial P}{\partial x_i} + \rho g_i = \rho \frac{Dv_i}{Dt}, \tag{2.7}$$

where i and j are coordinate indices, x_i and x_j are spatial coordinates. g_i is the i-th component of the gravity vector, ρ is local density and Dv_i/Dt is the time derivative of the i-th component of the velocity vector (acceleration).

Because the time derivative shown in the right-hand side of the Navier-Stokes equation is too small (plate motions are in the order of 10^{-9} m/s and mantle flow in the order of 10^{-22} m/s), this part of the equation becomes negligible in respect to g (10^{23} bigger than mantle flow), so the deformation and motion of highly viscous flows are described by the Stokes equation for *slow flow* (Gerya, 2010):

$$\frac{\partial \sigma'_{ij}}{\partial x_j} - \frac{\partial P}{\partial x_i} + \rho g_i = 0. \tag{2.8}$$

2.2.3 The Heat Conservation Equation

Because density and viscosity are important rock material properties and are fully dependent on temperature, the heat equation must also be computed according to the conservation assumption of continuous mechanics. Thus, the heat conservation equation accounts for the balance between heat conduction, advection and production in the following form:

$$\rho C_p \frac{DT}{Dt} = -\frac{\partial q_i}{\partial x_i} + H, \tag{2.9}$$

where ρ is density (kg/m^3), C_p is heat capacity at constant pressure (J/kg/K) and H is volumetric heat production (W/m^3). DT/Dt is the Lagrangian-Eulerian time derivative of temperature and q_i accounts for heat flux (W/m^2).

Because advection requires the velocity transport, then the Eulerian form of the equation is a better choice, so

$$\frac{DT}{Dt} = \frac{\partial T}{\partial t} + \nu_i \frac{\partial T}{\partial_i}. \quad (2.10)$$

Conduction is described by

$$q_i = -k \frac{\partial T}{\partial_i}, \quad (2.11)$$

where *i* stands for x, y and z directions (for 3D simulations), υ the velocity transport and *k* is the thermal conductivity.

In what follows, the heat conservation equation that is computed is of the following form:

$$\rho C_p \left(\frac{\partial T}{\partial t} + \nu_i \frac{\partial T}{\partial_i}\right) = \frac{\partial}{\partial_x}\left(k \frac{\partial T}{\partial_i}\right) + H. \quad (2.12)$$

2.3 Benchmarks

The use of benchmarks in numerical geodynamic modelling is crucial because it tests the robustness of the codes in the various situations of a geodynamic reality. Benchmarking is usually done by comparing the code's numerical solution to numerical results from other well-established codes or by using specific softwares that focus on error analysis, benchmarking and code verification (one can cite CIGMA – Computational Infrastructure for Geodynamics Model Analyser [2]).

Another widely used method of benchmarking is the comparison of the results with analogue models that are scaled for geological structures (Hubbert, 1937) since 1937 (until then, analogues were only descriptive) and have been still developing and compared to nowadays numerical solutions for either contractional or extensional tectonics (e.g. Ellis *et al*., 2004; Autin *et al*., 2013; Cappelletti *et al*., 2013). Analogue modelling for brittle behaviour is mainly done using sandbox experiments because quartz is considered a good material in terms of generating and recording microscale shear bands and microcracks. Ductile experiments usually use silicon putties with Newtonian behaviour. A good review on brittle and ductile analogue models is well reviewed in Schreurs et al. (2006). Finally, another type of benchmark is the comparison of the resulting model to natural data such as oceanic spreading (Gerya, 2013), continental rifting and graben interaction (Allken *et al*., 2013), rifted

[2] http://geodynamics.org/cig/software/cigma/

passive margins (e.g. Huismans & Beaumont, 2011; Brune *et al*., 2014), syntectonic sedimentation in fold-and-thrust belts (Fillon *et al*., 2012) or moutain building (Pysklywec, 2002).

2.4 State-of-the-art geodynamic numerical models on rifting

Most geodynamic numerical models that constrain the extensional history of the South Atlantic Rift Central Segment use 2-D thermo-mechanical codes, even though it is widely known that the rifting process is essentially 3-D, not only when concerning oblique rifting (Brune *et al*., 2012) but also when concerning along strike interactions (Allken *et al*., 2011, 2012). Well-accepted lithospheric stretching models, such as the pure-shear uniform extension kinematic model of Mckenzie (1978) and the simple shear model of Wernicke (1985), have succeeded in explaining some configurations of rifted margins, although quantitative and mechanical constrains are poorly constrained. Thermo-mechanical models of Buck (1991) have shown that a cold, strong crust with a thick brittle layer couples crustal and mantle deformation, leading to narrow rifted margins, whereas hot and weak crust decouples deformation and lead to a wide margin. For instance, these models fail to explain hyper-extended margins and asymmetric conjugate margins.

Thermo-mechanical finite-element experiments have shown the effects of strain-softening processes during lithospheric extension and its symmetric or asymmetric character. The experiments linearly decreased the internal angle of friction and the effective viscosity, and deformation is either tested in the case of continental crust and lithospheric mantle coupling and decoupling (Huismans & Beaumont, 2003). Results showed that strain-softening processes (accommodated in large and different sets of shear zones) promote asymmetry of the upper crust only if it is underlain by a low-viscosity middle or lower crust. Coupling, in this case, would not allow strain localization and thus strain-softening mechanisms. It was also shown that while frictional-plastic strength is independent of strain rate, viscous stress is not, and higher rifting velocities can favour viscous rheology and thus lithospheric decoupling.

Other finite-element simulations suggest that asymmetry and development of hyper-extended continental margins are the result of abrupt plate accelerations during rifting (Brune *et al*., 2016). The same authors also show that steady-state rifting migration (which is velocity-dependent) explains highly asymmetric continental margins. Strain-softening

deformation coupled to thermal-strengthening processes cause the rift to migrate towards new rifting-bounding faults that became active with time. Previously active faults are abandoned in the more extended part of the lithosphere (Brune *et al*., 2014).

Rheological layering of the continental lithosphere does not favour the uniform lithospheric extension model of McKenzie (1978), so depth-dependent lithospheric extension has been advocated (e.g. Davis & Kusznir, 2004; Huismans & Beaumont, 2011). Depth-dependency may generate complex rifted continental margins, but two main end-members have been proposed (Huismans & Beaumont, 2011, 2014): Type-I margins are characterized by: 1) development of major basin-forming faults that penetrate into the crust possibly rooting in the lower crust; 2) formation of narrow transitional regions (<100km); 3) clearly asymmetric geometry and uplift of the flanks; 4) breakup of the crust before breakup of the mantle lithosphere; 5) exhumation and exposure of continental mantle lithosphere in the transition between oceanic and continental crust; and 6) little surface magmatism during rifting. To the other hand, Type-II margins are characterized by: 1) ultra-wide regions (>350 km) of very thin continental crust, with little evidence for lower continental crust; 2) faulted early syn-rift sedimentary basins; 3) undeformed late syn-rift sediments; 4) continental mantle lithosphere replacement by hot asthenosphere (formation of sag basins); 5) lack of mechanical flexural rift flank uplift; 6) no mantle exhumation; and 7) limited magmatism during rifting.

Continental mantle lithosphere exhumation at distal domains of a rifted continental margin or at the transition between continental and oceanic crust has been modelled using 2-D finite elements codes on an upper-mantle scale (Beaumont & Ings, 2012). Results show that previously metasomatized mantle lithosphere (due to subduction in the Wilson Cycle) gets less viscous and more buoyant, which permits it to counterflow during continental rifting and being exhumed at distal domains of the conjugate continental margins.

2-D finite-difference models have attempted to simulate cratonic lithosphere extension, showing the effect of a mid-lithospheric weak layer. If the weak layer is relatively shallow and thin, narrow and localized mantle thinning is favoured, whereas widespread mantle necking is promoted otherwise. A weak layer may not alone promote the extension and breakup of a cratonic lithosphere, but once deformation is enhanced, the required extensional boundary forces (tectonic forces) are lower (Liao & Gerya, 2014).

Chapter 3 - Inheritance within the continental lithosphere

One of the main implications of the Wilson Cycle (Wilson, 1966) is that the continental crust is repeatedly reworked while the oceanic crust is repeatedly consumed. Thereby, after plate tectonic processes took place on Earth, the continental crust has been recording subsequent tectonic processes that involve magmatism, metamorphism and deformation. All of those processes develop inheritance features within the continental lithosphere, which can play important roles during subsequent tectonic events. Manatschal et al. (2015) enumerate three types of inheritance, namely: (1) thermal, which implies that inherited heat decreases with time; (2) compositional, that comprises all the lithological variation of a continental lithosphere; and (3) structural, referring to all mechanical weaknesses present in the continental lithosphere.

The observation that the Atlantic Ocean opened following older sutures or other orogen-related structures (e.g. Porada, 1989; Piquè and Laville, 1996; Vauchez et al., 1997; Buiter and Torsvik, 2014; Misra and Mukherjee, 2015), brings forth the importance of all types of inheritance, particularly the reactivation or not of orogenic structural inheritance during subsequent rifting.

3.1 Structural inheritance and reactivation

Structural inheritance is related to mechanical weaknesses in the continental lithosphere that resulted from previous tectonic events (Thomas, 2006). For instance, present-day and preserved ancient collisional orogens are thought to have undergone a subduction-related phase, with the closure of oceanic basins. The inversion of those basins re-use most of the tectonic structures associated to the basin formation. After the reactivation of the basin-related structures, orogenic contractional structures are developed so the resulting orogenic lithosphere has both extensional and orogenic structural inheritance. This inheritance occurs in the form of brittle-ductile and ductile shear zones that basically represent domains of decreasing strength of the lithosphere. Unless fault-healing processes have dominated (for

example if the time between formation and reactivation of structures is too long), those weaker domains will be prone for reactivation (Tommasi & Vauchez, 2001; Corti, 2012).

Besides the rheological discrepancies between inherited structures and the surrounding rocks, other factors may control reactivation, such as the relative orientation to the main extensional stress field and the extent of the inherited structures, particularly with depth. On the lithospheric scale, the former subduction zone of a collisional belt creates a deep strong anisotropy or weakness not only in the crust but also in the mantle lithosphere. Lattice-preferred orientation of olivine crystals in the mantle lithosphere are significant anisotropies that are prone to reactivation, and this connection of weaknesses between crust and mantle lithosphere could be one of the arguments why rifting took place over orogenic structural inheritance in the Atlantic Ocean (Tommasi & Vauchez, 2001, 2015; Cappelletti *et al*., 2013).

While lithospheric scale weaknesses can control early stages of rift, the inherited orogenic structures present on the continental crust are thought to play an important role in shaping the developing rifted continental margin. If we consider orogenic structural inheritance, then the reactivation of crustal thrust shear zones can readily occur during extensional gravitational collapse of the orogenic pile. With continuous rifting, orogenic crustal structures are subsequently reactivated or abandoned during stretching and thinning.

In the Norwegian North Sea region, geological and geophysical studies show the successive reactivations of intrabasement (inherited) structures (Phillips *et al*., 2016) during the development of the Norwegian rifted continental margin. Other studies have shown that the reactivation of inherited structures oblique to rift extension direction also play an important role of the final architecture of rifted margins (Fossen *et al*., 2016). In the Brazilian rifted margin (Central South Atlantic), magnetometric and gravimetric mapping of onshore structures (Ferreira *et al*., 2009) and offshore 3-D seismic interpretations (Fetter, 2009) show a first-order relationship between inherited structures in the onshore with the younger offshore structures controlling the development of the rifted passive margin.

Only a few numerical models have been run concerning structural inheritance, basically showing the effects of inherited orogenic structures on the segmentation of rifted margins (Manatschal *et al*., 2015) and the effects of inherited extensional structures on the overall structure of orogens (Erdős *et al*., 2014).

3.2 Rheology

High-resolution global maps derived from Bouguer gravity and topography correlations (Audet & Bürgmann, 2011) have shown that the effective elastic thickness of the lithosphere is higher in old Archean cratons than at its margins where orogenic belts are structured, which means that the latter are weaker. Cratonic lithosphere is stronger and more stable due to its dehydrated and refractory character (Peslier *et al*., 2010) and low heat flux (Sleep, 2003). To the other hand orogenic lithosphere, particularly in collisional orogens, concentrate heat-producing elements (U, Th, K) due to crustal thickening and thus have higher heat flux, besides more water content and a fertile character. In the weaker lithosphere, deformation is enhanced by concentrating strain in pre-existing fabrics, which during repeated tectonic cycles isolate continental interiors as strong cratons. In what follows, the rheological differences between orogenic and cratonic lithosphere are of great importance in terms of reactivation.

Rheology of the lithosphere is a function of its composition and structure, pressure and temperature (Fernandez & Ranalli, 1997), which are basically factors that affect thermal and compositional inheritance (*sensu* Manatschal et al., 2015) in the lithosphere. Besides the temperature-dependent and the compositional weakening of the lithosphere and the role of structural inheritance, the rheological variations in a layered lithosphere also affect rifted passive margin formation. As already mentioned in section 2.4, rheological variations between upper and lower crust and mantle lithosphere develop complex modes of depth-dependent lithosphere extension (Huismans & Beaumont, 2008, 2014).

Chapter 4 - From orogen to rifted margin

Because one of the main goals of the numerical simulations in this thesis is to investigate tectonic structural inheritance, it is important to build reference end-member descriptive models between which the numerical simulations are going to develop. The oldest end-member is the configuration of the Araçuaí-West Congo Belt (Neoproterozoic structural inheritance) in terms of pressure, temperature and structural conditions by the time Western Gondwana was finally amalgamated. These three features helped us to estimate how thick and wide and how was the structure of this orogen before rifting began. Brasiliano orogens are important because most of the rifting processes of Gondwana and the development of the Atlantic Ocean Basin began parallel to *orogenic* lithosphere. The youngest end-member for the simulations is illustrated by the current structure of the continental margin lithosphere, which was mainly interpreted from seismic sections along the main petroliferous Brazilian basins.

4.1 Brasiliano – Pan-African orogens

Prior to the South Atlantic Cretaceous rifting, the South American and African plates were assembled together in the Western Gondwana paleocontinent, which finally amalgamated during upper Neoproterozoic times, although Cambrian tectono-metamorphic events appear to have taken place in southeastern South America and southwestern Africa between 530-480 Ma (Schmitt *et al*., 2004, 2008; McGee *et al*., 2012). The configuration of Western Gondwana comprised Paleoproterozoic Archean cratonic blocks bordered by Neoproterozoic to Cambrian Pan-African and Brasiliano orogens (Figure 4.1).

Paleogeographic reconstructions indicate that the South American São Francisco Craton (SFC) was linked to the West African Congo Craton (CC) through a cratonic bridge (Porada, 1989).

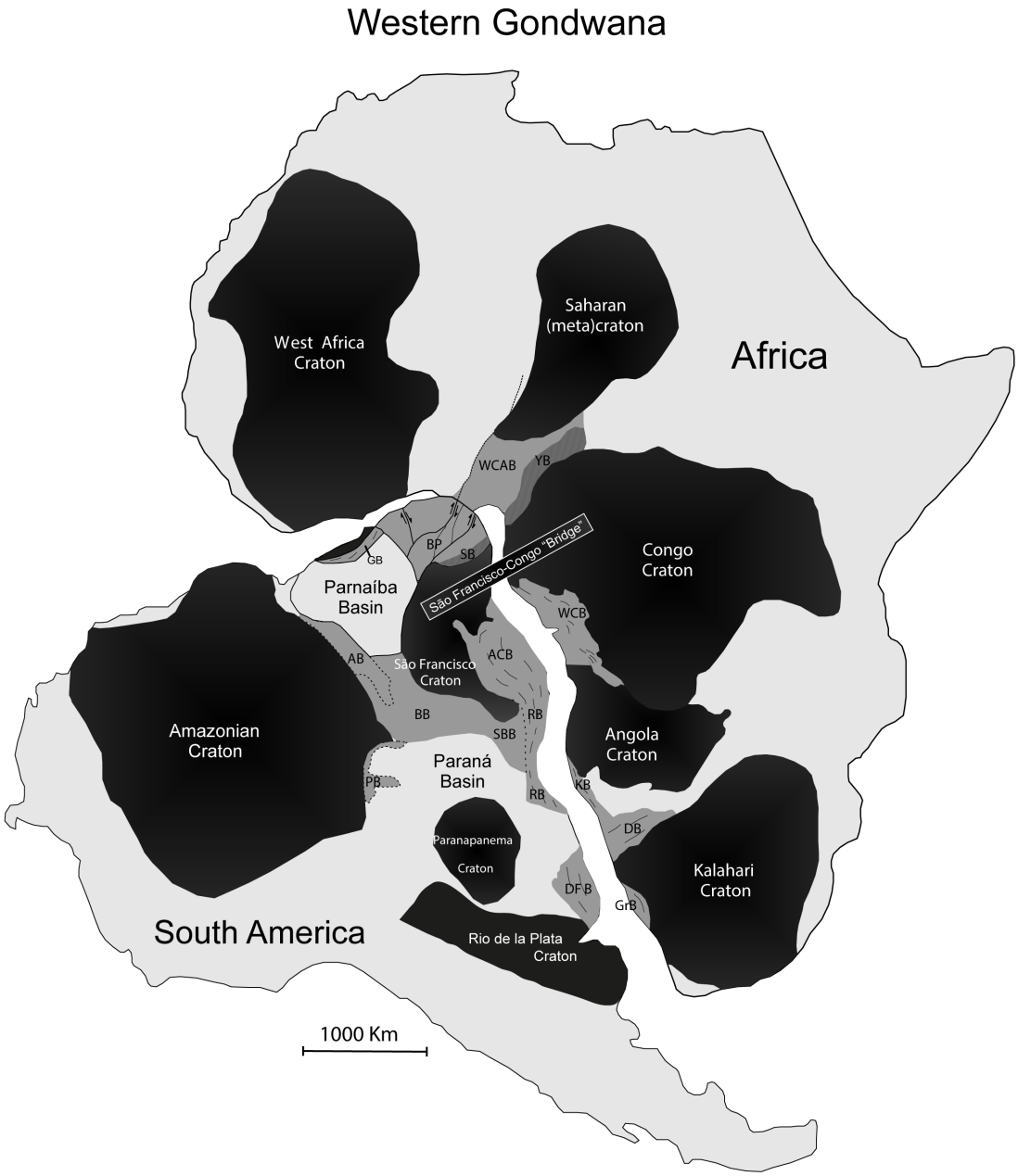

Figure 4.1 – Upper Proterozoic schematic configuration of Western Gondwana (modified after Almeida et al., 2013; Heilbron et al., 2008; Porada, 1989). In black, cratonic blocks and in dark grey Brasiliano/Pan-African orogens: Araçuaí Belt (ACB), Araguaia Belt (AB), Borborema Province (BP), Brasília Belt (BB), Dom Feliciano Belt (DFB), Damara Belt (DB), Gurupi Belt (GB), Gariep Belt (GrB), Kaoko Belt (KB), Paraguai Belt (PB), Ribeira Belt (RB), Southern Brasília Orogen (SBB), Sergipano belt (SB), West Congo Belt (WCB), West Central African Belt (WCAB) and Yaoundé Belt (YB). In light grey are represented Paleozoic basins and other undistinguished geological units of both South America and Africa.

The SFC is roughly composed of Archean to Paleoproterozoic cores of high-grade migmatitic-granulitic terranes, granite-greenstone terranes and Paleo- to Mesoproterozoic covers. Paleoproterozoic reworking is recorded in the 2.4 Ga Itabuna-Salvador-Curaçá orogen, which reached peak metamorphism around 2.05 Ga (van Schmus *et al*., 2008). The

CC exhibits an Archean core (3.1-2.5Ga) with Paleo- to Mesoproterozoic overprints along its margins (Alkmim *et al*., 2006). The 2.05 Ga high-grade Nyong Complex is thought to represent the Eburnian-Transamazonian amalgamation of the SFC and the CC (van Schmus *et al*., 2008).

South of the São Francisco-Congo cratonic bridge, roughly N-S-striking orogenic belts are developed until southeast Brazil and southwest Africa. From north to south, the onshore Brazilian rifted margin comprises the Araçuaí, Ribeira and Dom Feliciano orogens – all of which comprise the Mantiqueira Province (Almeida *et al*., 1981) -, while the onshore African rifted margin comprises the West Congo, Kaoko and Damara orogens (see Figure 4.1). The Mantiqueira Province evolved diachronously from south to north and its orogenic history admits a pre-collisional stage between 670-595 Ma, a syn-collisional stage between 620-550 Ma and a post-collisional stage between 560-490 Ma (Bento dos Santos *et al*., 2015).

4.2 The Araçuaí-West Congo Belt (AWCB)

The AWCB developed between the São Francisco and Congo cratons in the central domain of Western Gondwana (Figure 4.1) and is reckoned as a confined orogen due to its arc-shaped geometry within the so-called São Francisco-Congo cratonic bridge. Some authors in favour of a cratonic bridge during the Neoproterozoic Western Gondwana amalgamation (e.g. Alkmim et al., 2006; Barbosa and Sabaté, 2004; Porada, 1989) debate upon three arguments: (i) that the youngest tectono-metamorphic event between the two cratons took place 2.05 Ga; (ii) that their paleomagnetic poles indicate they were already assembled; (iii) and the development of narrow rifted passive margins across the bridge during the Cretaceous South Atlantic rifting, suggesting the latter to act as an old strong cratonic block that broke up without being stretched, unlike margins where orogenic belts were extended before actual breakup (Unternehr *et al*., 2010; Peron-Pinvidic *et al*., 2013a)

The orogen is thought to have formed due to the closure of a gulf-shaped precursor basin connected to the Adamastor paleo-ocean. Whereas some authors believe it was an inverted intracontinental rift (e.g. Trompette, 2000), others agree that the precursor basin was partially floored by oceanic crust (e.g. Pedrosa-Soares et al., 2008) that later underwent subduction during the Rio Doce Orogeny (Campos Neto & Figueiredo, 1995). The existence of ophiolite slivers (Pedrosa-Soares *et al*., 1998), the development of the Rio Doce magmatic arc (Campos Neto & Figueiredo, 1995) and the attempts of magmatic history construction

from pre-, syn- to post-collisional phases (Pedrosa-Soares *et al*., 2008; Gradim *et al*., 2014) would favour the closure of an oceanic basin.

Due to the gulf-shaped geometry of the AWCB precursor basin, kinematic models for its closure are still debatable. For instance, Alkmim et al. (2006) proposed the "nutcracker tectonics" model, where the anticlockwise rotation of the São Francisco craton would have caused basin closure. Nevertheless, this model requires the São Francisco-Congo bridge to shorten, and this is evidenced by the inversion of the Paramirim aulacogen, which runs approximately NNW-SSE (present day coordinates) between the São Francisco and Congo cratons. In what follows, it is more likely that the supposed cratonic bridge was not completely stable during Western Gondwana amalgamation.

4.2.1 The precursor basin of the Araçuaí-West Congo Belt

The AWCB precursor basin (hereafter referred to as Macaúbas basin) is thought to have formed between 1.0-0.65 Ga, from Tonian to upper Cryogenian periods (Pedrosa-Soares *et al*., 2008). In the São Francisco passive margin, the basin evolution is recorded in the Macaúbas Group, whereas in the Congo passive margin, it is recorded both in the Zadinian and Mayumbian Groups (Figure 4.2 A).

The Zadinian Group hosts rift-related siliciclastic rocks, anorogenic peralkaline granites and mafic volcanics. The A-type granites are at the base of the Zadinian Group, with U-Pb ages in zircon yielding 999 ± 7 Ma. The overlying 4 km thick Mayumbian Group consists mostly of felsic volcanics, ranging from 920 to 912 Ma. Both the mafic and felsic magmatism recorded in these two groups resemble a typical continental rifting bimodal magmatism (Tack *et al*., 2001). The overlying stratigraphic unit is the West Congolian Group, which hosts continental rift deposits, passive margin successions, carbonate platform deposits and two diamictite units.

In the São Francisco side, the basin development is mostly recorded in the 12 km thick Macaúbas Group with maximum depositional age around 900 Ma (Babinski *et al*., 2012). The Salto da Divisa A-type granite (Figure 4.2 A) is intruded in the Paleoproterozoic basement of the Macaúbas basin with a 875 Ma U-Pb age (da Silva *et al*., 2008), being younger than the continental rifting magmatism recorded in the Congo craton side and thus, suggesting the westward migration of the rift thermal axis (Pedrosa-Soares *et al*., 2008).

The youngest formation of the Macaúbas Group comprises metamorphosed turbidites, pelites, black shales, cherts, banded iron formations and mafic volcanics. The more distal portions of this formation contain ocean-floor sediments imbricated with ultramafic rocks (Figure 4.2 B), possibly representing a dismembered ophiolite (Pedrosa-Soares *et al*., 2008). Plagiogranites composing this ophiolite section yielded magmatic U-Pb ages of 650 Ma, being the maximum age of sea-floor spreading (Peixoto et al., 2013 and references therein).

Flysch sedimentation is recorded in the Salinas Formation, which is a thick sequence of turbiditic wackes and pelites with lenses of conglomerates and calc-silicate rocks (Figure 4.2 C). Maximum depositional age at 588 Ma brackets the time of sedimentary filling between the developing Rio Doce magmatic Arc and the Macaúbas passive margin (Pedrosa-Soares *et al*., 2008).

Even though the craton-confined gulf-shaped Macaúbas basin is considered as a narrow basin partially floored by oceanic crust, it experienced a long-lived evolution of 350 My (from 1000 to 650 Ma). Comparing to present day narrow and gulf-shaped basins with ultraslow sea-floor spreading of 15 $mm.yr^{-1}$ like the Red Sea (Augustin *et al*., 2014), the Macaúbas basin would have evolved to an Atlantic-type 5000 km wide basin. In what follows, some authors concluded that the Macaúbas basin was a protracted stagnant basin (Pedrosa-Soares *et al*., 2008).

4.2.2 Magmatism, metamorphism and orogenic phases

The time of the orogenic event in the AWCB is constrained by the pre-collisional magmatism between 630-585 Ma, the syn-collisional magmatism between 585-530 Ma, and the post-collisional magmatism between 530-490Ma (Pedrosa-Soares *et al*., 2008; Gradim *et al*., 2014). Subduction-related convergence led to the formation of the Rio Doce Magmatic Arc (Figure 4.2 D) with a calc-alkaline cordilleran-type plutonic magmatism (Campos Neto & Figueiredo, 1995), which dates from 630 to 585 Ma and is entirely located in the Araçuaí Belt (Brazilian part of the AWCB). Mantle and crustal processes were involved during the formation of this arc, suggesting an active continental margin setting (Gonçalves *et al*., 2015). The magmatic arc basement comprises Rhyacian rocks from the Juiz de Fora Domain and Pocrane Complex (Gonçalves et al., 2014 and references therein).

P-T conditions estimates are well-constrained in the Araçuaí Belt, which is thought to be part of the "hot orogens" group (e.g. Collins, 2002; Schulmann et al., 2008), with

temperatures varying from 700°-800°C in the western Araçuaí Belt, and 913°C in the hot back-arc zone during Brasiliano syn-collisional peak metamorphism around 580 Ma (Cavalcante *et al*., 2013; Gradim *et al*., 2014). Pressure estimates vary from 6.5 to 7.0 kbar in the western part of the orogen (Cavalcante *et al*., 2014; Peixoto *et al*., 2015) and 5.4 to 6.5 kbar in the eastern part (Gradim *et al*., 2014). Peak regional metamorphic conditions are thought to have been achieved between 580-570 Ma in the Araçuaí Belt (Pedrosa-Soares *et al*., 2008).

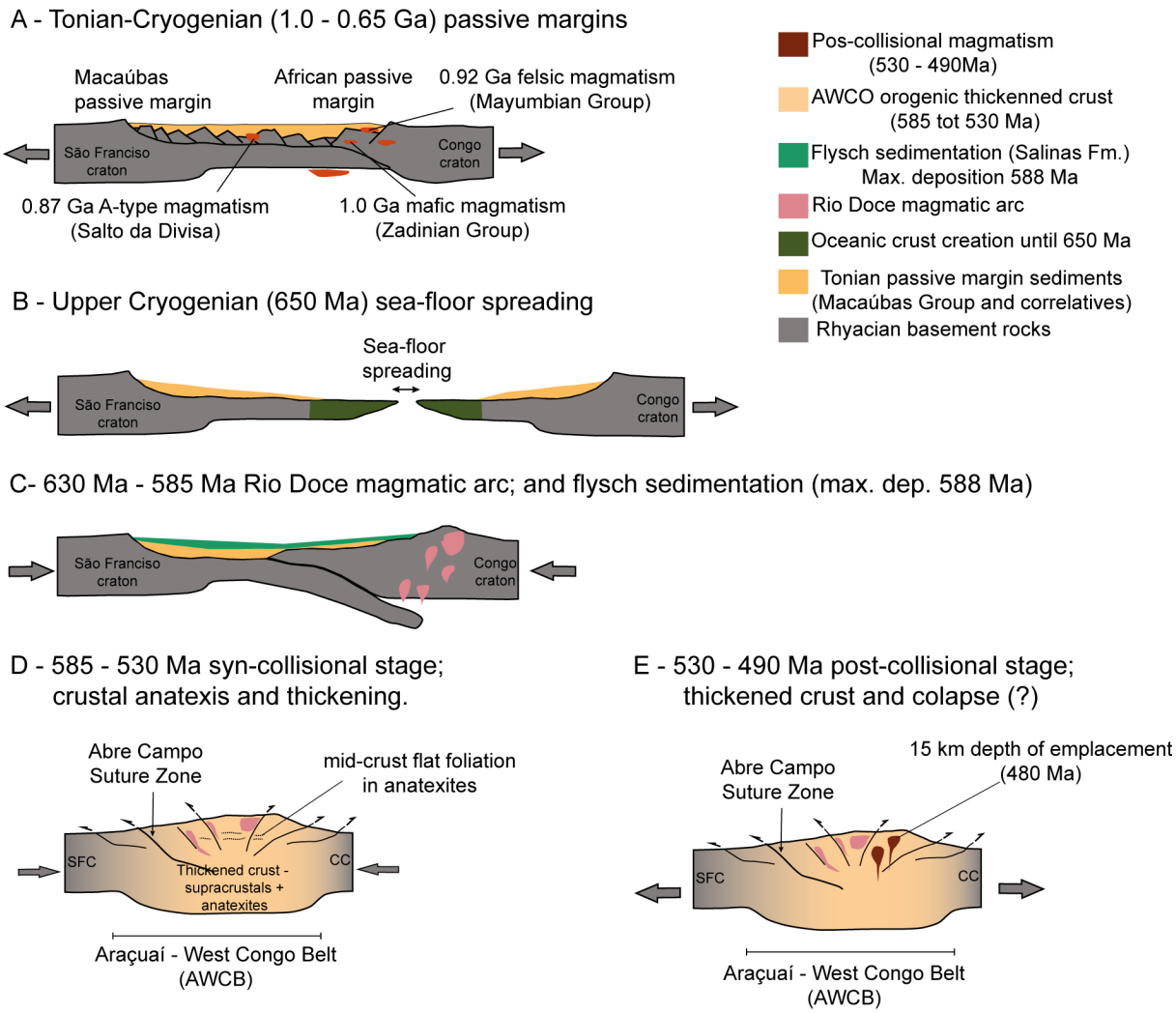

Figure 4.2 – Schematic evolution of the Araçuaí-West Congo Belt. See text for complete explanation.

The WCB experienced two main tectono-metamorphic events, one around 540 Ma (6-9 kbar and 680-750ºC) and another around 490 Ma (5-7 kbar and 610-670ºC). Peak metamorphic conditions of the West Congo Belt are 40-30 Ma younger than Araçuaí Belt (Monié *et al*., 2012), suggesting the hypothesis that the West Congo shared an orogenic history with the Brazilian Cabo Frio Domain, which in turn, is thought to have been accreted

to the southeastern extension of the Araçuaí Belt (da Silva *et al*., 2005) during early Cambrian (Schmitt *et al*., 2008).

4.2.3 Orogenic paleo-thickness and structure of the AWCB

Cross-sections from both Araçuaí and West Congo Belts are shown in Figure 4.3. A tectonic vergence reversal is preserved in the Araçuaí Orogen, which for some authors (e.g. Gradim et al., 2014) represents the suture zone. Nevertheless, the West Congo Belt would more likely represent an eastern foreland domain of the double-vergent Araçuaí-West Congo Belt (Figure 4.3). The suture is expected to be far west of the West Congo Belt, already in the Araçuaí Belt (Tack *et al*., 2001), where ophiolitc remnants, high-grade metamorphic rocks and granitoid batholiths (completely absent in West Congo Belt) occur. In fact, the suture zone should be located to the west of the Rio Doce magmatic arc, where the Abre Campo Shear Zone (Figure 4.3, 4.2D) hosts a suture-related accretionary wedge characterized by deep-sea deposits, tectonic slices of ophiolitic rocks and arc-derived sediments (Peixoto *et al*., 2015).

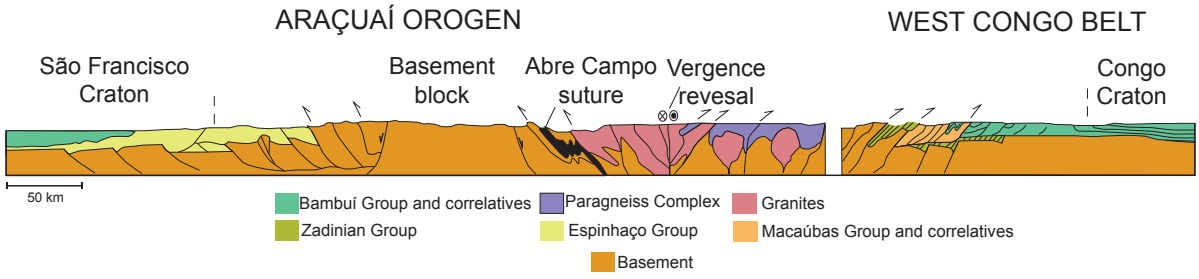

Figure 4.3 – Cross-sections of the Araçuaí and West Congo Belts. Note that a vergence reversal and all magmatism are restricted to the Araçuaí Belt (hinterland). Thin-skin tectonics prevails towards both Brazilian and African sides when units are being thrusted upon the cratons. Adapted from Alkmim et al. (2006).

As it can be pictured from the schematic regional cross-sections of the AWCB (Figure 4.3), the hinterland domain of the orogen is preserved in the Araçuaí Orogen (Brazilian side after Cretaceous breakup). This domain comprises most of the magmatic rocks from pre-, syn- and post-collisional stages and thus accounted for most of the crustal thickening. It also comprises the back-arc related rocks (Paraíba do Sul Complex) and the suture zone. In terms of structures, it is characterized by high-angle thrust faults with important strike-slip components. These faults show a vergence reversal that does not coincide with the suture zone and configure a double-vergent orogen.

Despite the high-angle thrusts, AMS-aided structural studies (Cavalcante *et al*., 2013) showed that the hinterland developed a consistent flat foliation in the mid-crustal syn-collisional anatectic rocks, suggesting an important gravitational component during syn-collisional thickening and a ductile regime in the middle and lower crust (Figure 4.2 D).

Estimations of hinterland crustal paleo-thickness can be done by summing present day depth to Moho - derived from seismic studies (Pasyanos & Nyblade, 2007; Tedla *et al*., 2011; Assumpção *et al*., 2013b) - and burial depth (Table 4), that is, the depth translated from pressure estimates in metamorphic rocks (Figure 4.4).

Table 4 – Estimations of paleo-thicknesses in metamorphic rocks and emplacement depth from intrusives. The samples chosen are the closest to cross-section shown in Fig. 4.

Metamorphic P-T estimations of metamorphic rocks									
Orogen	Location	Sample	Tectonics	Metamorphism Age (Ma)	Thermometry (Degree Celsius)*	Barometry (kbar)*	Estimated depth (km)**	Depth to Moho (km)	Paleo-thickness
West Congo Belt	W Africa	Metasediments[1]	syn-post-collisional	540	750	9	32,4	37	69,4
West Congo Belt	W Africa	Metasediments[1]	exhumation	490	670	7	25,2	37	62,2
Araçuaí Orogen	E Brazil	Migmatitic gneisses[2]	syn-collisional	580	913	6,5	23,4	37	60,4
Araçuaí Orogen	E Brazil	Migmatitic gneisses[2]	syn-collisional	580	800	7	25,2	37	62,2
Araçuaí Orogen	E Brazil	Granulites[3]	?	600-580	800	8	28,8	37	65,8
Araçuaí Orogen	E Brazil	Metassediments[3]	?	570	800	6,5	23,4	37	60,4
Intrusive rocks and emplacement depths									
Orogen	Location	Sample	Tectonics	Emplacement Age (Ma)	Thermometry (Degree Celsius)	Barometry (kbar)*	Emplacement Depth (km)**		
Araçuaí-Ribeira	ES State	VA-06[3]	Late-orogenic	508±8 (Rb-Sr)	980	6,6	15-20		
Araçuaí-Ribeira	ES State	VA-202[3]	Late-orogenic	508±8 (Rb-Sr)	980	5,53	15-20		
Araçuaí-Ribeira	ES State	VA-261.1[3]	Late-orogenic	508±8 (Rb-Sr)	?	6,7	15-20		
Araçuaí-Ribeira	ES State	StA-410A[3]	Late-orogenic	513±8 (U-Pb)	720	5,96	15-20		
Araçuaí-Ribeira	ES State	StA-410B[3]	Late-orogenic	513±8 (U-Pb)	720	11,4	15-20		

*** P-T data displayed in this table are the greatest values within data error**

**** Values calculated considering 3,6 km/kbar**
[1]Monié et al. (2012)
[2]Cavalcante et al. (2014)
[3]Weidemann et al. (2002)

In what follows, the maximum depths to Moho are those preserved in Brazilian side, around 41 km. During syn-collisional stages (580-530 Ma), the Araçuaí Belt records between 23-25 km burial depth, while the West Congo Belt records up to 32 km of burial depth. Crustal paleothickness for both sides yield 66-67 km thick. Intrusive post-collisional granitic rocks in the Araçuaí Belt show maximum emplacement depths of 20 km between 510-500 Ma and maximum emplacement depths of 15 km around 480 Ma (Wiedemann *et al.*, 2002). In what follows, the crust must have kept ~56-60 km thick at least until 480 Ma.

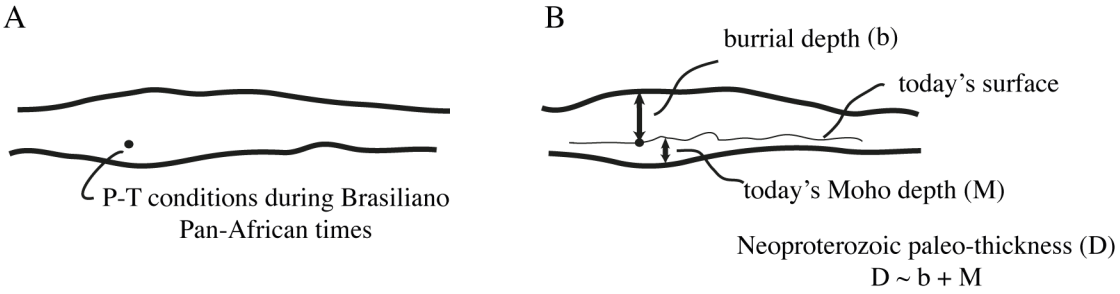

Figure 4.4 – Schematic representation of paleo-thickness estimation. (A) Shows thickened crust during peak orogenic stage and preservation of Brasiliano P-T conditions. (B) Shows the same thickened crust and today's surface. By summing burial depth (b), which is estimated by P-T data, to today's depth to Moho (M), then we find a good estimation for crustal paleothickness during peak orogenic stage in the Neoproterozoic.

From the hinterland westwards, the orogen has uplifted basements rocks and a thin-skinned thrust-and-fold belt over the São Francisco Craton. Basement uplifts (e.g. Guanhães Block) show magmatic crystallization ages of 2.7 Ga, Paleoproterozoic metamorphism at 2.05 Ga and Brasiliano/Pan-African metamorphism overprint at 0.56 Ga (Peixoto *et al.*, 2015), which indicates that basement rocks were reworked during the AWCB building up. Sediments of the Macaúbas basin and older Espinhaço rift are thrusted upon the cratonic margin under thin-skin deformation.

In the African side, the West Congo Belt shows thin-skinned fold-and-thrust belt over the Congo Craton. Mostly pre-rift and syn-rift rocks are correlatives of the Macaúbas basin.

4.3 From Western Gondwana amalgamation to the onset of Juro-Cretaceous rifting

The time between the final Gondwana amalgamation (~Eo-Paleozoic) and the onset of its breakup (Juro-Cretaceous) was a period of quiescence. Intraplate deformation is thought to

have ruled during this period, mainly as a result of the cratonward propagation of regional flexural subsidence caused by the Gondwanides Belt in western Gondwana (Milani & Ramos, 1998; Ramos, 2003). From the Neoproterozoic to the Ordovician, rift structures formed small basins that were later covered by Silurian-Devonian sediments (Almeida *et al*., 2013). Proterozoic shear zones within the crystalline basement of the Ribeira Belt were reactivated, such as the Itu-Jundiuvira Shear Zone at 477 Ma (Hackspacher *et al*., 2004), the Camburu Shear Zone at 402 Ma and later at 310 Ma (Mora *et al*., 2013) and the Bocaina Plateau at 303 Ma (Hiruma *et al*., 2010).

The rifting process of Gondwana is suggested to have begun around 180 Ma, during the Karoo Magmatic Event in Africa and Argentina, and together with the ~132 Ma Paraná-Etendeka Magmatic Province, these are the two main age peaks of pre-breakup magmatism (Almeida *et al*., 2013). In what follows, rifting started in the south of Gondwana and propagated northwards (present coordinates), until it reached the Jatobá-Recôncavo-Tucano aborted rifts in northeast Brazil. North-south orthogonal rifting ceased by Aptian-Albian times, when extension became oblique and characterized the Transform Equatorial Segment of the South Atlantic Rift System. At ~100 Ma, oblique rifting started and fully open oceanic conditions were established around 94-62 Ma (Macdonald *et al*., 2003; Pérez-Díaz & Eagles, 2014).

4.4 The Central South Atlantic

The South Atlantic Rift System is separated from the Central Atlantic Rift System by the Marathon Fracture Zone (Figure 4.5). In what follows, the South Atlantic Rift System is divided into four different segments (Moulin *et al*., 2010): from north to south, the Equatorial Segment, the Central Segment (limited by the Ascension and Rio Grande Fracture Zones), the Austral Segment and the Falkland Segment (Figure 4.5).

The Central Segment - or Central South Atlantic - comprises magma-poor rifted conjugate margins, being one of the three main archetypal Atlantic rifted margins (*sensu* Peron-Pinvidic et al., 2013). Besides the evident fit between the South American and African conjugate margins, some misfits during lower Cretaceous reconstructions (e.g. Heine et al., 2013) have shown that extension of the lithosphere must have occurred following non-uniform stretching models, that is, depth-dependent extension (e.g. Huismans and Beaumont, 2011, 2014; Lentini et al., 2010). Depth-dependency causes the lithosphere to stretch

differently with depth, so in some domains the crust might be hyper-extended (> 100 km, Unternehr et al. (2010)), whereas in other domains, mantle lithosphere could be exhumed. These differences are the main causes of misfits in paleogeographic plate reconstructions. Non-uniform stretching models are also favoured in order to explain higher accommodation space creation for anomalously thick sag sequences in the Brazilian and African conjugate margins. Resulting brittle deformation due to uniform stretching (pure-shear models) seems to underestimate the magnitude of lateral extension needed to create very thick sag basins (Lentini *et al*., 2010; Reston, 2010)

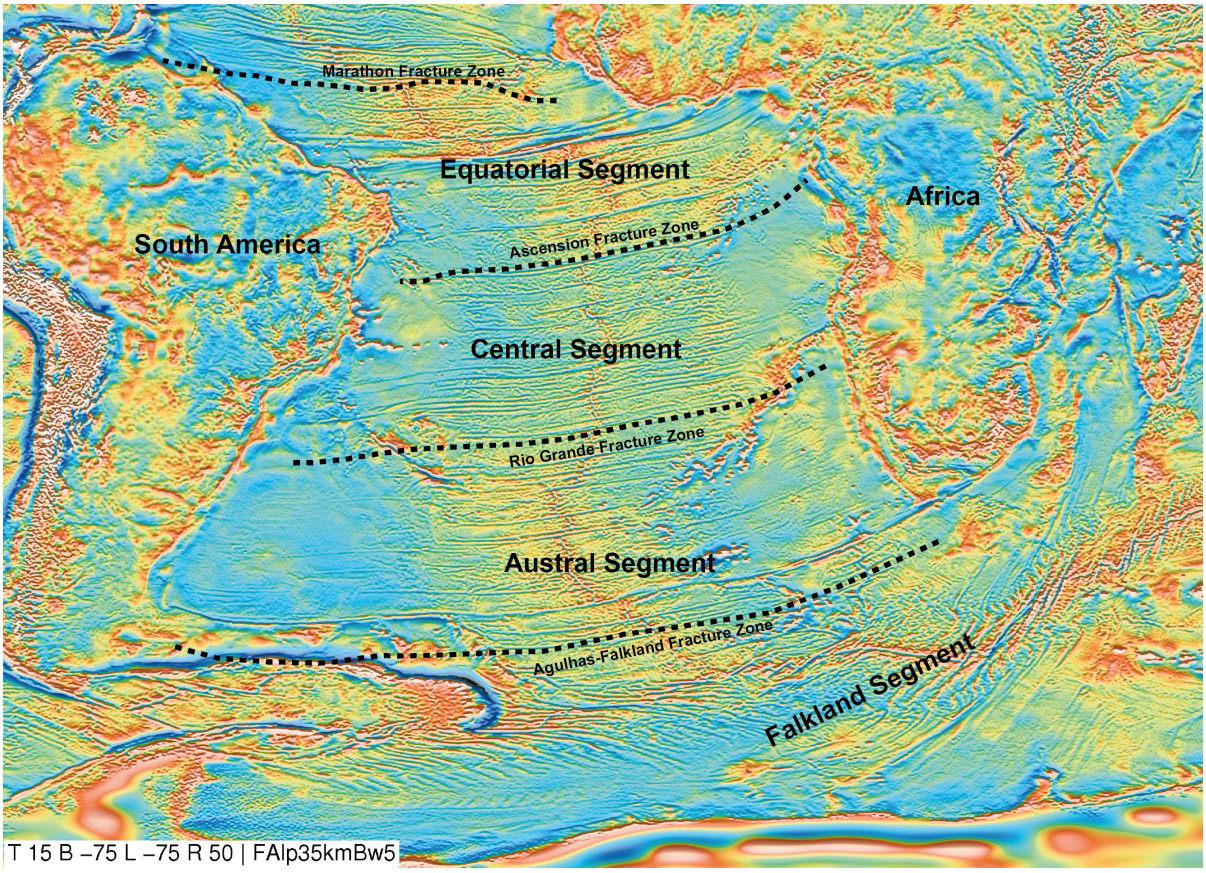

Figure 4.5 – Free-air gravity filtered image (Heine *et al*., 2013) of the South Atlantic Rift System showing its four main segments and bounding fracture zones.

By following the continent-ocean boundary (COB) in the Central Segment, it is observed that hyper-extension is particularly present where lithosphere was thermal-mechanically reactivated during Ediacaran Brasiliano/Pan-African orogenesis, whereas old and stable cratonic lithosphere (i.e. São Francisco and Congo Cratons) somehow precluded hyper-extension. Lentini et al. (2010) argued that differential subsidence (and associated creation of thicker pre-salt accommodation space) appears to reflect basement heterogeneity, concluding that orogenic crust (or "soft crust") is a first order control on subsidence patterns,

whereas cratonic (or "hard crust") precludes higher rates of differential subsidence. These observations seem to agree with well-accepted classifications of rifted passive margins either as wide or narrow (*sensu* Buck, 1991), since wide passive margins in the Central South Atlantic developed on Brasiliano/Pan-African orogens, while narrow configurations developed on cratonic lithosphere.

The conjugate margin in the Central Segment developed through orthogonal rifting, that is, with extensional forces orthogonal to rift axis (Matos, 2000). Is it also observed that rift axis and rift propagation developed sub-parallel to pre-existent lithospheric anisotropies represented by either Neoproterozoic fabrics of the Brasiliano and Pan-African orogens (e.g. Fetter, 2009) and by the Paleoproterozoic fabrics around Archean cratonic borders (Ferreira *et al*., 2009).

As aforementioned, the Central Segment is thought to represent a magma-poor rifted margin, that is, without voluminous magmatism expressed as flood basalts, without seaward-dipping reflectors (SDRs) and with high-velocity lower crustal underplatings. Instead, magma-poor margins are controlled by tectonic processes and are characterized by hyper-extended crust accompanied by normal faulting and lithospheric mantle exhumation between oceanic and continental lithosphere (Blaich *et al*., 2011). However, these characteristics seem not to occur throughout the entire Central Segment. The southern part of the Central Segment includes the African Kwanza Basin, which displays brittle deformation accompanied by significant block faulting (von Nicolai *et al*., 2013) and extreme thinning, but lack mantle exhumation at the COB. This is explained by magmatic activity, that is, intruding magmas that sealed detachment faults responsible for exhumation processes (Blaich *et al*., 2011; von Nicolai *et al*., 2013). This syn- to late-rift volcanic activity shows the transition between the magma-poor Central and magma-rich Austral Segments of the South Atlantic Rift System.

4.5 A brief review on the evolution of the sedimentary basins in the Central South Atlantic

The Brazilian eastern passive margin extends from the southern Pelotas Basin to the northeastern Potiguar Basin. Four large stages are likely to have occurred during the development of the Central South Atlantic: pre-rift, syn-rift, post-rift and drift (Cainelli & Mohriak, 1999; Brownfield & Charpentier, 2006; Milani *et al*., 2007).

The pre-rift phase is an early evolutionary stage during the upper Jurassic and the lower Cretaceous (~145 Ma) characterized by flexural subsidence induced by processes of lithospheric stretching and leading to sag-type basins. Pre-rift successions comprise reddish sediments derived from fluvial, lacustrine and eolian continental contexts. In Brazil, pre-rift successions are recorded in the Recôncavo-Tucano-Jatobá basins, Sergipe-Alagoas, Camamu and Foz do Amazonas, whereas in Africa, only within the Congo (more than 1 km thick) and Gabon basins.

The following syn-rift phase is characterized by the intense activity of normal faults and mechanical subsidence, generating deep lakes with uplifted flanks. Sedimentation is mainly conglomeratic close to the border faults and anoxic distal shales. The latter are important hydrocarbon-generator rocks, as exemplified by the Lagoa Feia Group (Campos Basin) and the Barra de Itiúba Formation (Sergipe-Alagoas basins). Magmatism is characterized by igneous basic rocks from 145 to 125 Ma, specially between Pelotas and Espirito Santos magma-rich continental margin. Except for the Paraíba and Pernambuco basins, all eastern marginal basins of Brazil preserved syn-rift sediments. In Africa, it is well recorded in the Gabon, Congo and Kwanza basins.

A following period of quiescence is typical of the post-rift phase, which is characterized by thermal cooling and a new generation of sag-type basins that subsided either by thermal contraction and sediment loading. During the Aptian (or so-called Alagoas Stage) restricted marine conditions prevailed and deposited large packages of evaporites (mostly halite and gypsum-anhydrite), comprising the Santos Basin (Ariri Formation), Campos Basin (Retiro Formation of the Lagoa Feia Group) and Espírito Santos Basin (Itaúnas Member of the Maririco Formation). Evaporitic successions extend to the north until Sergipe-Alagoas region (see Fig. 4.14) and are above reservoir microbialites. Santos, Campos and Espirito Santos basins have the thickest salt layers. The lack of salt layers in the Potiguar basin corroborates to a south-to-north direction of rifting during the South Altantic Rift System. During the Aptian (~120 Ma), the Recôncavo-Tucano-Jatobá basins are already aborted.

The final drift phase begun with the installation of the oceanic crust and the progressive separation of the continents. Continental drifting and sediment loading generated regional uplift in the continental margin, defining present-day physiography (Mohriak *et al*., 2008).

4.6 Current rifted passive margin structure of the Central South Atlantic

The current lithospheric structure of the rifted passive margin in the Central South Atlantic was mainly constrained by published seismic sections that are shown in Figure 4.6. In order to constrain structural inheritance, rheology and lithospheric structure in the Central Segment, two conjugate offshore seismic sections were selected based on the fact that they are approximately parallel and show minor offset when paleo-reconstructions are made (Figure 4.6 B), as well as minor magmatic activity, once they are in magma-poor margins.

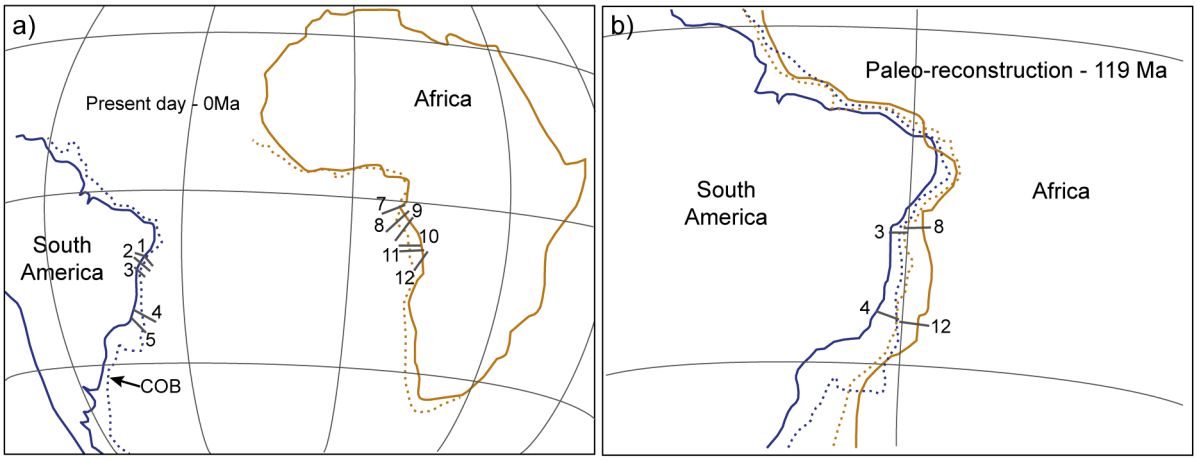

Figure 4.6 - (A) Available seismic sections in the Brazilian and Africa rifted margins of the Central South Atlantic (spherical projection). Dashed lines in the margins denotes the transition continent-ocean crust. 1: Tucano-Sergipe Sections (Blaich *et al*., 2008), 2: Recôncavo-Jacuípe Sections (Blaich *et al*., 2008), 3: Camamu Section (Blaich *et al*., 2011; Heine *et al*., 2013), 4: Espírito Santo Section (Zalán *et al*., 2011; Peron-Pinvidic *et al*., 2013), 5: Campos Section (Aslanian *et al*., 2009; Zalán *et al*., 2011), 7: Gabon Section (Blaich *et al*., 2011), 8,9: North and South Gabon Sections (Dupré *et al*., 2011), 10: North Angola Section (Aslanian *et al*., 2009), 11: South Angola Section (Peron-Pinvidic *et al*., 2013), 12: Kwanza Section (Blaich *et al*., 2011). (B) Paleo-reconstruction (119 Ma) closing the South Atlantic Rift System according to Heine et al. (2013) showing the selected pairs of conjugate sections Camamu-Gabon and Espírito Santo-Kwanza.

The first conjugate sections are located in the Brazilian Camamu basin and the African Gabon basin, while the second pair is located in the Brazilian Espírito Santo Basin and the African Kwanza Basin (Figure 4.7). In the Camamu basin, lithospheric extension took place on the older cratonic lithosphere of the São Francisco Craton, whereas its African conjugate Gabon basin extension took place on the Neoproterozoic West Congo Belt.

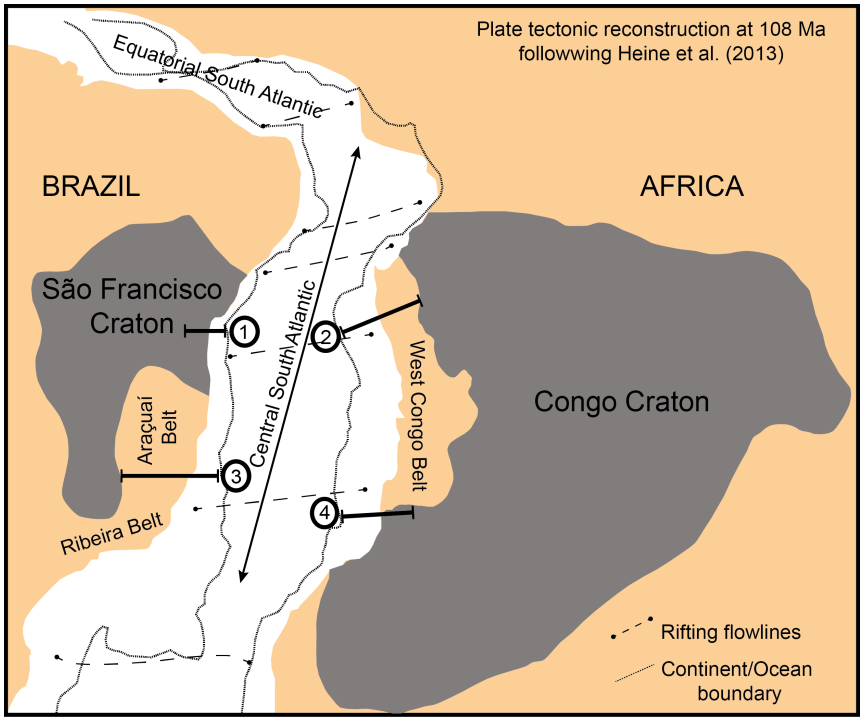

Figure 4.7 - Plate tectonic reconstruction at 108 Ma (Heine et al., 2013) of the South American and African plates. Numbers 1-2 represent the Camamu-Gabon conjugate transections and 3-4 represent the Espírito Santo-Kwanza transections.

Towards the south, the Espírito Santo basin formed due to the extension of the Neoproterozoic-Cambrian Araçuaí Belt, whereas the Kwanza basin developed in the limits between the southern part of the West Congo Belt and the Congo Craton. Onshore geology was connected to the offshore seismic sections and together they compose four main transections to constrain the Central Segment of the South Atlantic (Figure 4.7).

4.6.1 Camamu basin and onshore connections

The Camamu basin seismic section shows that the continental crust extends across 100 km oceanwards (Figure 4.8). At the necking domain (*sensu* Peron-Pinvidic et al., 2013), the continental crust thins from 35 km thick to 10 km thick along 40 km towards the offshore, with a stretching factor β=1,43. In the next 70 km oceanwards, in the distal domain, the crust again thins from 10 km thick to 4 km thick and a β=2,9. The calculated[3] stretching factor for

[3] Stretching factor β was calculated using initial length (L_0) and present-day length (L) as $\beta=L/L_0$. L_0 was, in turn, calculated considering equal-areal restorations through the relation $L_0=Area/h_0$. Area was calculated using Adobe Illustrator Software and h_0 is assumed: for late Jurassic, crustal thickness equals depth-to-Moho estimates, while for Paleoproterozoic or Neoproterozoic it is equal to the sum of present-day depth to Moho and pressure-derived burial depth translations (see Figure 8.1 for details).

the Camamu basin as a whole, considering late Jurassic crustal thickness of 35 km in the proximal domain, is β=3.9.

According to the thick syn-rift sedimentary succession overlying the thinned continental crust, thinning was not governed by brittle deformation (Blaich *et al*., 2010). Although lower crustal segments were not interpreted in the Camamu Basin by Blaich et al. (2011), the nearby Almada Basin shows reflective lower crust (Gordon *et al*., 2012).

The same authors refute the idea of mantle exhumation in the transition between the continental and oceanic crust (COB) in the Almada Basin, but Caixeta et al. (2009) propose mantle exhumation for the Camamu Basin at the COB.

Towards the onshore, the Camamu Basin is linked to the São Francisco Craton (SFC). Is this region (Bahia State, NE Brazil), it comprises the Neoarchean Jequié Block and the Paleoproterozoic 2.4 Ga Itabuna-Salvador-Curaçá Belt, which reached peak metamorphism around 2.05 Ga (van Schmus *et al*., 2008). Peak metamorphic conditions are estimated in 7 kbar and 850ºC (Barbosa & Sabaté, 2004), which translates into 25 km of burial depth. Present day depth to Moho onshore the Camamu Basin is 35 km (Assumpção et al. 2013), so an estimate of Paleoproterozoic crustal paleo-thickness is around 60 km.

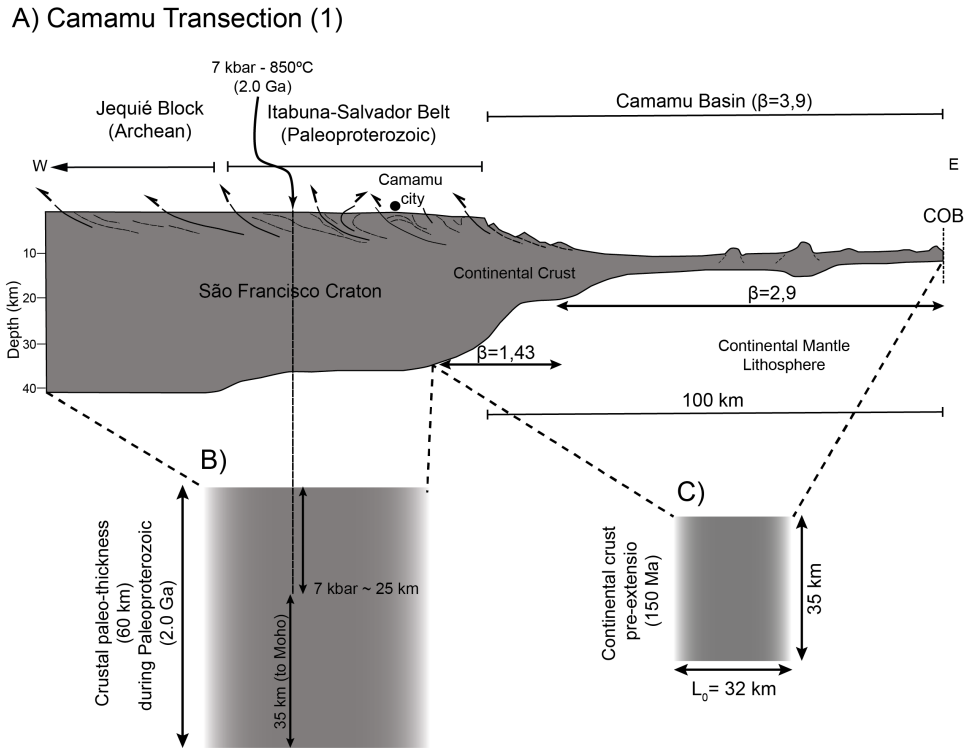

Figure 4.8 – A) Camamu transection. See localization in Figure 4.7. Onshore geological configuration was extracted from Barbosa and Sabaté (2004) and offshore configuration from Blaich et al. (2011). B) Crustal paleo-thickness during Paleoproterozoic assuming a 60 km thick Itabuna-Salvador Belt (25 km of burial depth and 35 km to Moho). C) Continental crust restored (equal-area) to pre-extension setting 150 Ma.

The basement structures are mainly Archean-Paleoproterozoic low-angle faults and Paleoproterozoic high-angle faults (Ferreira *et al*., 2009). The main faults in the Camamu Basin follow older low-angle structures, whereas intrabasinal local faults follow younger high-angle faults (Gordon *et al*., 2012).

4.6.2 Gabon Basin and onshore connections

The Gabon Basin seismic sections show hyper-extended continental crust across 230km oceanwardsm (Figure 4.9). The crust thins from 35 km thick to ~14 km thick along the 120 km long necking domain, with β=1,74. The distal domain thins from 14 km thick to 4 km thick along another 110 km oceanwards, with a β=1,94. The calculated stretching factor for the Gabon basin as a whole, considering late Jurassic crustal thickness of 35 km in the proximal domain, is β=2,5.

Seismic interpretations by Blaich *et al*. (2011) and seismic and gravity analysis by Dupré *et al*. (2011) show that both upper and lower crust (2,85 g/cm^3) were stretched, although upper crust is more stretched. Compressional wave velocities in the Gabon extended margin shows an increase oceanwards, from 6400 m/s for a pure continental crust, to 6700-7000 m/s for transitional crust and to 7200 m/s for oceanic crust Dupré et al. (2011). The COB along Gabon margin is characterized by flat Moho and flattening of gravity anomalies Blaich et al. (2011). The same features are mirrored to the conjugate Camamu extended margin.

Onshore, the Gabon section connects to the Neoproterozoic West Congo Belt, which is reckoned to be an inverted intracontinental rift. This belt is thrust by the Paleoproterozoic Kimezian basement, and both nappe stacks thrust the margin of the Congo Craton with top-to-east vergence (Tack *et al*., 2001). The West Congo Belt experienced two main tectono-metamorphic events (Monié *et al*., 2012), one around 540 Ma (6-9 kbar and 680-750ºC) and another around 490 Ma (5-7 kbar and 610-670ºC).

Considering Brasiliano-Pan/African orogenesis around 540 Ma, the West Congo Belt reached 9 kbar, which translates to 32 km of burial depth. Present day depth to Moho onshore the Gabon basin is around 35 km (Tedla *et al*., 2011), which gives a Neoproterozoic crustal paleo-thickness of 67 km. If we perform equal-area restoration of the orogenic crust to 540 Ma when the crust was thickened to at least 67 km, the calculated initial length (L_0) of the West Congo Belt was around 113,4 km wide.

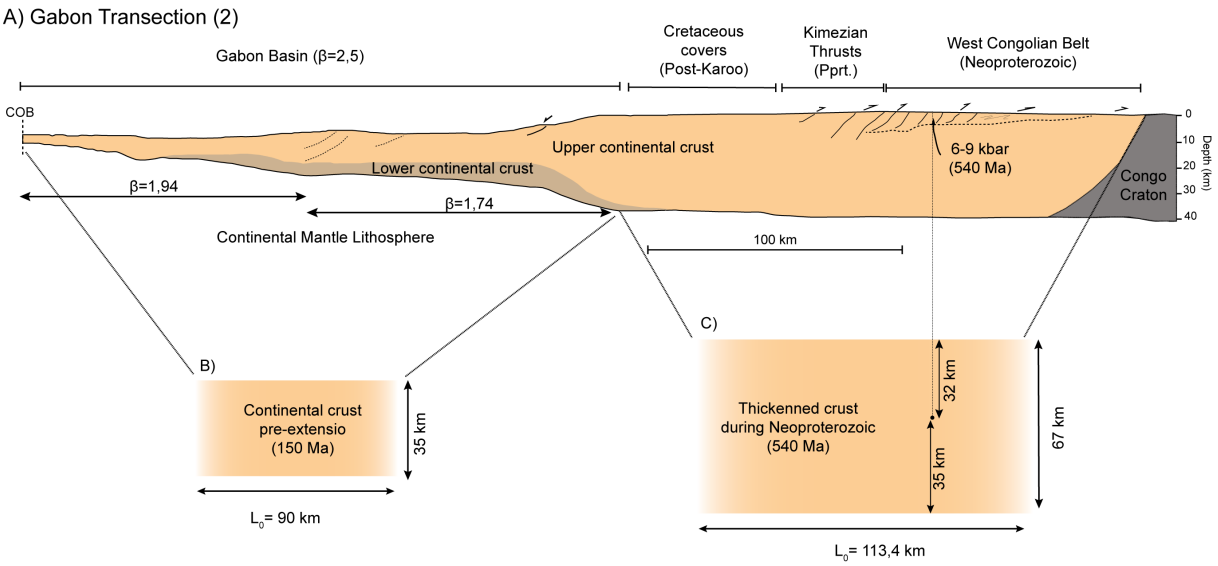

Figure 4.9 - A) Gabon transection. See localization in Figure 4.7. Onshore geological configuration was extracted from Tack et al. (2001) and offshore configuration from Blaich et al. (2011) and Dupré et al. (2011). B) Crustal paleo-thickness during Paleoproterozoic assuming a 67 km thick West Congo Belt (32 km of burial depth and 35 km to Moho). C) Continental crust restored (equal-area) to pre-extension setting 150 Ma.

The Gabon faults mainly inherited the low-angle structures of the east-verging West Congo Belt. The extended continental crust does not show prominent brittle deformation.

4.6.3 Espírito Santo Basin and onshore connections

The section along the Espírito Santo Basin shows that the continental crust was stretched and thinned oceanwards (Figure 4.10). In the proximal domain, around 30-40 km oceanwards, the continental crust underwent necking, as shown by the shallowing of the Moho from 35 km depth to 25 km depth, and by the generation of accommodation space in the basin up to 5 km deep. The necking domain has a stretching factor $\beta = 1{,}72$. Moving towards distal domains, the crust is highly thinned and stretched, achieving minimum thicknesses of 8 km. Stretching factor for this domain is $\beta = 3{,}73$.

Seismic interpretation by Zalán *et al.*, (2011) shows that both upper and lower continental crust were stretched, although the lower crust is highly thinned and stretched, indicating that it accounted for most of the ductile deformation. Furthermore, all Santos, Campos and Espírito Santo basins show mantle exhumation in the transition between continental and oceanic crust, as well as very shallow Moho.

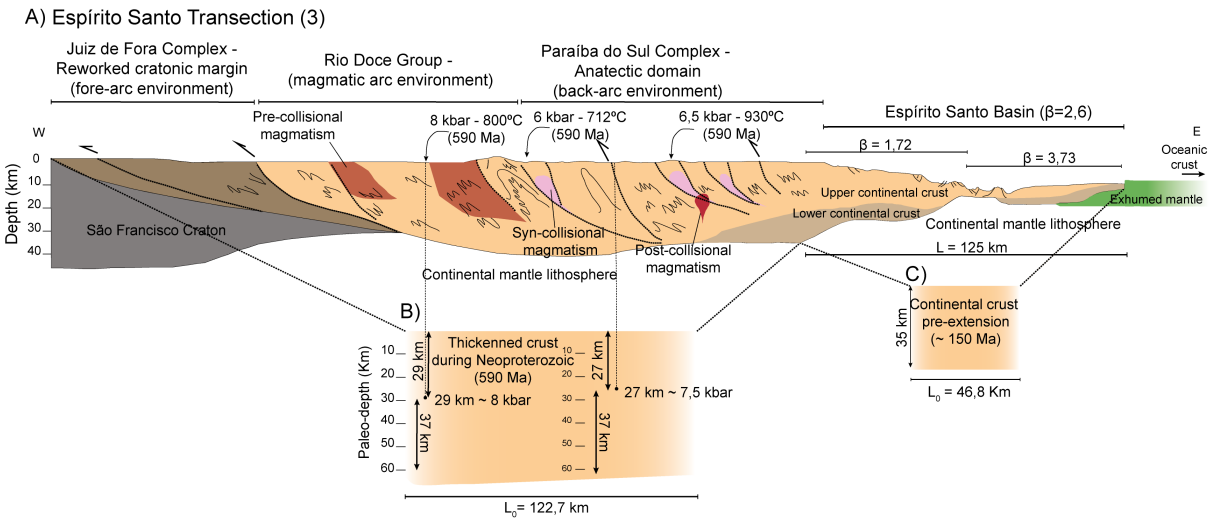

Figure 4.10 – Espírito Santo Transect. Onshore geology was interpreted following gravity-based geological sections of Wiedemann et al. (2002) and offshore crustal structure was interpreted after seismic sections of Blaich et al. (2011) and Zalán et al. (2011). Lower boxes are equal-area restorations showing the initial length of the rifted passive margin during the onset of rifting (~150Ma) and the initial length of the Araçuaí Belt during Neoproterozoic metamorphic peak (~580Ma).

According to the seismic interpretations by Blaich et al. (2011) and Zalán et al. (2011), the main type of faults in the basin are both synthetic and antithetic listric normal faults. In the proximal domain, these faults are relatively shallow, and die out in the upper continental crust, whereas in the distal highly thinned domains, they die out at the Conrad Discontinuity. The synthetic normal faults probably follow the Neoproterozoic onshore fabrics of the Araçuaí Belt, which is characterized by high-angle reverse faults top-to-the craton (west).

Towards onshore, the Espirito Santo section is connected to the southern part of the Araçuaí Belt. This belt is roughly divided into three units (Figure 4.10), from east to west, The Paraíba do Sul Complex (back-arc environment), the Rio Doce Group (Magmatic Arc environment) and the Juíz de Fora Complex (fore-arc environment, reworked cratonic margin). P-T conditions estimates are well-constrained in the Araçuaí Belt, with temperatures varying from 700°-800°C in the western fore-arc, and 913°C in the hot back-arc zone during Brasiliano prograde metamorphism (Cavalcante *et al.*, 2013; Gradim *et al.*, 2014). Pressure estimates vary from 6,5 to 7,0 kbar in the west part of the orogen (Cavalcante *et al.*, 2014; Peixoto *et al.*, 2015) and 5,4 to 7,5 kbar in the eastern part (Wiedemann *et al.*, 2002; Gradim *et al.*, 2014). 7-7,5 kbar translates to 25-27 km of burial depth, and the depth to Moho in the onshore Espírito Santo is around 37 km (Assumpção *et al.*, 2013a), so an estimated crustal

paleothickness for the Araçuaí Belt during late Neoproterozoic is around 62 km. If we perform equal-area restoration of the orogenic crust to 580 Ma when the crust was thickened to at least 62 km, the calculated initial length (L_0) of the Araçuaí Belt was around 123,2 km wide.

4.6.4 The Kwanza Basin and onshore connections

The seismic sections along the Kwanza Basin show that the continental crust extends across ~340 km oceanwards (Figure 4.11). Along the proximal 200 km in the onshore Kwanza Basin, the continental crust is stretched and accommodate brittle deformation in antithetic normal faults and minor synthetic ones along the upper crust. Both synthetic and antithetic faults create troughs, such as the Calomboloca trough (Guiraud *et al*., 2010), in the inner Kwanza Basin (Hudec & Jackson, 2004). Thinning along the 200 km long Inner Kwanza turns a 35 km thick crust into an 18 km thick crust, with consequent shallowing of the Moho and creation of accommodation space (~5 km depth) in the surface. Stretching factor in the inner Kwanza Basin is β=1,65. Reflection seismic interpretations and gravity modelled transects by Blaich et al. (2011) and Contrucci et al. (2004) indicate that lower continental crust is present along 190 km oceanwards with maximum thickness of 9 km, which is correlated to better-constrained lower crust in neighbouring southern Gabon margins.

In the outer Kwanza Basin, the crust is more thinned than stretched, reaching minimum thickness of 5 km (β=2), and showing no evidence for the interpretation of a lower continental crust. This domain shows higher densities (~2.9kg/m^3), but lack of seaward dipping reflectors indicated this is still continental crust (Blaich *et al*., 2011). The Moho is even shallower in this domain, and there is no evidence for exhumation of the continental mantle lithosphere at the COB. The stretching factor for the whole Kwanza Basin is β = 2,3.

Kwanza Basin onshore geology is related to the West Congo Belt. Type cross section of the West Congo Belt (Tack et al., 2001) shows that a basement nappe (Paleoproterozoic Kimezian Group) is thrust on top of the West Congo Orogen, which in turn, thrusts the Congo-Angola Craton to the east as a foreland thin-skinned fold-and-thrust belt. Assuming 7 kbar of baric peak during West Congo development (Monié *et al*., 2012) in the hinterland, which translates into 25 km of burial depth, and present day Moho depth at 37 km (Tedla *et al*., 2011), Neproterozoic paleothickness of the West Congo Belt is estimated as 62 km. If we perform equal-area restoration of the orogenic crust to 540 Ma when the crust was thickened

to at least 62 km, the calculated initial length (L_0) of the West Congo Belt was around 108 km wide.

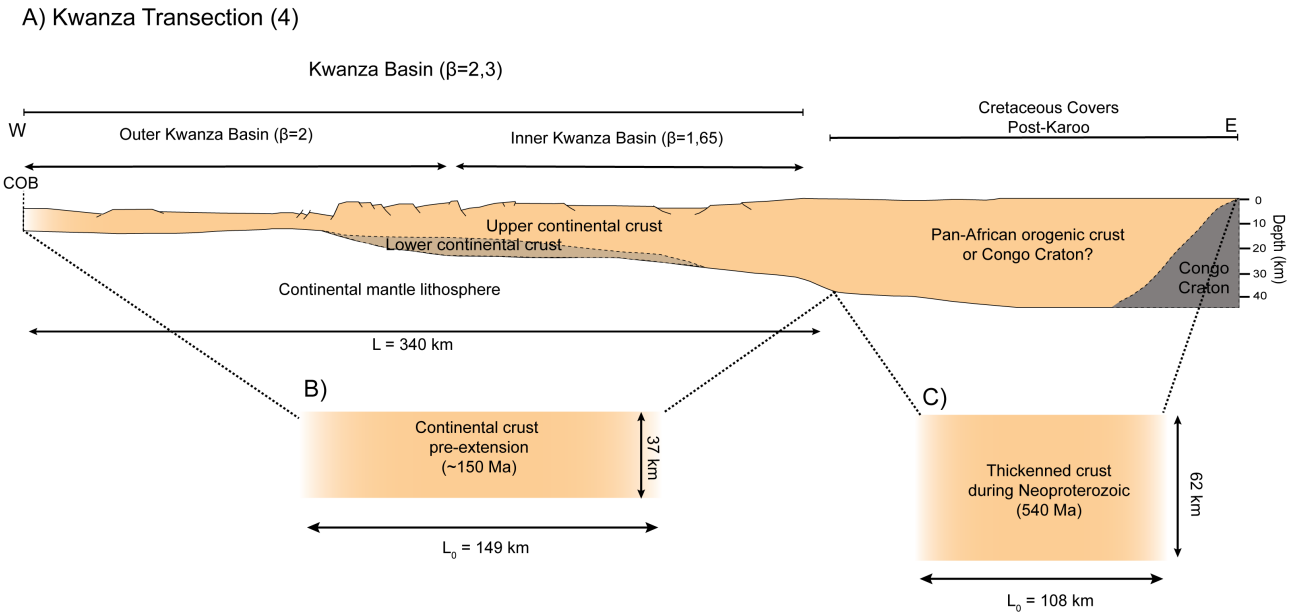

Figure 4.11 – A) Kwanza Transect. Onshore geology was interpreted after geological type cross sections of (Tack *et al*., 2001) and offshore crustal structure was interpreted after seismic sections of Blaich et al. (2011), structural maps by Guiraud et al. (2010), regional transect made by Hudec and Jackson (2004) and gravimetric modelling by von Nicolai et al. (2013). B) Shows a schematic continental crust pre-extension (~150Ma), with initial length (L_o) of 149 km. C) Shows a schematic thickened crust during Neoproterozoic. West Congolian Belt in this domain was ~108 km long.

Chapter 5 - Materials and methods

All the geodynamic numerical simulations presented in this thesis were carried out at the University of Bergen, Norway, where I spent one year as a PhD guest. Being there, it took me a few months to get used to the code (and coding language) we used, after which I could start with primary test simulations. After many tests and debugging – which as very well-stated by Gerya (2010) "*...99% of your time will be for debugging*" – we finally created a first model that we considered more realistic as model set up and then we were able to start testing structural inheritance.

Numerical modelling was actually run at NOTUR, the Norwegian Metacenter for Computational Science[4], where high performance computation can be done either in sequential or parallel jobs. NOTUR is a national program of computational science in Norway that covers most of the Norwegian universities, including UiB. This thesis simulations were made in the realm of a project at NOTUR entitled "3D forward modelling of lithosphere extension", led by my co-supervisor.

5.1 Numerical approach used in this thesis

For the numerical simulations we use a modified highly efficient version of the Arbitrary Lagrangian-Eulerian finite-element code FANTOM (Thieulot, 2011; Erdős *et al*., 2014) to model thermal-mechanically coupled, plane-strain, viscous-plastic creeping flows. We investigate the behavior of a layered lithosphere and the sublithospheric mantle with frictional-plastic and thermally activated power law viscous rheologies in both contractional and extensional regimes.

When stress is below the frictional-plastic yield criterion, deformation is viscous and described by temperature-dependent non-linear power-law rheologies based on laboratory measurements.

Viscous deformation of rocks occurs by solid-state creep, which is the non-recoverable deformation of crystalline materials under stresses. Solid-state creep is the main deformation mechanism of rocks both in the Earth's crust and mantle (Gerya, 2010).

[4] Check http://notur.no website for details on the systems used in the lithosphere extension project: Hexagon and Vilje.

Diffusion creep and dislocation creep are the two main types of creep, where the first dominates under relatively low stresses during diffusion of atoms, and the second predominates under higher stresses during the dislocation of imperfections in the crystalline lattice of minerals. Diffusion creep shows a linear (e.g. Newtonian) relationship between deviatoric stress and strain rate, whereas dislocation creep is non-linear. Because most of the rocks in the lithosphere rarely show a Newtonian behavior (Stüwe, 2007), both diffusion and dislocation creep are parameterised together (using Dorn's law or power-law) in terms of differential stress (σ_d) and resulting strain rate ($\dot{\gamma}$), as follows:

$$\dot{\gamma} = A_m . \sigma_d^n . exp\left(-\frac{Q+V.P}{RT}\right), \tag{5.1}$$

where A_m is a material constant, n is the stress exponent (n=1 is diffusion and n>1 is dislocation creep), Q is activation energy, V is activation volume, P is pressure, T is temperature and R is the gas universal constant.

An important parameter in deforming materials is viscosity, which characterizes the material resistance to thermally-activated plastic deformation. Viscosity relates stress and strain in the following form for non-linear relationships:

$$\sigma^n = 2\eta\dot{\gamma}, \tag{5.2}$$

where n is the stress exponent. For numerical modelling, it is necessary that equation 5.1 is reformulated in terms of effective viscosity, which is a function of the second invariant of both deviatoric stress tensor (σ_{II}) and strain rate tensor ($\dot{\varepsilon}_{II}$):

$$\eta_{eff} = \frac{\sigma_{II}}{2\dot{\varepsilon}_{II}}. \tag{5.3}$$

The result of this reformulation (Gerya, 2010) and the addaptation for our numerical approach (Huismans & Beaumont, 2003; Erdős *et al*., 2014) is of the following form:

$$\eta_{eff} = f . A^{-1/n} . \dot{\varepsilon}_{II}^{\frac{1-n}{2n}} . \exp\left(\frac{Q+V.P}{nRT}\right), \tag{5.4}$$

where f is a scaling factor that creates strong lower crust without additional flow laws (Huismans & Beaumont, 2003, 2014), A is the pre-exponential scaling factor, n is the power law exponent, $\dot{\varepsilon}_{II}$ is the second invariant of the deviatoric strain rate tensor $\left(\frac{1}{2}\ \dot{\varepsilon}'_{ij}\dot{\varepsilon}'_{ij}\right)$, Q is activation energy, V is activation volume, P is pressure, T is temperature, and R is the universal gas constant. A, n, Q and V are derived from laboratorial measurements of "wet"

and “dry” olivine (Karato & Wu, 1993) and “wet” quartz (Gleason & Tullis, 1995) and are given in Table 6.1.

When stress exceeds the yield criterion, frictional-plastic deformation is modeled by a pressure-dependent Drucker-Prager yield criterion, which is equivalent to Coulomb criterion given incompressible deformation assumption in plane-strain. Frictional-plastic deformation is according to the following equation:

$$\sigma_y = (J_2')^{\frac{1}{2}} = C.\cos\phi_{eff} + p.\sin\phi_{eff}\ , \tag{5.5}$$

where J_2' is the second invariant of the deviatoric stress, ϕ_{eff} is the effective internal angle of friction given as p . sin(ϕ_{eff}) = (p - p_f) . sin(ϕ) for pore-fluid pressure p_f and cohesion C.

This yield criterion approximates frictional sliding in rocks and the effect of pore-fluid pressures. Strain-dependent rheologies play an important role during lithospheric deformation (Huismans & Beaumont, 2002, 2003), so in our models strain-softening effects are introduced by the linear decrease of the internal angle of friction from 15° to 2°, with simultaneous decrease of cohesion from 20 MPa to 4 MPa for accumulated strain values between 0.05 and 1.05. $\phi_{eff}(\varepsilon) \sim 15°$ corresponds to the effective ϕ when the pore fluid pressure is approximately hydrostatic.

The mechanical and thermal systems are coupled through the temperature dependence of viscosity and density and are solved sequentially during each simulating time step. In what follows, the heat transport equation is solved also in two dimensions (i=1,2):

$$\rho\ .\ C_p\ .\left(\frac{\partial T}{\partial t} + v_i\frac{\partial T}{\partial x_i}\right) = \frac{\partial}{\partial x_i}\ .\left(k\frac{\partial T}{\partial x_i}\right) + H\ , \tag{5.6}$$

where ϱ is density, C_p is heat capacity, t is time, v_i and x_i are the velocity and spatial components in the i direction, k is thermal conductivity and H is heat production per unit volume. Density temperature dependence is given by

$$\rho\ (T) = \rho_0\big(1 - \alpha(T - T_0)\big), \tag{5.7}$$

where the thermal expansion coefficient α is $3.1\text{x}10^{-5}\,°\text{C}^{-1}$ for lithosphere and sublithospheric mantle.

5.2 Numerical set-up used in this thesis

The model domain is set to represent the lithosphere and the sublithospheric mantle and its dimensions are L_x = 1200 km and L_z = 600 km (Figure 6.1). The lithosphere comprises a 35 km thick continental crust and a 90 km thick mantle lithosphere. The continental crust layering is first represented by a 25 km thick upper crust and a 10 km thick lower crust. The upper 4 km of the upper crust are represented by pre-deformation sediments, with a 3 km thick frictional upper layer overlying a 1 km thick weak layer portraying a *décollement* horizon. This setup allows for the interaction of both thin- and thick-skinned tectonic regimes.

A strain-weakened seed of 6 x 6 km is positioned at the top of the lower crust layer in order to ensure that deformation localizes in the center of the model rather than at its sides, where velocity boundary conditions are set. Once the initial conditions are symmetrical, subduction initiates with a random polarity.

The experiment Eulerian grid has 2400 elements in the horizontal and 300 elements in the vertical dimension, respectively. In the vertical direction, the elements are distributed as 125 for the upper crust, 125 for the lower crust and mantle lithosphere and 50 elements for the sublithospheric mantle. In what follows, vertical resolution is 200 m for the upper crust, 800 m for the lower crust and mantle lithosphere and 9.5 km for the sublithospheric mantle. The horizontal resolution is 500 m for the entire model. Each element of the Eulerian grid has nine Lagrangian material nodes, which allows for tracking of the material throughout space and time.

Velocity boundary conditions applied to each side of the lithosphere are V/2 = 0.5 cm yr^{-1}, and a velocity field in the opposite direction is applied in the rest of the vertical boundary in order to balance the inflow of lithospheric material. The upper horizontal boundary is free and allows for topography, whereas the basal horizontal boundary is set for free slip conditions.

Thermally, the lateral boundaries do not allow for heat flow, whereas the upper and top boundaries are set for constant temperature values. The initial temperature field varies parabolically with depth from the surface (T_o = 0 ˚C) to the Moho (T_m = 550 ˚C) as a result of radioactive heat production in the crust (h_c = 0.9 μWm^{-3}). Below the Moho, temperature follows a linear gradient until the base of the lithosphere (T = 1330 ˚C) and basal heat flux of q_{ml} = 19.5 mWm^{-2}. In the sublithospheric mantle, the temperature gradient is adiabatic until

the base of the model, initially set as T = 1520 ˚C. Higher thermal conductivity on the sublithospheric mantle triggers higher heat flux (q_{sl} = 48.6 mWm^{-2}), which allows for a convective behavior unlike the conductive lithosphere.

Chapter 6 – The Wilson Cycle and the effects of tectonic structural inheritance on rifted passive margin formation

Claudio A. Salazar-Mora[1,2*], Ritske S. Huismans[1], Haakon Fossen[3], Marcos Egydio-Silva[2]

[1]Department of Earth Sciences, University of Bergen, Norway. Allégaten 41, 5007. Bergen, Norway.

[2]Geosciences Institute, São Paulo University (USP), Brazil. Rua do Lago, 562, CEP 05508-080. São Paulo, Brazil.

[3]University Museum of Bergen – The Natural History Collections, University of Bergen, PO Box 7800, 5020 Bergen, Norway.

[*]Corresponding author at: Geosciences Institute, São Paulo University. E-mail: claudio.asm@hotmail.com

Abstract

The parallelism between older collision belts and younger rift systems is widely known and particularly well portrayed along the Atlantic Ocean. The relationship between lithospheric inherited shear zones and nucleation of rift systems has been focus of many studies. Nevertheless, it is still poorly understood how inherited tectonic and new-formed shear zones (i.e. during extension) affect the final architecture of rifted conjugate passive margins. Here we present lithospheric thermo-mechanical numerical models that self-consistently create extensional and contractional tectonic inheritance, allowing us to investigate of their influence during the development of conjugate rifted margins. The amount of prior extension and contraction is systematically varied. Our results show that: 1) reactivation first occurs along the former lithospheric suture zone; 2) upper crustal thick-skinned basement thrusts are partially or fully reactivated depending on the amount of prior contraction and size of the orogen; 3) with a small amount of contraction, thick-skinned thrusts are efficiently reactivated in extension and provide the template for rifted margin formation; 4) with larger amounts of

pre-extensional contraction, thick-skinned thrusts distal to the lithospheric suture zone do not reactivate in extension; 5) reactivation of prior contractional shear zones dominates during the early stages of rifting, whereas during the final stage of rift-passive margin formation new-formed extensional shear zones dominate. We compare our models to present-day rifted conjugate margins in the North and Central South Atlantic.

Keywords: Numerical modeling; Structural inheritance; Rifting; Rifted margins; Wilson Cycle; Geodynamics

6.1 Introduction

During the Wilson Cycle, the continental lithosphere is repeatedly weakened and reworked at its margins (Wilson, 1966) during subduction, orogeny and rifting, while continental nuclei remain undeformed. Lithospheric pre-existing shear zones have been suggested to be a key factor controlling rift development, as illustrated by the parallelism between older orogenic belts and younger rift systems during the breakup of Western Gondwana and the development of the North, Central and South Atlantic rifted margins (Piquè & Laville, 1996; Vauchez *et al*., 1997; Buiter & Torsvik, 2014). Cratonic lithosphere is strong and tectonically stable owing to dehydration, a prevalence of refractory crustal composition (Peslier *et al*., 2010) and low heat flux conditions (Sleep, 2003). On the other hand younger continental lithosphere is generally weaker resulting from a more fertile composition, including hydrated minerals, and a higher concentration of heat-producing elements and higher background mantle-related heat flow. This may lead to preferential localization of deformation during regional tectonic events in weaker non-cratonic lithosphere. In addition to these nominal contrasts in strength, strain localization along faults and shear zones may lead to significant structural weaknesses.

Structural inheritance relates to mechanical weaknesses in the continental lithosphere that result from previous tectonic events (Thomas, 2006). Tommasi and Vauchez (2001, 2015) suggest that crystallographic lattice preferred orientation of olivine crystals in the lithospheric mantle provided pre-existing weakness zones that played a significant role during Mesozoic South Atlantic rifted margin formation. Similarly, correlation of magnetometric and gravimetric mapping of onshore old Pan African shear zones (Ferreira *et al*., 2009) and offshore 3-d seismic interpretations (Fetter, 2009) along the Brazilian rifted margin suggest a

first-order control of older orogenic structure on the development of the rifted passive margin. However, while the concept of the Wilson Cycle is widely accepted, it is not clear how both nominal variations in continental lithospheric rheology and structural inheritance control variations in the structural style of rifts and passive margins.

Previous numerical modeling studies have investigated the role of nominal variations in continental crust rheology, thermal state and strain-rate on the style of rifted margin formation (e.g. Brune et al., 2014; Huismans and Beaumont, 2011, 2014; Naliboff and Buiter, 2015). Here we present a study of the role of structural inheritance created during extensional and contractional events prior to the development of rifted passive margins by means of high-resolution, plane-strain, thermo-mechanical numerical models. We focus in particular on the role of varying amounts of pre-orogenic extension and orogenic shortening.

6.2 Numerical modeling method

For the numerical simulations we use a modified highly efficient version of the Arbitrary Lagrangian-Eulerian finite-element code FANTOM (Thieulot, 2011; Erdős *et al.*, 2014) to model thermal-mechanically coupled, plane-strain, viscous-plastic creeping flows. We investigate the behavior of a layered lithosphere and sub-lithospheric mantle with frictional-plastic and thermally activated power law viscous rheologies in both contractional and extensional regimes.

When stress is below the frictional-plastic yield deformation is viscous and described by temperature-dependent non-linear power law viscous rheologies based on laboratory measurements. The effective viscosity in the power-law rheology is of the following form:

$$\eta_{eff} = f.A^{-1/n}.\dot{\varepsilon}^{\frac{1-n}{2n}}.\exp\left(\frac{Q+V.p}{nRT}\right) \quad , \quad (1)$$

where f is a scaling factor that allows modifying viscous strength without recourse to additional flow laws (Huismans & Beaumont, 2014), A is the pre-exponential scaling factor, n is the power law exponent, $\dot{\varepsilon}$ is the second invariant of the deviatoric strain rate tensor $\left(\frac{1}{2}\ \dot{\varepsilon}'_{ij}\dot{\varepsilon}'_{ij}\right)$, Q is activation energy, V is activation volume, p is pressure, T is temperature, and R is the universal gas constant. A, n, Q and V are derived from laboratorial measurements of "wet" and "dry" olivine (Karato & Wu, 1993) and "wet" quartz (Gleason & Tullis, 1995) and are given in Table 6.1.

Table 6.1 – Input parameters for all models.

Units	*Décollement* layer	Upper Crust + Pre-collision Sediment	Lower Crust	Mantle Lithosphere	Sub-lithospheric Mantle
			Mechanical Parameters		
Thickness (km)	1	21 + 3	10	90	475
Reference density (kg m^{-3}) ρ_0	2300	2800	2800	3300	3300
Internal friction angle $\phi_{eff}(\varepsilon)$	1°	15° - 2°	15° - 2°	15° - 2°	15° - 2°
Strain range of softening	0.05-1.05	0.05-1.05	0.05-1.05	0.05-1.05	0.05-1.05
Cohesion (Pa), C	2.10^6	2.10^7 - 4.10^6	2.10^7 - 4.10^6	2.10^7 - 4.10^6	2.10^7 - 4.10^6
Flow law	-	Wet Quartz	Wet Quartz	Dry Olivine	Wet Olivine
Scaling factor (f)	1	1	100	1	1
A (Pa^{-n} s^{-1})	$8.574\ 10^{-28}$	$8.574\ 10^{-28}$	$8.574\ 10^{-36}$	$2.4168\ 10^{-15}$	$1.393\ 10^{-14}$
Activation Energy (J mol^{-1}) Q	$222\ 10^3$	$222\ 10^3$	$222\ 10^3$	$540\ 10^3$	$429\ 10^3$
Power law exponent (n)	4	4	4	3.5	3
Activation Volume (m^3 mol^{-1}) V	0	0	0	$25\ 10^{-6}$	$15\ 10^{-6}$
Gas constant (J mol^{-1} $°C^{-1}$) R	8.1344	8.1344	8.1344	8.1344	8.1344
			Thermal Parameters		
Heat capacity (m^2 K^{-1} s^{-2}) C_p	803	803	803	682	682
Thermal cond. (W m^{-1} K^{-1}) k	2.25	2.25	2.25	2.25	48.6
Thermal expansion (K^{-1}) α	$3.1\ 10^{-5}$	$3.1\ 10^{-5}$	$3.1\ 10^{-5}$	$3.1\ 10^5$	$3.1\ 10^5$
Heat productivity (W m^{-3}) A	$0.9\ 10^{-6}$	$0.9\ 10^{-6}$	$0.9\ 10^{-6}$	-	-
Heat flux (mW.m^2)	-	-	-	19.5	19.5
Temperature surface (ºC)	-	0	-	-	-
Temperature Moho (ºC)	-	-	550	-	-
Temperature base lithosphere (ºC)	-	-	-	1330	-
Temperature base of model (ºC)	-	-	-	-	1520

When stress exceeds the plastic yield criterion, frictional-plastic deformation is modeled by a pressure-dependent Drucker-Prager criterion, which in plane-strain is equivalent to a Coulomb criterion :

$$\sigma_y = (J_2')^{\frac{1}{2}} = C.\cos\phi_{eff} + p.\sin\phi_{eff}\ , \quad (2)$$

where J_2' is the second invariant of the deviatoric stress $\left(\frac{1}{2}\ \dot{\sigma}_{ij}'\sigma_{ij}'\right)$, ϕ_{eff} is the effective internal angle of friction given as p . sin(ϕ_{eff}) = (p - p_f) . sin(ϕ) for pore-fluid pressure p_f and

cohesion C. This yield criterion approximates frictional sliding in rocks and the effect of hydrostatic pore-fluid pressures. Strain-dependent rheologies allow for the formation of localized frictional-plastic shear zones during lithospheric deformation (Huismans & Beaumont, 2003). In our models strain-softening effects are introduced by a linear decrease of the effective internal angle of friction ϕ_{eff} from 15° to 2°, with a simultaneous decrease of cohesion from 20 MPa to 4 MPa for accumulated strain values between 0.05 and 1.05 (Figure 1). $\phi_{eff}(\varepsilon) \sim 15°$ corresponds to the effective ϕ when the pore fluid pressure is approximately hydrostatic.

The mechanical and thermal systems are coupled through the temperature dependence of viscosity and density and are solved sequentially during each model time step. In what follows, the heat transport equation is solved in two dimensions:

$$\rho \,.\, C_p \,.\, \left(\frac{\partial T}{\partial t} + v_i \frac{\partial T}{\partial x_i}\right) = \frac{\partial}{\partial x_i} \,.\, \left(k \frac{\partial T}{\partial x_i}\right) + H \quad , (3)$$

where ϱ is density, C_p is heat capacity, t is time, v_i and x_i are the velocity and spatial components in the i direction, k is thermal conductivity and H is heat production per unit volume. Density depends on temperature $\rho\,(T) = \rho_0\big(1 - \alpha(T - T_0)\big)$, where the thermal expansion coefficient α is $3.1\text{x}10^{-5}\,°\text{C}^{-1}$ for the lithosphere and sub-lithospheric mantle.

6.3 Model design

The model represents the lithosphere and the sub-lithospheric mantle in a 1200 km wide and 600 km deep domain (Figure 6.1). The lithosphere comprises a 35 km thick continental crust and a 90 km thick mantle lithosphere. Continental crustal layering is given by a 25 km thick upper crust and a 10 km thick lower crust. The upper 4 km of the upper crust are formed by pre-deformation sediments, with a 3 km thick frictional upper layer overlying a 1 km thick weak layer portraying a *décollement* horizon. This setup allows for the interaction of both thin- and thick-skinned tectonic deformation. A strain-weakened seed of 6 x 6 km is positioned at the top of the lower crust to seed initial localization. Once the initial conditions are symmetrical, subduction initiates with a random polarity.

The Eulerian grid has 2400 elements in the horizontal and 300 elements in the vertical dimension, respectively. In the vertical direction, the elements are distributed as 125 for the upper crust, 125 for the lower crust and mantle lithosphere and 50 elements for the sub-lithospheric mantle resulting in a vertical resolution of 200 m for the upper crust, 800 m for

the lower crust and mantle lithosphere and 9.5 km for the sub-lithospheric mantle. The horizontal resolution is 500 m for the entire model. Velocity boundary conditions applied to the vertical sides of the lithosphere are V/2 = 0.5 cm yr^{-1}, with an influx velocity in the sub-lithospheric mantle in order to keep the volume in the model domain constant.

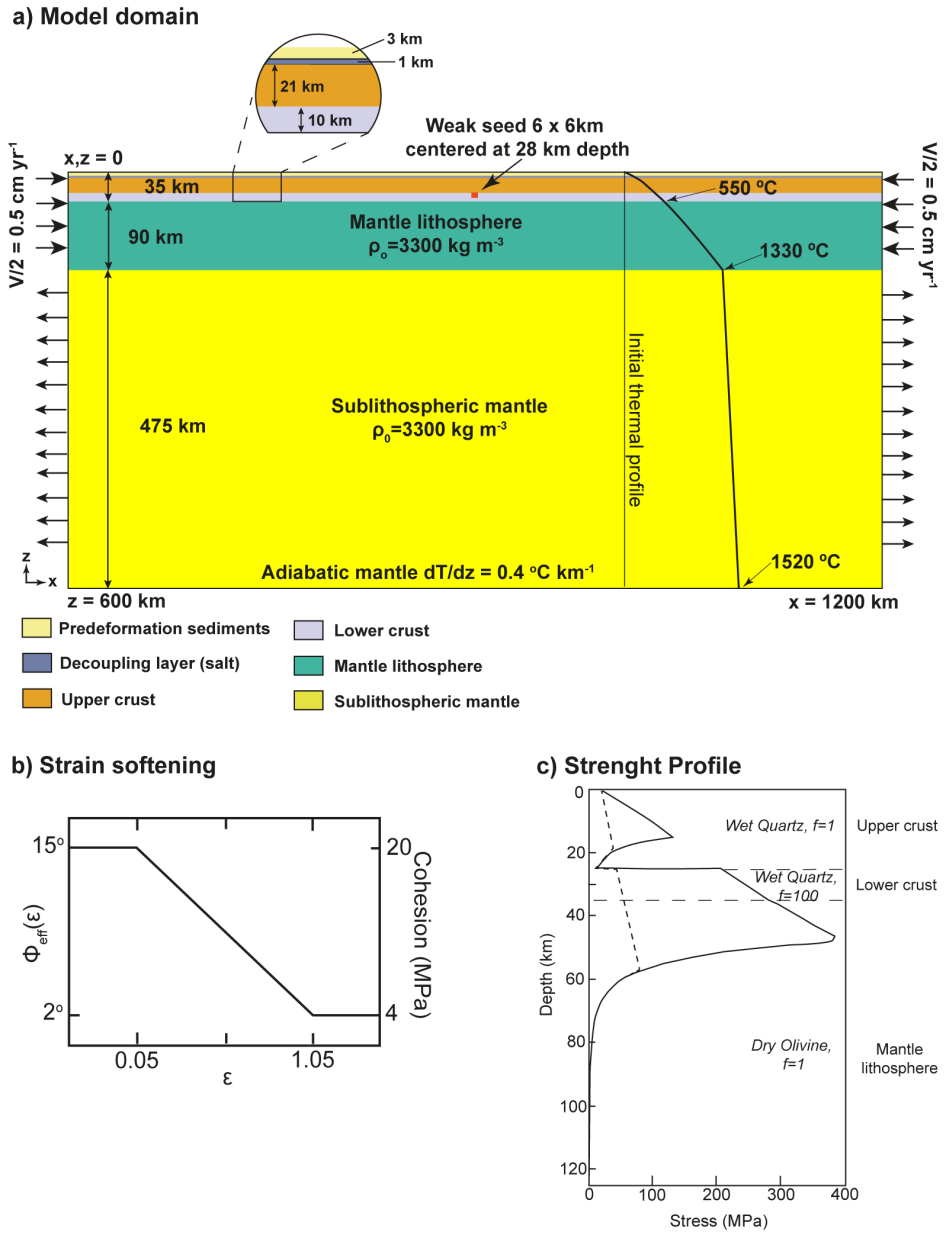

Figure 6.1 – Model design showing the initial layering of the crust, lithosphere and sub-lithospheric mantle. Also portrayed are the initial thermal profile and velocity boundary conditions. All parameters used in the simulations are given in Table 1. The lower part of the figure shows strain softening and the initial stress profile (dashed line represents fully strain-weakened lithosphere).

The upper horizontal boundary is free and allows for topography, whereas the basal horizontal boundary is has a free slip condition and zero vertical flow.

The thermal model setup includes lateral boundaries with zero heat flow, and constant temperature at upper and lower boundaries. The initial temperature field varies parabolically with depth from the surface (T_o = 0 ˚C) to the Moho (T_m = 550 ˚C) as a result of radioactive heat production in the crust (h_c = 0.9 μWm^{-3}). Below the Moho, temperature follows a linear gradient until the base of the lithosphere (T = 1330 ˚C) and basal heat flux of q_{ml} = 19.5 mWm^{-2}. In the sub-lithospheric mantle, the temperature gradient is adiabatic until the base of the model, set as T = 1520 ˚C. Thermal conductivity increases linearly to 48.6 W m^{-1} k^{-1} at 1330 °C in the sub-lithospheric mantle corresponding to scaling the thermal conductivity by the Nusselt number of upper mantle convection. The enhanced conductivity maintains a constant heat flux to the base of the lithosphere and an adiabatic thermal gradient in the sub-lithospheric mantle (e.g. Pysklywec and Beaumont, 2004).

6.4 Model results

We explore first the effect of orogenic structural inheritance in model set 1 (M1-M2, Table 6.2) characterized by two-phases, with phase 1 lithosphere shortening followed by phase 2 lithosphere extension. To allow for a broader range of orogenic shear zones model set 2 (M3-M6, Table 6.2) exhibits three-phases in which the lithosphere shortening is preceded by extension: with phase 1 lithosphere extension, phase 2 shortening and final phase 3 extension models differ by varying amount of prior shortening and extension its effect on rifted margin formation.

Table 6.2 – List of models and varying parameters.

Model		**Amount of Extension**	**Amount of Contraction**	**Amount of Extension**	**Figure**
Two-phase models	**M1**	-	150 km	250 km	Figure 6.2
	M2	-	300 km	400 km	Figure 6.3
Three-phase models	**M3**	50 km	150 km	250 km	Figure 6.4
	M4	50 km	300 km	350 km	Figure 6.5
	MS1	100 km	150 km	250 km	S1
	M5	100 km	300 km	250 km	Figure 6.6

3.1 Contraction-extension models

3.1.1 Model 1: 150 km contraction followed by extension

Model 1 is characterized by 150 km of contraction leading to a small and narrow crustal scale orogen with three deeply rooted thick-skinned thrusts covered by thin-skinned thrust sheets on the pro-wedge (Figure 6.2a). Elevation is up to 5 km whereas the retro-foreland basin is 500 m deep and the pro-foreland basin is 1.5 km deep. During convergence, the first contractional conjugate frictional-plastic shear zones bound a primary pop-up structure (shear zones 1 and 1'), rooted in the weak middle crust (Figure 6.2a). The mantle lithosphere and strong lower crust exhibit asymmetric subduction and subsequent thick-skinned crustal basement thrust sheets 2-4 form in sequence on the pro-wedge towards the foreland. Towards distal parts of the orogen, contraction is accommodated by thin-skinned tectonics. The leading edge of the subducting plate develops a highly ductile wedge of upper crust that is decoupled from the lower crust, which in turn subducts coupled to the mantle lithosphere to 100 km depth. Retro-wedge deformation is limited to an incipient shear zone and large-scale upwarping above pro-wedge subducted mid-lower crust and mantle lithosphere.

In Phase 2 velocity boundary conditions are reversed. At t = 30 Ma and after 150 km of extension, the contractional shear zones 1 to 4 are efficiently re-used completely reversing the initial contraction (Figure 6.2b) forming a set of synthetic normal faults, while extension in the mantle lithosphere is localized on the orogenic subduction shear zone. New extensional shear zones 5-6, antithetic with respect to shear zones 1-4, allow exhumation of previously subducted upper continental crust. With continued extension and thinning of the lithospheric mantle, the pro-wedge crust thins and its lower crust ruptures (Figure 6.2b). Extensional reactivation on the retro-wedge is limited to shear zone 1. With continued extension, deformation in the mantle lithosphere shifts from the orogenic suture zone to a narrow viscous necking zone with upwelling sub-lithospheric mantle (Figure 6.2c). New crustal extensional shear zones 7-8 form during final lithosphere break-up attenuating the retro-wedge margin (Figure 6.2c)

The final passive margin architecture is asymmetric with broad crustal extension on the pro-wedge and narrow extension on the retro-wedge side. The distal portion of the wide margin accommodates extension by reactivating contractional shear zones 3 and 4 (Figure 6.2c). From shear 2 ocean wards the necking zone accommodates crustal thinning reusing

contractional shear 1 and forming new counter regional shear zones 5 and 6. Within the necking zone, the crust is attenuated from ~30 km to 5 km thickness with the lower crust being removed towards the most attenuated portion of the margin. The very narrow conjugate 'retro-wedge' margin is thinned across 50 km through new-formed shear zones 7 and 8, achieving 5 km of thickness. Also this margin has its lower crust removed, with minor exhumation of mantle lithosphere to the surface and the orogenic suture rooting below the narrow margin.

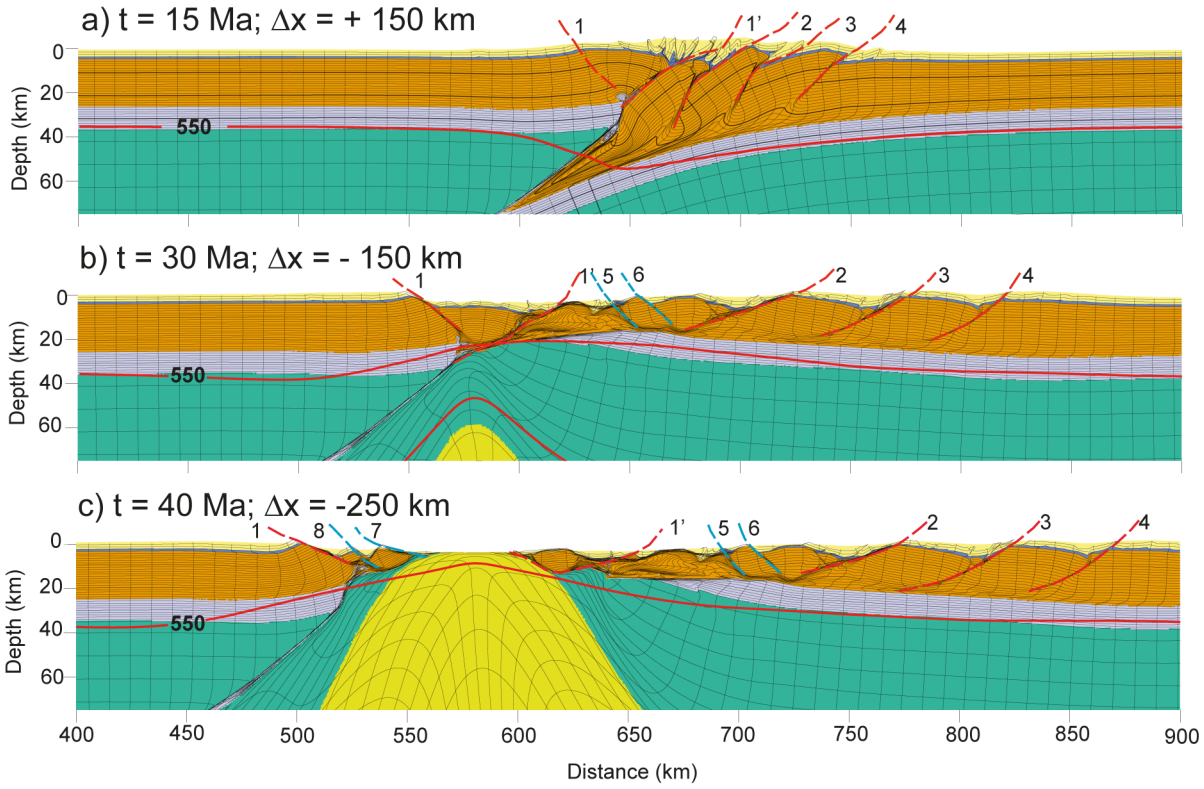

Figure 6.2 – M1. (a) Full orogenic structure after 150 km of contraction, (b) extension of 150 km and (c) final passive margin configuration after 250 km of extension. Legend for colors is the same as for Figure 1. Dashed lines represent frictional-plastic shear zones, where red ones are contractional and blue ones are new-formed extensional shear zones. Numbering represents the chronologic development of shear zones. When shear zones are assigned the same number, they represent simultaneous faulting.

3.1.2 Model 2: 300 km of contraction followed by extension

Model 2 has 300 km of contraction leading to a large asymmetric crustal scale orogen with eight deeply rooted thick-skinned thrusts covered by thin-skinned thrust sheets on the pro-wedge covered by thin-skinned deformed pre-collisional sediments on both pro- and retro-wedge (Figure 6.3a). On the pro-wedge, contractional shear zones 1 to 9 form in

sequence. On the retro-wedge, contractional shear 1 is more developed in comparison with Model M1, with one thin-skinned thrust sheet towards the foreland. The lower crust subducts along with the mantle lithosphere to 150 km depth as in model M1.

Phase 2 rifted passive margin formation leads, similarly to model M1, to narrow localization along the orogenic mantle lithospheric shear zone and broad distributed extensional deformation within the crust, with a broad domain of crustal extension on the former pro-wedge side and a very narrow extensional domain on the retro-wedge margin (Figure 6.3b and c). One of the main differences with respect to model M1 is that not all pro-wedge orogenic shear zones are reactivated. Shear zones 1 to 4 proximal to the necking zone are fully reactivated, while distant orogenic shear zones 5 to 9 are not, resulting in preservation of the orogenic structure in the proximal domain of the rifted margin system (Figure 6.3b and c). Previously subducted upper crust is exhumed to shallow crustal levels through extensional reactivation of shear zones 2-4 and new-formed extensional shear 10. The conjugate retro-wedge margin accommodated extension with the reactivation of the previously contractional shear zones 1', without formation of new extensional shear zones resulting in a very narrow necking zone (Figure 6.3c). Lower crust is removed on both conjugate margins. The orogenic suture zone roots similarly to model M1 under the retro-wedge margin, leaving tracts of lower crust in the mantle lithosphere.

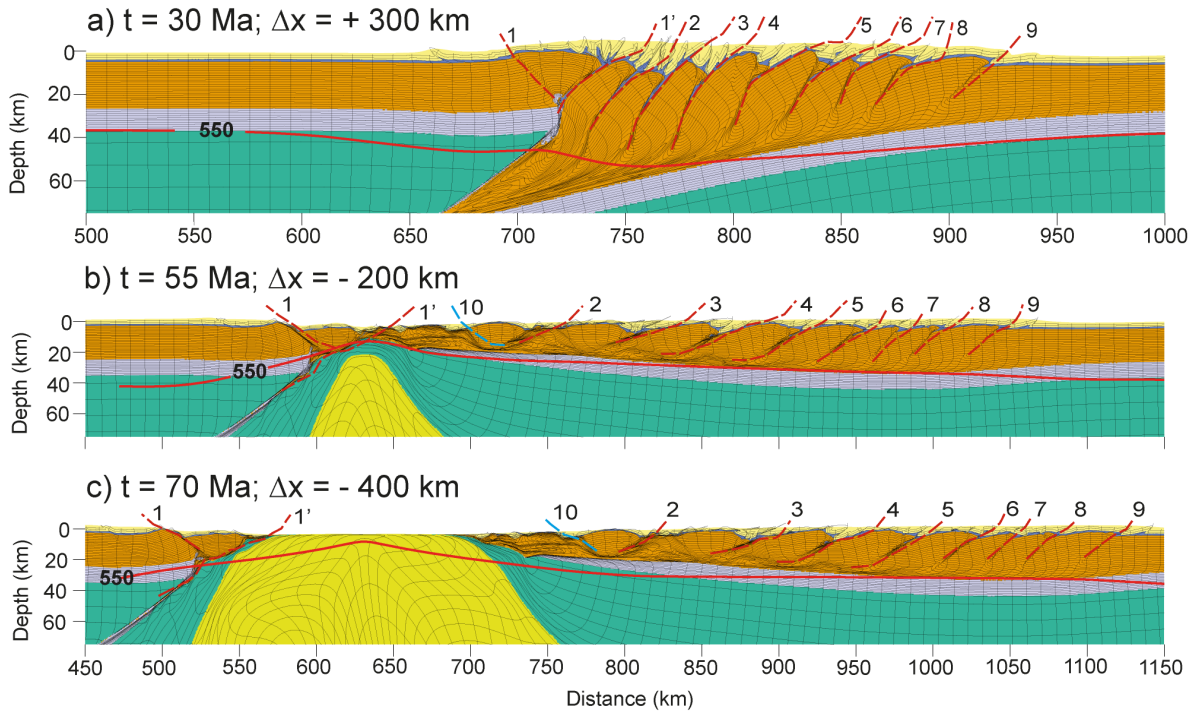

Figure 6.3 – M2. (a) Full orogenic structure after 300 km of contraction. (b) and (c) show extension of 200 km and 400 km respectively. Note that structures 6-9 are not reactivated. Color coding of shear zones is the same as Figure 2.

3.2 Extension-contraction-extension Models

3.2.1 Model 3: 50 km extension, 150 km contraction, followed by extension

Model 3 is characterized by a first phase of 50 km of extension, followed by 150 km of contraction and subsequent extension. Initial moderate rifting leads to a small symmetric continental rift basin with two main conjugate extensional shear zones rooting in the strong lower crust and upper mantle lithosphere (Figure 6.4a). The lower crust is completely removed from the base of the graben. The central domain of the graben exhibits a second set of smaller scale conjugate normal shear zones (Figure 6.4a). During contraction Phase 2, conjugate shear zones 2 first reactivate and invert followed by shear zones 1, developing a doubly-vergent pop-up structure transported onto the retro-wedge (Figure 6.4b). Further shortening leads to outward propagating thick-skinned basement thrusts sheets on the pro-wedge and subduction of the continental mantle lithosphere at depth. At the surface thin-skinned thrusting affects pre-collision sediments on both pro- and retro-wedge (Figure 6.4b). The resulting doubly vergent orogen has two main thick-skinned thrust sheets bounded by new contractional shear zones 3 to 6. The retro-wedge is much more structured in comparison with models M1 and M2 with pure contraction and controlled by reactivation of previously developed extensional shear zones. The subducting plate also develops a highly ductile wedge of upper continental crust that subducts along with the lower crust.

In Phase 3 the boundary conditions are reversed to extension. The mantle lithospheric suture zone initially localizes strain quite efficiently. Within the crust strain localizes in the central domain of the orogen, whereas the pro-wedge orogenic shear zones are efficiently reused during extension (Figure 6.4c). Extensional shear 7 to 9 develop as a result of exhumation of previously deeply buried continental crust, and represent the transition from extension to thinning. Thermal weakening and upwelling of the sub-lithospheric mantle causes the orogenic suture to be abandoned, and resulting in extensional reactivation of retro-wedge shear zones 1 and 2 (Figure 6.4d). The final rifted passive margin configuration (Figure 6.4d) is asymmetric, with a wide ‘pro-wedge’ margin and a narrow ‘retro-wedge’ margin. The structure of the proximal wide margin is controlled by orogenic inherited shear zones 4 to 6. The necking zone, ocean wards from shear 4, accommodates extension on reactivating long-lived orogenic and prior extension shear zones and on new-formed extensional shear zones 7 to 9 in the distal margin (Figure 6.4d). The conjugate narrow rifted margin resulting from extension of the former orogenic retro-wedge reuses inherited

extensional shear zones 2 from phase 1 (Figure 6.4d) and exhumes lower crust to very shallow crustal levels. Both sides of the final rifted conjugate passive margin exhibit minor exhumation of mantle lithosphere in the ocean continent transition zone.

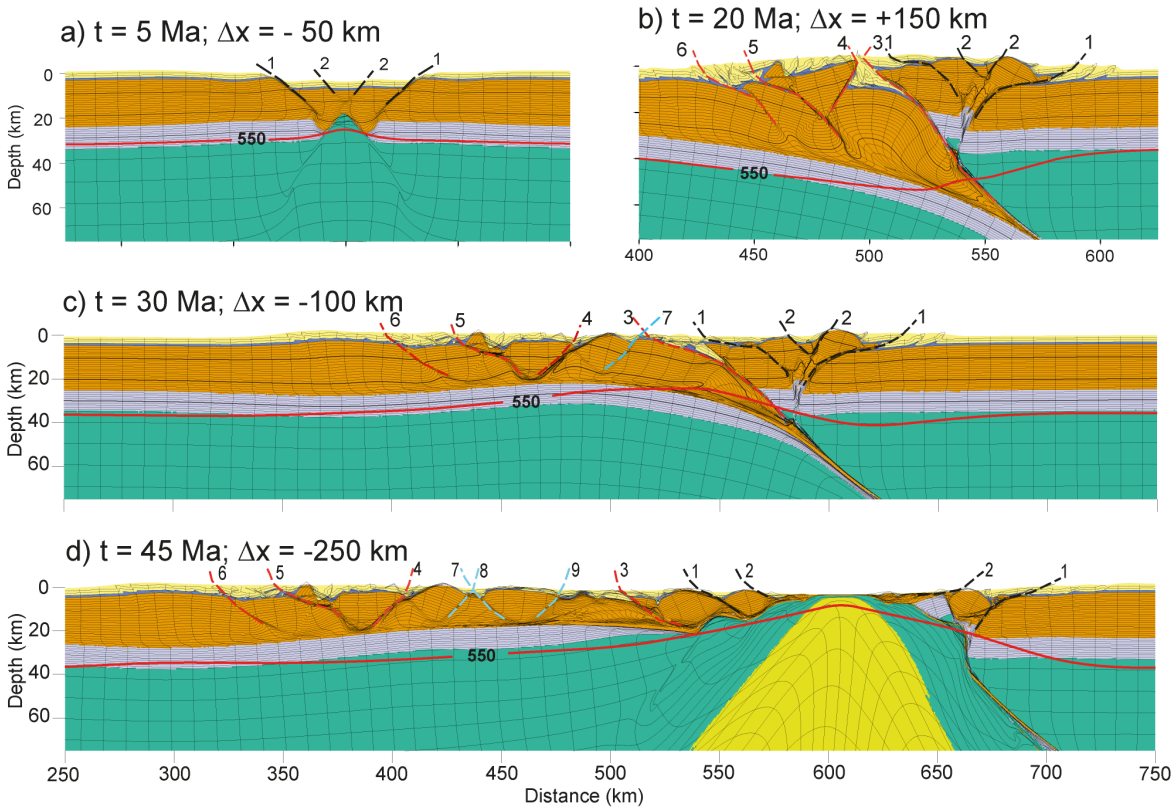

Figure 6.4 – M3. (a) 50 km of pre-orogenic extension showing simultaneous faulting during the development of pre-orogenic extensional shear zones (black dashed lines). (b) Full orogenic structure after inversion of 50 km of extension and contraction of 150 km. (c) Continued extension (100 km) and development of new-formed extensional structure 7 on the pro-wedge. (d) Final passive margin configuration and crustal breakup following inherited extensional shear zones on the retro-wedge.

3.2.2 Model 4: 50 km extension, 300 km contraction, followed by extension

Model 4 is characterized by a first phase of 50 km of extension, followed by 300 km of contraction and subsequent extension. Phase 1 extension and early Phase 2 contraction are the same as in Model 3. The orogenic configuration at t = 35 Ma and 300 km of contraction exhibits 6 thick-skinned thrusts (bounded by shear zones 3 to 10) covered by thin-skinned deformed pre-collisional sediments on the pro-wedge (Figure 6.5a). Below the pro-wedge, ductile upper continental crust is subducted to 90 km depth. Inverted extensional shear zones 1 and 2 structure the retro-wedge.

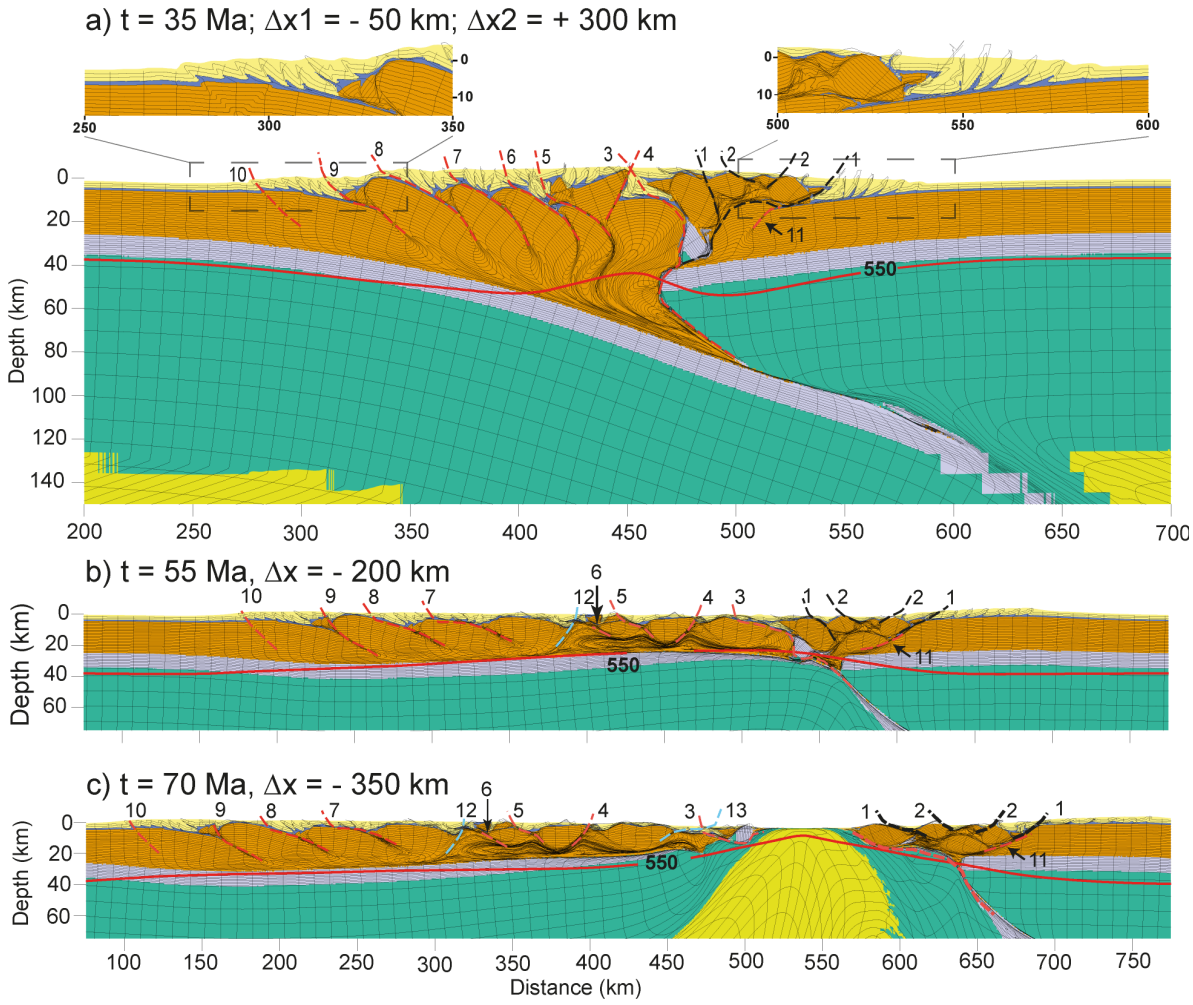

Figure 6.5 – M4. (A) Full orogenic structure after inversion of 50 km of pre-orogenic extension plus 300 km of contraction. Inlets show thin-skin deformation in the forelands. (B) Extension of 200 km in Phase 3. Full reactivation of all contractional shear zones on the pro-wedge and development new-formed extensional structure. (c) Final passive margin configuration. Note that crustal breakup did not follow neither inherited nor new-formed shear zones. Instead, it followed the contact between a tract of lower crust with the upper crust.

During Phase 3 at 55 Ma and 200 km of extension, shear zones 1 to 6 and 11 are fully reactivated accommodating extension, whereas shear zones 7 to 10 do not reactivate and preserve part of the orogenic structure (Figure 6.5b). Extensional reactivation of pro-wedge shear zones 3 to 6 exhumes upper continental crust previously subducted to large depths. Retro-wedge shear zones 1, 2 and 11 accommodated extension in the retro-wedge, with new shear 11 transporting Phase 1 shear zones 1 and 2 to the rifted margin. Break-up occurs after about 70 Ma and 350 km of extension. The orogenic suture zone with remnants of lower continental crust roots below the extended retro-wedge margin (Figure 6.5c). The resulting conjugate rifted passive margin (Figure 6.5c) is highly asymmetric. The former pro-wedge develops into a very wide and complexly structured passive margin, ~400 km long. Its proximal domain is controlled by inherited contractional shear zones, which were not

efficiently reactivated, preserving orogenic thick- and thin-skinned structures. The intermediate and distal margin show interplay between inherited contractional and extensional shear zones, resulting in extension and thinning of the continental crust from ~40 km to < 5 km in the distal margin. A small block of lower continental crust originating from the orogenic retro-wedge exhumes in the ocean-continent transition zone. The very narrow conjugate 'retro-wedge' passive margin is mostly extended by reactivation of inherited extensional and contractional shear zones.

3.2.3 Model 5: 100 km extension, 300 km contraction followed by extension

Model 5 and supplementary Model 1S test the effect of larger Phase 1 extension leading to lithospheric break-up on subsequent Phase 2 orogenic structure and Phase 3 rifted margin formation. At t = 10 Ma and 100 km of extension the crust has fully ruptured along conjugate extensional shear zones 1 and 2 leading to exhumation of mantle lithosphere to the surface (Figure 6.6a). Phase 2 orogenic structure after 300 km shortening is similar to Model M4 with 5 basement thrust sheets on the pro-wedge and inversion of the crustal extensional shear zones in a pop-up structure on the retro-wedge margin. The main difference with respect to Model 4 is the incorporation of a large fragment of mantle lithosphere in the inversion structure in the retro-wedge at a very shallow crustal level (Figure 6.6b).

During Phase 3 extension (Figure 6.6b-c), extensional reactivation occurs on shear zones proximal to the mantle lithospheric necking zone, similar to the previous models. As the pro-wedge is educted, extension is accommodated first by reactivation of contractional shear zones 4 to 10 in the proximal domain of the developing wide margin (Figure 6.6c). With continued extension, new extensional shear zones 11 to 13 form when the deeply buried basement thrust 5 exhumes to the surface. Strain accumulation migrates to the necking zone of the evolving margin, preserving the orogenic structure (contractional shear zones 4 to 10) and crustal thicknesses in the proximal margin (Figure 6.6b). The final rifted passive margin configuration is, as in previous models, asymmetric with a 400 km wide 'pro-wedge' margin and a 150 km wide 'retro-wedge' margin (Figure 6.6d). Inherited orogenic shear zones control the proximal 'pro-wedge' margin. The necking zone is characterized by crustal thinning from 35 km to less then 5 km over a distance of about 175 km. The narrow 'retro-wedge' margin is thinned from its original thickness to the OCT over 150 km with fragments of mantle lithosphere as shallow as 5 km in the extended crust (Figure 6.6d). Both margins

exhibit a minor area of exhumed mantle lithosphere between the edge of the continental crust and new ‘oceanic’ lithosphere.

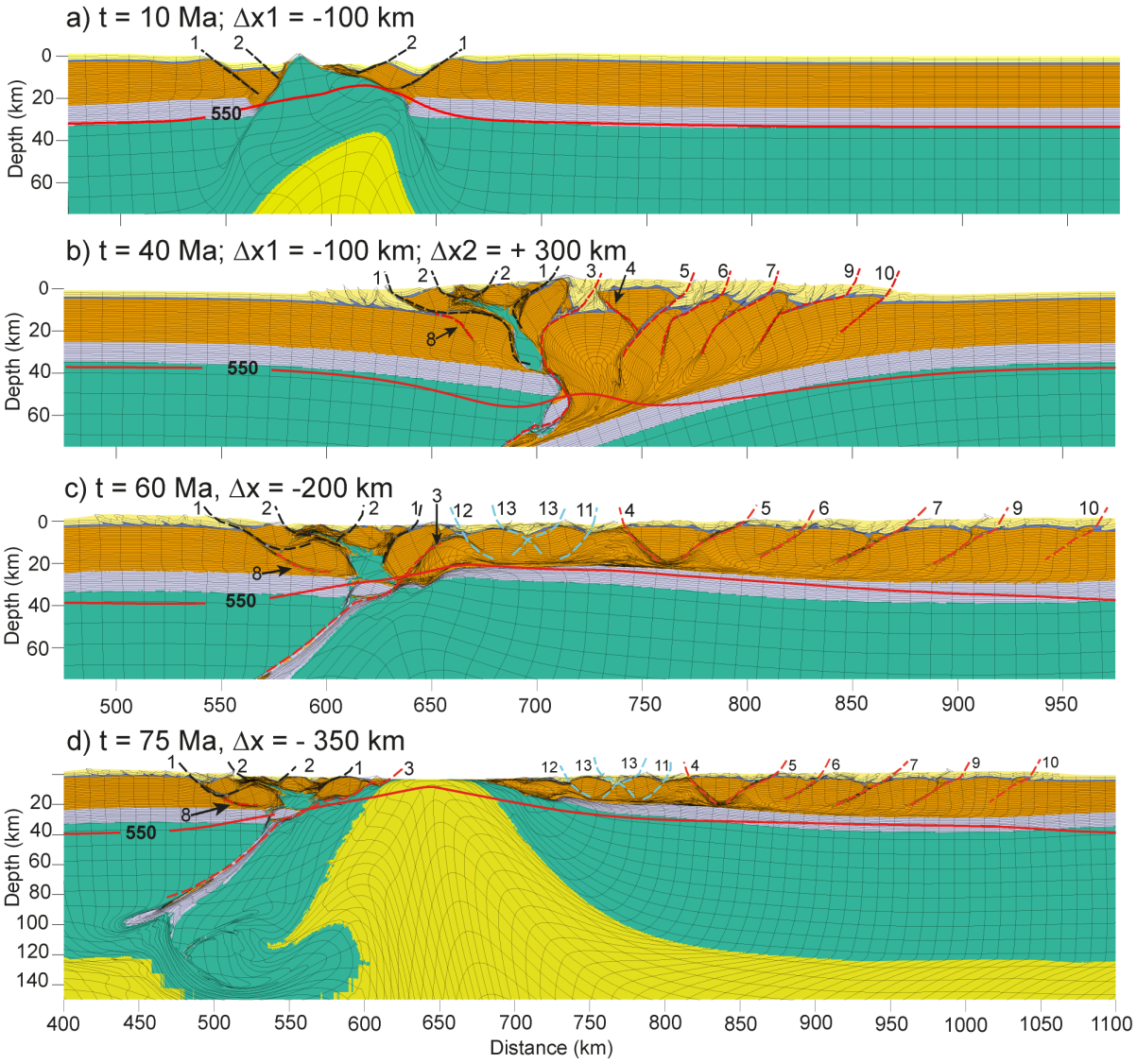

Figure 6.6 – M5. (a) Full orogenic structure after 100 km of pre-orogenic extension and 400 km of contraction. (b) After 200 km of extension, the pro-wedge shows fully and partially reactivated contractional shear zones and development of new-formed extensional shear zones sequentially (11 and 12) and later simultaneously (13). (c) On the retro-wedge, extension occurs with the interplay between inherited extensional (1) and contractional (8) shear zones to form a main border fault of the rifted passive margin. (d) Final crustal breakup occurs along the suture zone.

6.4. Discussion

6.4.1 Role of structural inheritance on reactivation and margin style

All models show similar general characteristics: 1) initial subduction of the continental lithosphere during the contractional phase; 2) decoupling of the upper and lower continental crust with subduction of lower crust with the mantle lithosphere and formation of an upper crustal orogenic wedge; 3) asymmetric orogenic accretion on the pro-wedge in case of pure contractional models; 4) when a precursor extensional Phase 1 is added to the model, inherited extensional structures permit the migration of deformation to the orogenic retro-wedge, resulting in a more symmetric orogenic style in contractional Phase 2; 5) deformation during Phase 3 extension is highly localized in the mantle lithosphere as a result of the weak orogenic suture zone; 6) decoupling in the mid crust and distributed extension of the orogenic wedge by reactivation of weak upper crustal shear zones.

We identified the following primary factors that control the structural style of rifted margin formation in the presence of orogenic structural inheritance: 1) the strength of orogenic shear zones in the upper crust and upper mantle lithosphere, which in the models is controlled by strain weakening. The single weak mantle lithospheric orogenic suture zone exerts a main control on margin structure by highly efficient localization of extensional deformation upon reactivation, multiple weak upper crustal orogenic shear zones control extensional basin and rifted margin structure; 2) the degree of decoupling between upper crust and the strong lower crust-lithospheric mantle layer controls the distance over which the highly localized strain in the weak mantle suture zone can connect with offset weakness zones in the upper crust (e.g. Braun & Beaumont, 1989); 3) the amount of shortening and size of the orogen. More orogenic shortening leads to larger offset between the weak mantle shear zone and offset weaknesses in the upper crust and reduced potential for reactivation of crustal orogenic shear zones in a position distal to the suture zone; 4) pre-orogenic extensional inheritance provides a primary control on orogenic structure by reducing orogenic asymmetry and promoting retro-wedge shortening. As a result the distribution of orogenic structural weakness in the upper crust is more symmetric with respect to the underlying orogenic suture zone, which in turn results in a more symmetric margin structure.

During the development of Phase 3 rifted margin formation, extensional shear zones inherited from Phase 1 and used during contraction Phase 2, reactivated to accommodate stretching on the retro-wedge, whereas contractional inherited shear zones control 'pro-wedge' stretching. All three-phase models form new extensional shear zones on the pro-wedge with continued rifting, and models with a lower amount of contraction during Phase 2 result in more new-formed structures as compared with models with larger amounts of shortening. This is because models with a lower amount of pre-cursor contraction leave larger domains without orogenic structure and a greater propensity for formation strain-weakened shear zones.

6.4.2 Model limitations

Here we have focused on the role of orogenic structural inheritance on the structural style of rifted margin formation. The models presented here are by no means exhaustive and a number of other factors that influence the configuration of rifted passive margins such as variations in rheological, compositional, and thermal structure investigated in earlier studies (e.g. Huismans and Beaumont, 2011, 2014) are not included here. Models shown in this study represent moderately strong lower crust. Other factors that may modify inherited structural weaknesses from early orogenic events such as thermal relaxation, healing of fault zones and erosion are not investigated here and their consequences remain to be tested. Furthermore, our numerical models are 2D, and any 3D effects such as obliquity between the rift extension direction and pre-existing basement structure, which may play an important role during reactivation (Fossen *et al*., 2016) are not included here.

6.4.3 Comparison to natural systems

We next compare model results with observations from two natural systems: a transect through Southern Norway with inherited Caledonian structure and the Mesozoic North Sea rift (Christiansson *et al*., 2000; Fichler *et al*., 2011); and a conjugate margin transect in the South Atlantic with the Brazilian Espírito Santo (Blaich *et al*., 2011; Zalán *et al*., 2011) and West African Kwanza (Hudec & Jackson, 2004; Blaich *et al*., 2011) rifted margins with the onshore inherited Pan-African orogenic structure of Araçuaí (Pedrosa-soares *et al*., 2001;

Wiedemann *et al*., 2002) and Congo (Tack *et al*., 2001) orogens. Three characteristic domains predicted by the forward models can be recognized in both natural systems. Domain A with un-reactivated orogenic structure in a very proximal position with respect to the main locus of extension. An intermediate Domain B with partial reactivation of orogenic structure, and a Domain C at the main locus of extensional basin formation with a combination of reactivated and new-formed extensional structures. In the Norwegian example (Figure 6.7a), domain A comprises un-reactivated inherited contractional structure with basement thrust towards the east on top of the Hardanger Baltica basement, the external frontal zone of the Caledonides in the Oslo area and slightly thickened 40 km thick crust (Fossen *et al*., 2014). Domain B exhibits extensional reactivation of orogenic thick-skinned thrusts and progressive thinning of the crust. Domain C is the extended rift area with demonstrated orogenic inheritance in early rift normal faults and the location of the postulated Caledonide suture zone at depth under the North Sea rift basin (e.g. Fossen et al., 2016). The development of domains A-C supports an important role for Caledonian orogenic inheritance on post-collisional extension and rift basin formation (Fossen, 2010). Domain A represents orogenic structure distal to the locus of extension which appears controlled by the inferred mantle suture zone beneath Domain C, consistent with model predictions. Intermediate Domain B, with the onshore extensional reactivation of the major Hardanger and Lærdal-Gjende basement thrust sheets and can be compared with models M4 and M5 with large amount of precursor contraction (e.g. Figures 6.5 and 6.6).

In the Central South Atlantic (Figure 6.7b), Domain A is represented by the Pan-African Araçuaí orogen in East Brazil and the Congo orogen in West Africa (Tack *et al*., 2001; Wiedemann *et al*., 2002). The Pan-African orogenic structure was reactivated by early post-collisional extension that most likely restored the crust to close to its present day thickness of between 35 and 40 km (Bento dos Santos *et al*., 2015) but remained stable during Mesozoic rifting and passive margin formation. While there is no documented evidence for a role of orogenic inheritance, we postulate based on our model predictions that proximal extension is partially controlled by orogenic structure and indicate Domain B in both margins (Figure 6.7b) with crustal thicknesses of ~25 km. The distal margin is likely controlled by a combination of inherited and new structures and is therefore considered Domain C.

Reconstructions of the late Pre-Cambrian Araçuaí-West Congo orogen (Pedrosa-Soares et al., 2001) suggest a pre-orogenic extensional basin setting with subsequent west-ward subduction with the pro-wedge located on the Brazilian side and the retro-wedge on the African side. We speculate based on sights derived from our three-phase models that Domains

B and C on the African side may have reactivated the extensional structures inverted in contraction during orogeny onto the retro-wedge. On the Brazilian rifted margin Domains B and C may represent a combination of reactivation of contractional inheritance and new-formed structures.

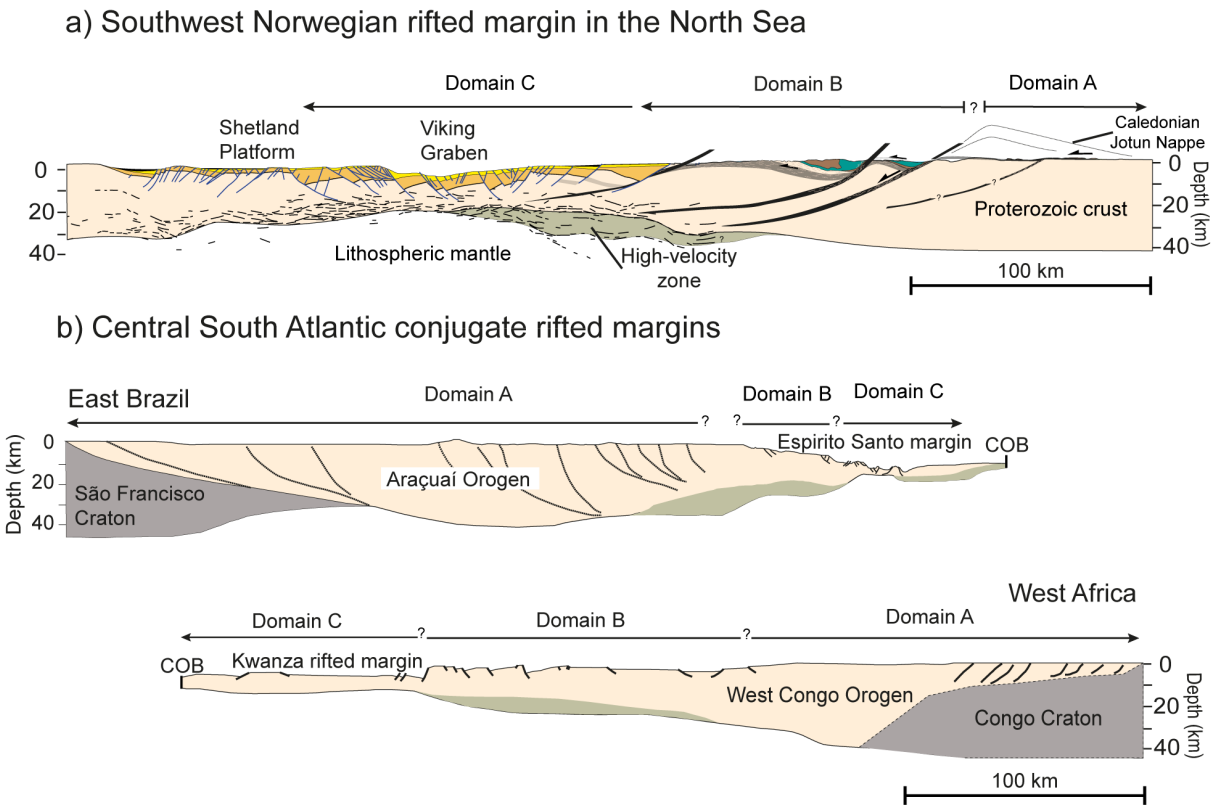

Figure 6.7 – (a) Present-day rifted margin in Southwest Norway, North Sea. This transection was interpreted by Christiansson et al. (2000) and Fichler et al. (2011) through deep seismic reflection and refraction data plus gravity and magnetic data. Note that the high velocity zone at the bottom tip of the faults is interpreted as eclogitized lower continental crust. (b) Present-day conjugate sections of rifted passive margins in the Central South Atlantic. Left shows Brazilian passive margin with the Espírito Santo Basin and its Araçuaí Orogen onshore connection. Onshore geology was interpreted following gravity based geological sections of Wiedemann et al. (2002) and offshore crustal structure was interpreted after seismic sections of Blaich et al. (2011) and Zalán et al. (2011).Right side of the figure shows the African conjugate passive margin with the Kwanza Basin and it West Congo Orogen onshore connections. Onshore geology was interpreted after geological type cross sections of (Tack *et al*., 2001) and offshore crustal structure was interpreted after seismic sections of Blaich et al. (2011), structural maps by Guiraud et al. (2010), regional transect made by Hudec and Jackson (2004) and gravimetric modelling by von Nicolai et al. (2013). See text for further interpretations. See text for explanations of domains A-C.

Interestingly the inferred suture of the Araçuaí-West Congo orogen is onshore on the Brazilian side (Alkmim *et al*., 2006) implying that Mesozoic extension did not reactivate it and largely ignored the associated lithospheric mantle shear zone. Model M4 indicates how the suture zone may be left below the margin (Figure 6.5c) with crustal breakup following a domain between exhumed lower crust (Figure 6.5c) and upper crust. The long interval

between orogeny and extension that may have allowed for healing of the lithospheric mantle shear zone may explain why it did not fully reactivate and did not guide crustal breakup. Alternatively 3D rift localization effects with lateral propagation of rifting, and magmatic mantle weakening away from the suture zone are likely to have played a role during the formation of South Atlantic rifted margins. Lastly weak crustal rheologies, not included here, are inferred as a major control on wide rifted margin formation as in the South Atlantic (Huismans & Beaumont, 2011, 2014; Brune *et al*., 2014). The efficient decoupling layer between upper crust and mantle may therefore mask reactivation of mantle shear zones beneath the rifted margin.

6.5. Conclusions

In this paper we have used self-consistent forward thermo-mechanical models to explore how tectonic structural inheritance affects the development and structural style of conjugate rifted passive margins. Models presented here self-consistently create structural inheritance by including prior extensional and contractional phases explicitly. We conclude that:

1. Primary factors that control the structural style of rifted margin formation in the presence of orogenic structural inheritance identified here are: i) The strength of orogenic shear zones in the upper crust and upper mantle lithosphere; ii) The degree of decoupling between upper crust and the strong lower crust-lithospheric mantle layer; iii) The amount of shortening and size of the orogen; iv) The role of pre-orogenic extensional inheritance on orogenic wedge structure.
2. The weak mantle lithospheric orogenic suture zone exerts a main control on margin structure by the highly efficient localization of extensional deformation upon reactivation, and multiple weak upper crustal orogenic shear zones control extensional basin and rifted margin structure
3. The offset between the weak mantle lithospheric orogenic suture zone and orogenic upper crustal weakness zones and the strength of the mid-crustal decoupling horizon are the main controlling factors for extensional reactivation. A weak decoupling horizon promotes linkage between the mantle suture zone and upper crustal orogenic shear zones with a large offset. In contrast a strong mid crust inhibits linkage of mantle and crustal shear zones with a large offset and promotes reactivation in a narrow zone.

4. We define three characteristic domains. Domain A distal to the mantle lithosphere suture zone with little to no propensity for extensional reactivation. Intermediate Domain B with partial extensional reactivation of orogenic structure. Domain C, close the suture zone characterized by full reactivation of orogenic structure and formation of new extensional structures. These domains were discussed in the case of Central South Atlantic and North Sea natural systems
5. With a small amount of contraction, thick-skinned thrusts are efficiently reactivated in extension and provide the template for rifted margin formation. With larger amounts of precursor contraction, thick-skinned thrusts distal to the mantle lithospheric suture zone do not reactivate in extension.
6. During the extension of the pro-wedge, reactivation of inherited contractional structures prevail, whereas the extension of the retro-wedge is mainly controlled by Phase 1 inherited extensional structures.
7. Relative importance of new-formed versus reactivated extensional shear zones during rifting depends on the amount of extensional and contractional inheritance. Small amounts of precursor extension and contraction result in less inherited structure and promote formation of new-formed extensional shear zones during Phase 3 extension.
8. Reactivation of contractional shear zones dominates during the early stages of rifting, whereas during the final stage of rift-passive margin formation extension occurs on an combination of new-formed and inherited structures.
9. Systems with pre-orogenic extensional inheritance promote retro-wedge deformation and inversion during mountain building. These retro-wedge structures guide strain localization and concentrate crustal breakup upon subsequent extension.

Acknowledgements

We would like to thank CAPES and SIU for financial support through the collaboration project *Integrated orogen-sedimentary basin studies*, and Petrobras for granting a PhD scholarship to the first author.

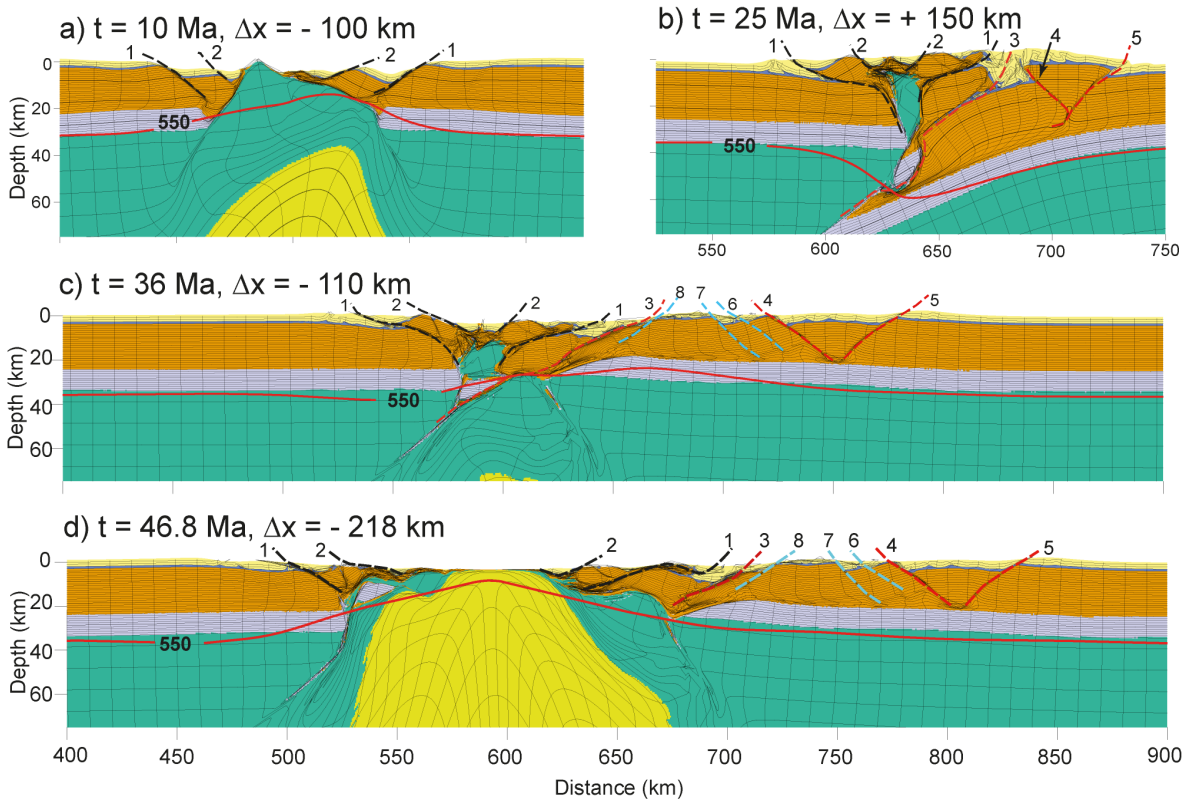

Figure 6.8 S1 – MS1. (a) Simultaneous faulting during the development of pre-orogenic extensional shear zones due to 100 km of stretching. This amount of extension permitted crustal breakup and exhumation of mantle lithosphere. (b) Full inversion and reactivation of inherited extensional shear zones and initiation of continental subduction. Note tracts of mantle lithosphere within the retro-wedge pop-up. (c) After 110 km of extension, contractional shear zones are fully reactivated on the pro-wedge and new-formed shear zones develop. Inset shows strain rate details, where red colors are high rates and blue low rates of strain. (d) Final passive margin configuration with crustal breakup following inherited extensional shear zones on the retro-wedge.

Chapter 7 - Lower continental crust removal during eduction prior to magma-poor rifted margin development

Claudio A. Salazar-Mora[1,2] and Ritske S. Huismans[2]

[1]*Department of Earth Sciences, Bergen University (UiB), Bergen N-5007, Norway*

[2]*Geosciences Institute, São Paulo University (IGc-USP). Rua do Lago 562, CEP 05508-080, São Paulo, Brazil*

Abstract

Structural inheritance in the continental lithosphere is thought to result from previous Wilson Cycles. For instance, the rifting process of the Atlantic Ocean preferentially reactivated ancient Western Gondwana suture zones. In addition, there are a few examples of fossil subduction zones in the mantle lithosphere under Atlantic-type passive margins. One of the main features in the crustal structure of magma-poor rifted margins is the lack of lower continental crust towards the continent-ocean boundary. Depth-dependent extension is advocated to explain mantle lithosphere exhumation and lower continental crust removal during extension. Alternatively, we use 2-D thermo-mechanical numerical models to show how lower continental can be removed during previous tectonic events before rifting. Our models show that rheological differences between upper and lower continental crusts cause them to decouple both during subduction and subsequent eduction. The latter process, associated to thermal necking of the upwelling asthenosphere, is responsible to leave slivers of previously subducted lower continental crust within the eduction channel in the mantle lithosphere. In what follows, lower continental crust of the former subducting plate can be removed long before depth-dependent extension during magma-poor rifted margin development.

Keywords: Numerical Modeling; Geodynamics; Continental subduction; Eduction; Lower crust.

7.1 Introduction

Typical examples of magma-poor conjugate rifted margins are the Iberia-Newfoundland in the North Atlantic and the Brazil-Angola in the Central South Atlantic (Franke, 2013; Peron-Pinvidic *et al*., 2013), both of which resulted from Western Gondwana continental breakup that occurred along ancient orogenic belts (Vauchez *et al*., 1997; Buiter & Torsvik, 2014; Tommasi & Vauchez, 2015). A common feature between these two conjugated margins is the presence of transitional crust towards the rift axis instead of normal seismically identified lower continental crust. Average seismic velocities around 6,8 km/s are usually used to interpret lower continental crust, but recent reviews show that an average up to 7,2 km/s could still resemble lower crust, but with a more mafic composition (Hacker *et al*., 2015). Transitional crust between the continental and oceanic crust at magma-poor margins has been documented to have seismic velocities between 7,2 and 7,8 km/s. This transitional character can either represent exhumation of sublithospheric mantle, which is represented by the increase of seismic velocities from 5 to 8 km/s with depth and lack of reflective Moho, or exhumation of lower continental crust, which varies from 6,9 to 7,1 km/s (Sibuet & Tucholke, 2013).

Removal of lower continental crust at magma-poor margins has been explained by its lateral flow towards the maximum extension area at the continent-ocean transition (e.g. Pérez-Gussinyé, 2013; Sibuet and Tucholke, 2013). Numerical models corroborate this lateral flow based on depth-dependent extension, showing that weak lower crust can be extruded towards the rifting axis like a channel flow (Huismans & Beaumont, 2011), a mechanism that can explain the formation of metamorphic cores complexes like in the Basin and Range (Huismans & Beaumont, 2014). The same authors also show strong lower crust being laterally advected and removed coupled to the mantle lithosphere. Other numerical simulations suggest lateral flows of lower continental crust to be a result of rift migration (Brune *et al*., 2014).

In this paper, we present numerical models that self-consistently create tectonic structural inheritance on a lithosphere that undergoes rifting, showing that lower crust removal can be also a result of rheological decoupling during eduction of the lower plate, that is, long before rift-related extension.

7.2 Numerical modeling

Our numerical simulations used a modified version of the Arbitrary Lagrangian-Eulerian finite-element code FANTOM (Thieulot, 2011; Erdős *et al*., 2014) to model thermal-mechanically coupled, plane-strain, viscous-plastic creeping flows. We investigate the behavior of a layered lithosphere and the sublithospheric mantle with frictional-plastic and thermally activated power law viscous rheologies in both contractional and extensional regimes. Because our models consider tectonic structural inheritance, they are allowed two previous tectonic phases, one extensional and one contractional (see Table 7.1), before final rifting and development of the conjugate passive margins. Thereby, our models self-consistently create tectonic/structural inheritance, which has already been efficiently tested by Huismans and Beaumont (2003), Jammes and Huismans (2012) and Erdős et al. (2014).

The model domain is set to represent the lithosphere and the sublithospheric mantle and its dimensions are L_x = 1200 km and L_z = 600 km. The lithosphere comprises a 35 km thick continental crust and a 90 km thick mantle lithosphere. The continental crust layering is first represented by a 25 km thick upper crust and a 10 km thick lower crust. The upper 4 km of the upper crust are represented by pre-deformation sediments, with a 3 km thick frictional upper layer overlying a weak 1 km thick layer portraying a *décollement* horizon. This setup allows for the interaction of both thin- and thick-skinned tectonic regimes. Vertical resolution is 200 m for the upper crust, 800 m for the lower crust and mantle lithosphere and 9.5 km for the sublithospheric mantle. The horizontal resolution is 500 m for the entire model (see GSA Data Repository for method details).

7.3 Model results

We have run six different models to test the role of decoupling between upper and lower crust during the eduction of a subducted continental lithosphere that experienced different amounts of contraction and pre-contraction extension (Table 7.1). Different amounts of both extension and contraction let us to create tectonic structural inheritance, that is, structures derived from previous tectonic events, such as precursor basin formation and inversion, and development of an orogenic belt. It is beyond the scope of this paper to discuss the role of all created tectonic structural inheritance within the lithosphere before rifting. Here

we focus on the behavior of the subducting continental lithosphere and its later eduction, prior to rifting.

In purely contractional models it is observed that the subducting lithosphere goes deeper with increasing amounts of contraction (Models 1 and 2 in Table 1). Decoupling between upper and lower crust is also a function of contraction, since lower crust goes 30 km deeper than the upper crust in Model 1 and 65 km deeper in Model 2. The same occurs with the mantle lithosphere.

Table 7.1 – Varying amounts of extension and contraction of all run models and depth achieved by upper and lower crusts and mantle lithosphere during the contractional phase.

		Depth with subduction (km)		
		Upper crust	**Lower crust**	**Mantle lithosphere**
Model 1	150 km C*	75	105	200
Model 2	300 km C	85	150	255
Model 3	50 km E, 150 km C	85	115	205
Model 4	50 km E, 300 km C	85	180	275
Model 5	100 km E, 150 km C	65	90	180
Model 6	100 km E, 300 km C	80	150	245
*C= contraction; E=extension				

When a previous extensional phase is added (Models 2 and 4 in Table 1), increasing decoupling is also observed with increasing amounts of contraction, although the upper crust does not subduct to greater depths with greater amounts of contraction. With doubled amounts of previous extension (Models 5 and 6), both upper and lower crusts achieve greater depths with increasing contraction. In what follows, the greater depths achieved by the lower crust during continental subduction is primarily affected by the greater amounts of contraction and smaller amounts of previous extension (Model 4).

Figure 7.1-A shows Model 6 after all previous extensional and contractional phases and a resulting ~300 km wide orogenic belt. During contraction and after subduction commenced, the boundary between the upper and lower crusts concentrates deformation and thus forms a principal decoupling surface, through which the lower crust detaches from the upper crust and

goes deeper into the mantle lithosphere. Note that the lower crust of the upper plate remains relatively untouched.

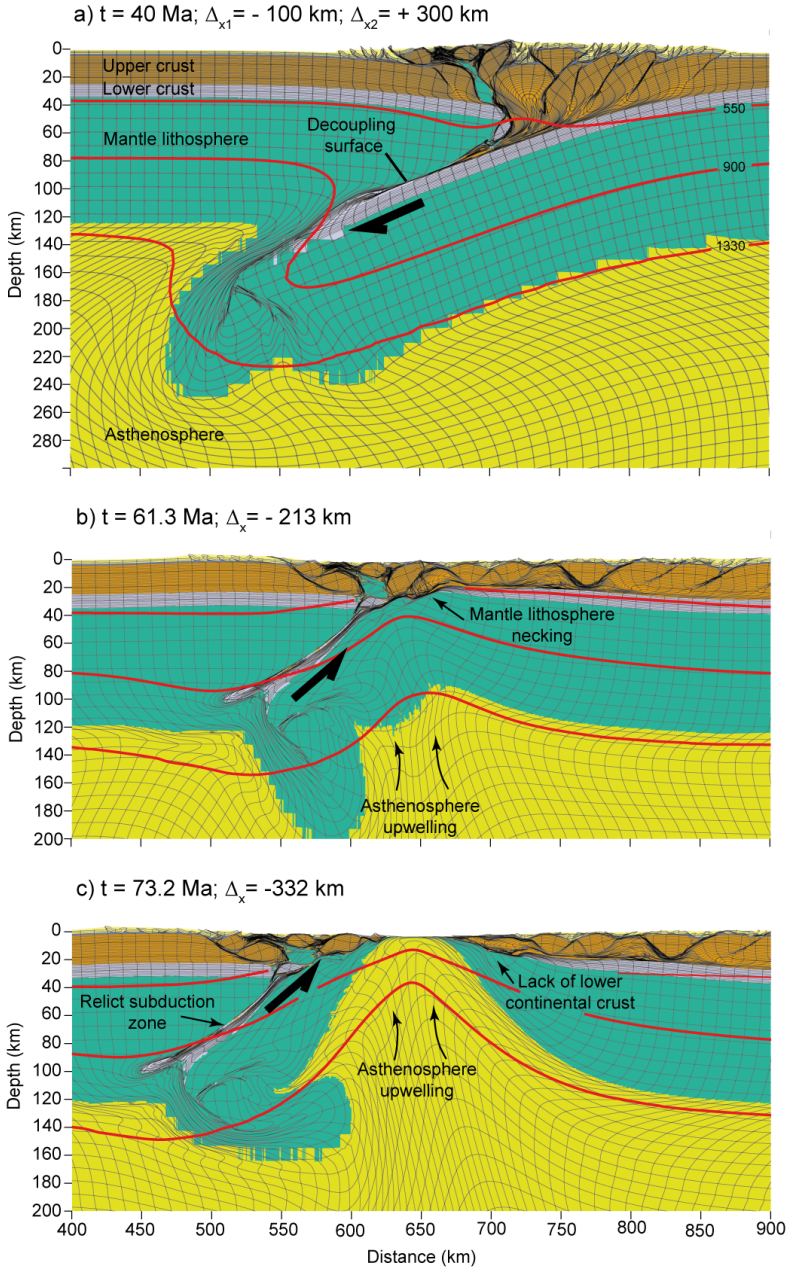

Figure 7.1 – Evolution for Model 6. Positive Δ_x means contractions and negative Δ_x means extension. See text for explanation and a complete animation in GSA Data Repository).

When velocity boundary conditions are inverted to extension (Figure 7.1-B), the decoupling surface is efficiently re-used as a sliding surface that facilitates the eduction process. During this process, part of the previously subducted upper continental crust is exhumed through the eduction channel and the detached lower continental crust is continuously left in the mantle lithosphere. As eduction goes on, the upwelling asthenosphere creates an upward force on the educting plate which caused the mantle lithosphere to neck the

educting lower crust and underlay the upper continental crust (Figure 7.1-B). This process finally separates tracts of lower continental crust that are left within the eduction channel in the mantle lithosphere. Thermal necking of the upwelling asthenosphere causes the mantle lithosphere to break up after the upper continental crust, allowing for mid-ocean spreading center to form and finally isolate the eduction channel in the mantle lithosphere, which is now a relict of a subduction zone (Figure 7.1-C).

After crustal breakup, both conjugate margins lack lower continental crust towards the transition between continental and oceanic crust. In the case of the wider margin, lower crust removal (x=675-725 km in Figure 7.1-C) occurred because it was left behind within the mantle as a relict subduction zone. The narrower margin, in turn, has mantle lithosphere at its base, emplaced due to asthenosphere upwelling and mantle lithosphere breakup.

7.4 Discussion

Deep seismic reflection surveys have long suggested relics of subduction zones in the mantle lithosphere (Morgan *et al*., 1994), and their link to suture zones has been well-pointed by the compilations of Heron et al. (2016). For instance, in the rifted conjugate margins between Norway and Greenland in the North Sea (North Atlantic), relicts of subduction zones were seismically interpreted and associated to the Caledonian orogenic belt (Schiffer *et al*., 2014), which is the suture through which the following North Sea rifting took place. The same authors show that the relict subduction zone has seismic velocities around 8,4 km/s, which could be eclogitized oceanic crust or be originated from lower continental crust. Another interesting example with relicts of subduction zones near present-day rifted conjugate margins is the Newfoundland-Iberia (Central Atlantic), which represents the accretion of Avalonia into Laurentia during the Silurian to Devonian (van der Velden & Cook, 2005).

The final conjugate margins of Model 6 can be compared to the present-day Newfoundland-Iberia conjugate (Figure 7.2). The Iberian side of the seismically interpreted section shows good correlation with the right-hand side margin of Model 6, in which the continental crust necks from ~ 30 km thick to ~ 15 km thick (x = 375-500 km in Fig. 7.2-a and 2-b). From x = 300 km oceanwards, our model shows lack o lower continental crust with a shallowing Moho from 15 km to 0 km deep, which is compared to the “petrological Moho” (Mohn *et al*., 2015) of the seismic interpretations that implies in exhumation of mantle

lithosphere (Sibuet & Tucholke, 2013). Except for the shallow tract of mantle lithosphere in the narrow margin of our model (left-hand side), this margin is very similar to the Newfoundland margin.

In what follows, the lack of lower continental crust at the base of the wide margin could be accounted by the amount of continental crust left behind in the fossil subduction zone within the mantle lithosphere. Our models show that the decoupling between the upper crust and the stronger lower crust is a key factor during both subduction and eduction. The difference in strength between the upper and lower continental crusts is the key factor permitting decoupling and thus letting the lower crust to achieve greater depths during subduction. Subduction of the strong lower crust is observed in orogens like Himalayas, Pirenees and Central Alps (Erdős *et al.*, 2014). It has been numerically shown that bulk crustal strength plays a key role in building realistic orogenic piles. Alternatively, if the lower crust is too weak, then its highly ductile behavior precludes subduction (Jammes & Huismans, 2012). The weak decoupling surface efficiently localizes strain during both subduction and eduction, possibly because of it link to the mantle lithosphre. Nevertheless, during eduction, healing processes due to long periods of time between orogeny and rifting, could preclude thorought eduction and thus facilitate the preservation of crustal rocks as fossil subduction zones.

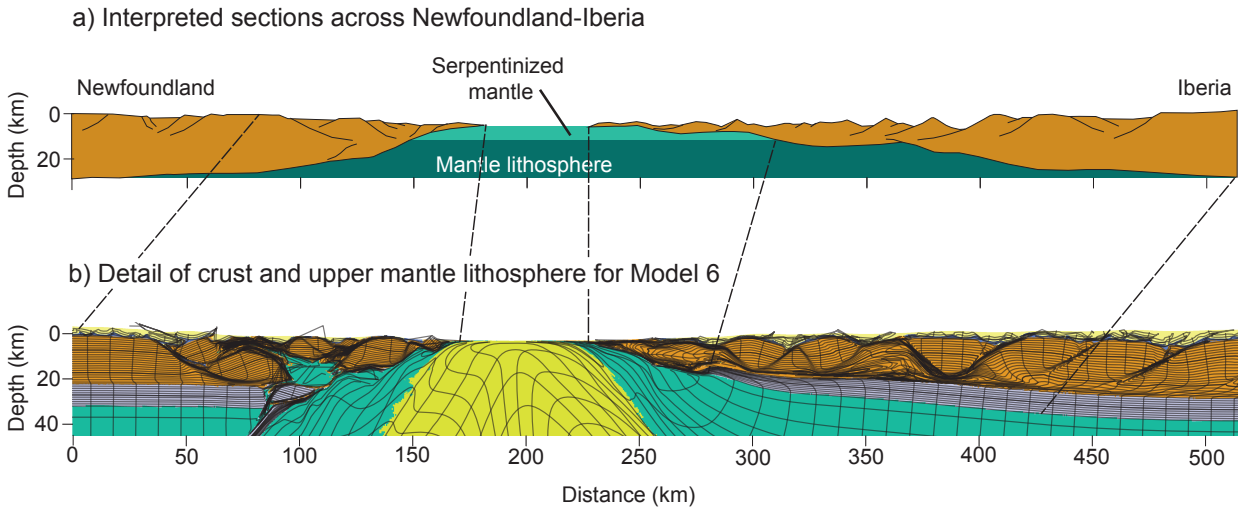

Figure 7.2 – (A) Seismic interpretation of the Newfoundland-Iberia rifted conjugate margins by (Mohn *et al.*, 2015). Serpentinized mantle is inferred by the authors with drilling until the "petrological moho" in the very thinned continental crust. Upper and lower continental crusts are not distinguished. (B) Results of Model 6 and comparison to seismic section in A. Dashed lines show three comparing domains, one from 0 to 160 km, another from 225 to 275 km and a final one between 275 to 425 km. See text for details.

7.5 Conclusions

Based on our numerical models, we showed that the relatively lack of lower continental crust towards the axial zone of magma-poor rifted conjugate margins can be accounted for its removal long before the rifting process. During the eduction of the ancient subduction zone, rheological decoupling of upper and lower continental crusts plus the effect of thermal necking due to asthenosphere upwelling permit that tracts of lower continental crust are left in the mantle lithosphere. Thereby, the rifting evolution of the previously subducted lithosphere already begins lacking amounts of lower continental crust. This means that lower continental crust removal or lateral movements are not only the result of depth-dependent extension during rifting.

Chapter 8 - Discussion and conclusions

Even though some previous discussion and conclusions on tectonic structural inheritance (Chapter 6) and rheology (Chapter 7) have already been presented, in this chapter I want to discuss and integrate these results in terms of rifted margin formation in Brazil (Central South Atlantic) and its Precambrian inheritance associated with the evolution of the Araçuaí-West Congo orogen. I therefore begin with a few words on how I constrained the two modelling end-member scenarios and how the models relate to the Araçuaí-West Congo evolution. Then I follow with a discussion of tectonic inheritance and rheology in the Wilson Cycle context. Conclusions are in the last section of this thesis.

8.1 Constraining the numerical models end-member scenarios

As aforementioned, the numerical simulations in the present thesis focused on testing Precambrian structural inheritance in the orogenic lithosphere during the development of the Cretaceous rifting process of the Central South Atlantic. Because numerical simulations allow us to "observe" the whole evolution *from orogen to rifted passive margin*, the Neoproterozoic end-member scenario should agree with what our models created as orogenic structure, as well as the final passive margin configuration. The latter brings fewer complications because it is aided by seismic and geophysical interpretations that produce good visualizations of the present-day rifted margin configuration and structure (described in Section 4.6).

To the other hand, constraining the Precambrian scenario for our models is far more difficult because the tools that allow us to elucidate about orogenic paleo-thickness, width and structure are: petrology-derived burial depths, 2-D equal-area restorations and regional schematic geological sections, respectively. Estimations of paleo-thickness are shown in Section 4.2.3 and Table 4, being derived from pressure and temperature calculations of metamorphic rocks formed during the syn-collisional phase of the Araçuaí Orogen.

In terms of width during the Neoproterozoic, the Araçuaí Orogen is not well constrained, for there is no estimation of shortening in the literature. Therefore, in this thesis I used 2-D equal-areal restorations to estimate the orogenic width during the Neoproterozoic.

Through the sections that connect onshore and offshore margin configuration

(Sections 4.6.3 and 4.6.4), we first restored the current rifted passive margin length to Jurassic length, that is, before actual rifting. We followed by restoring Jurassic length to find the Neoproterozoic length, which can be a first estimate of orogenic width. The restoration process is presented in Figure 8.1

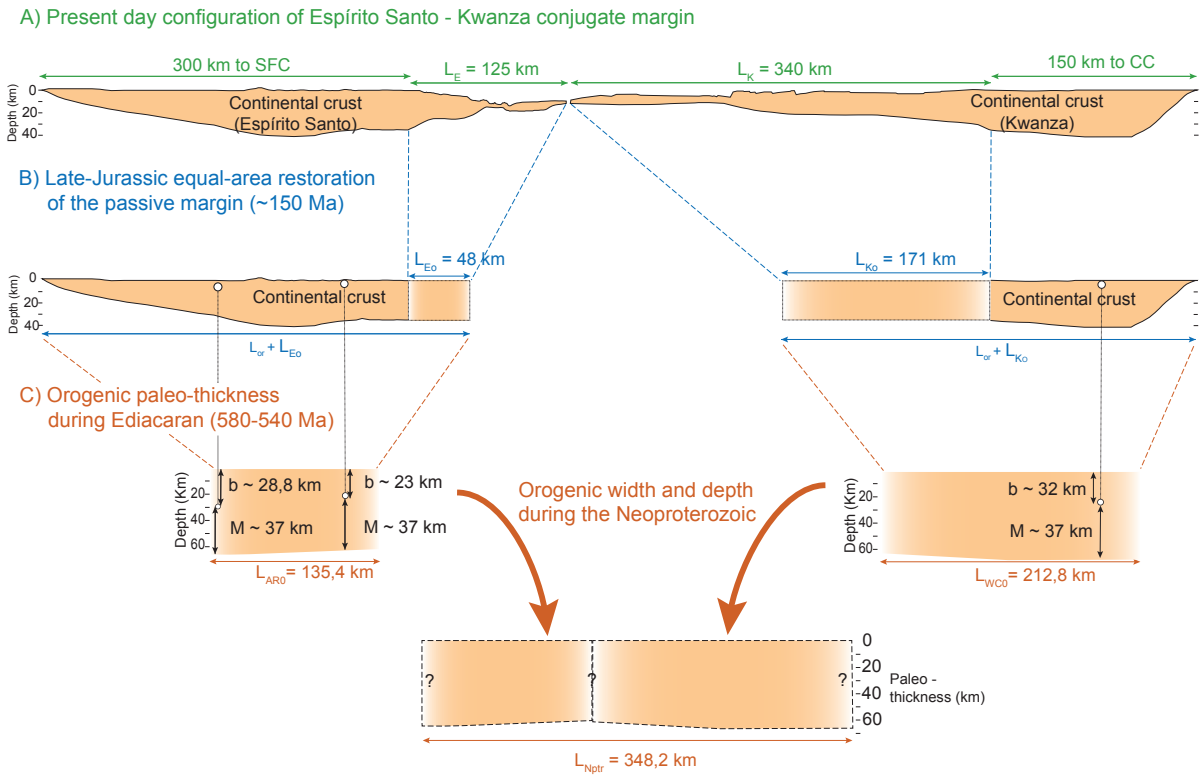

Figure 8.1 - 2-D equal-area restoration procedure in order to estimate Neoproterozoic orogenic width. (A) Present-day conjugate margins connecting onshore (orogenic crust) and offshore (rifted crust). L_E and L_K are the current lengths of Espírito Santo and Kwanza basins, respectively. (B) Rifted margin length restored to 35 km thick crust during Late-Jurassic. L_{E0} and L_{K0} are the initial lengths, that is, before rifting. (C) Restored orogenic length (width) during the Neoproterozoic calculated for thickened crust estimated by burial depth (b) added to present-day depth to Moho (M). By summing the estimated lengths of both margins for the Neoproterozoic, we have a first 2-D *estimation* of orogenic width. Calculation is made by the simple relation: L_0=Area/h_0, where L_0 is the unstretched length, h_0 is the height before stretching and Area refers to the stretched region.

The equal-area restoration procedure may be debatable, but it is reinforced here that it is used as an *estimation* of orogenic shortening due to lack of literature data. As it can be seen in Figure 8.1, maximum estimated width was 348 km, and all our models that considered 300 km of contraction created orogens 300 km wide, regardless of their previous extensional phases. Orogenic wedges created in the 300 km wide orogens have their maximum thickness of around 70-80 km, which is in agreement with paleothickness estimations in Table 4. In what follows, the difference of around 48 km in width between equal-area restoration and the numerical models, could be accounted for the 2-D instead of 3-D analysis.

In terms of structure, the Araçuaí-West Congo orogen is not well-constrained regarding its deeper parts, but the cross-section shown in Figure 4.3 shows and overall bi-vergent structure with thicker thrusts involving the basement in the orogenic hinterland, turning to a thin-skin deformation towards both cratonic domains. The model with pure contraction of 300 km does not form very well developed thin-skin deformation (Figure 6.3 – Model II), whereas 300 km wide orogens with a previous extensional phase show very well developed thin skin deformation in the forelands (Figure 6.5 – Model IV).

In what follows, the numerical simulations that result in a closer overall orogenic style (width, paleothickness and thin-skin foreland development) comparable to the Araçuaí-West Congo Orogen is model M II (Figure 6.5). The 50 km of extension before inversion and formation of the orogenic pile can represent the formation of a narrow intracontinental basin. As it can be seen in Figure 6.4a, 50 km of extension was sufficient to break the lower continental crust, whereas the upper crust was not broken. Despite all debatable characteristics of the Araçuaí-West Congo orogen precursor basin (see section 4.2.1), current geotectonic models attest it to be a very narrow and protracted basin. Therefore, our model M IV is consistent in the previous tectonic events it simulated to create all the tectonic inheritance present in the lithosphere before the Cretaceous rifting process of the Central South Atlantic.

The simulation of the final rifting phase in model M IV shows the reactivation of inherited structures and the development of new structures during rifting, and the role of each type of structure is fully discussed in Chapter 6. Because there is no well-constrained data in the literature about which types of orogenic structures of the Araçuaí-West Congo orogen were reactivated or not during the younger rifting process, our model M IV better constrains the overall lithospheric structure of the Espírito Santo-Kwanza rifted conjugate margins, as discussed in section 6.6.2.

8.2 Structural inheritance, rheology and the Wilson Cycle

When I refer to the Wilson Cycle in this thesis I am addressing to the subsequent ancient tectonic events that reworked the continental lithosphere and thus imprinted tectonic structural inheritance to it. In the case of the Araçuaí-West Congo orogen, as previously discussed, the geotectonic record reinforced the building of inheritance in model M IV, but the lack of geological data on the reactivation or development of structures during the rifting

process of the Central South Atlantic led to the a detailed interpretation of the numerical model itself. Therefore, in the Brazilian-African example, the numerical models show a better correlation in their end-member scenarios, once the final rifted conjugate margin overall structure (sections in topics 4.6.3, 4.6.4) agrees with the simulated final rifted margin. Although the reactivation or development of new structures is not geologically constrained, M model M IV is a consistent possibility of how structures behaved, either being reactivated during stretching or being newly formed during thinning. The code used for the numerical simulations has been consistently tested and compared to other scenarios of both mountain building and rifting (Erdős *et al*., 2014; Huismans & Beaumont, 2014). In what follows, the evolution of M IV in between end-members scenarios is a good approximation to the evolution from orogen to rifted passive margin formation.

A good natural example that shows reactivation of structures during rifting comes from the southwest Norwegian margin in the North Sea, where seismic imaging and systematic mapping of structures give consistent geological data (see section 6.6.1). The distal part of the Norwegian margin shows great similarity to the reactivation of orogenic structures during the following rifting phase, as well as the preservation of orogenic structure (Model M III and Figure 6.8).

Another good example, also seismically aided, comes from the Iberia-Newfoundland rifted conjugate margins, in the Central Atlantic. As discussed in Chapter 7, this example corroborates the Wilson Cycle because it shows relicts of subduction zones in the mantle lithosphere underneath the rifted passive margins. Moreover, this margin is also thought to have nucleated rifting from ancient suture zones. These fossil subduction zones we also modelled in this thesis, and is a result of rheological differences between upper and lower crust both during subduction and eduction.

In summary, the models and the code used in this thesis are in solid agreement with end-member scenarios – in the case of the Brazilian example –, with the dynamics of reactivation of orogenic structures or preservation of orogenic structure – in the North Sea Norwegian case – and with the rheological behaviour of upper and lower continental crust during subduction and later eduction – as in the Iberia-Newfoundland case. One important feature of the models presented in this thesis is that it takes the Wilson Cycle into account by self-consistently creating the tectonic inheritance, unlike most of the numerical simulations in the literature that address inheritance as initial inputs in the models.

8.4 Conclusions

In terms of tectonic structural inheritance and rheology and considering subsequent tectonic events, the following conclusions can be drawn having the modeling limitations in mind:

1) First reactivations occur along the lithospheric former suture zone;
2) Upper crustal thick skinned basement thrusts are partially or fully reactivated depending on the amount of prior contraction and size of the orogen;
3) With a small amount of contraction, thick skinned thrusts are efficiently reactivated in extension and provide the template for rifted margin formation. With larger amounts of precursor contraction, thick skinned thrusts distal to the lithospheric suture zone do not reactivate in extension, thus preserving orogenic structure;
4) The offset between the weak mantle lithospheric orogenic suture zone and orogenic upper crustal weakness zones and the strength of the mid-crustal decoupling horizon are the main controlling factors for extensional reactivation. A weak decoupling horizon promotes linkage between the mantle suture zone and upper crustal orogenic shear zones with a large offset. In contrast a strong mid crust inhibits linkage of mantle and crustal shear zones with a large offset and promotes reactivation in a narrow zone;
5) Reactivation of prior contractional shears dominates during the early stages of rifting, whereas during the final stage of rifted passive margin formation newly-formed extensional shears dominate;
6) Relative importance of new-formed versus reactivated extensional shear zones during rifting depends on the amount of extensional and contractional inheritance. Small amounts of precursor extension and contraction result in less inherited structure and promote formation of new-formed extensional shear zones during Phase 3 extension;
7) Systems with pre-orogenic extensional inheritance promote retro-wedge deformation and inversion during mountain building. These retro-wedge structures guide strain localization and concentrate crustal breakup upon subsequent extension;
8) Rheological discrepancies between upper and lower continental crust causes them to decouple during both subduction and eduction;
9) Decoupling and mantle upwelling force slivers of lower crust to be left behind in the mantle lithosphere as fossil subduction zones;

10) Lower continental crust removal in the axial zones of magma-poor rifted margins are not only the result of depth-dependent extension, but also a result of fossil subduction zones.

In terms of comparing the numerical results to the Araçuaí-West Congo orogen and the following Central South Atlantic rifting process, our models successfully portrayed the end-member scenarios, and provided predictions on which types of structures took part during the rifted passive margin development, which are summarized in the aforementioned paragraphs 1 to 7. Additionally, rheological differences within the layered continental lithosphere also brought insights in the case of fossil subductions zones and lower crustal removal prior to continental rifting.

References

Alkmim F.F., Marshak S., Pedrosa-Soares A.C., Peres G.G., Cruz S.C.P., & Whittington A. 2006. Kinematic evolution of the Araçuaí-West Congo orogen in Brazil and Africa: Nutcracker tectonics during the Neoproterozoic assembly of Gondwana. *Precambrian Research*, **149**(1–2):43–64.

Allken V., Huismans R.S., Fossen H., & Thieulot C. 2013. 3D numerical modelling of graben interaction and linkage: a case study of the Canyonlands grabens, Utah. *Basin Research*, **25**(4):436–449.

Allken V., Huismans R.S., & Thieulot C. 2011. Three - dimensional numerical modeling of upper crustal extensional systems. *Journal of Geophysical Research*, **116**:1–15.

Allken V., Huismans R.S., & Thieulot C. 2012. Factors controlling the mode of rift interaction in brittle-ductile coupled systems: A 3D numerical study. *Geochemistry Geophysics Geosystems*, **13**(1):Q05010.

Almeida F.F.M., Hasui Y., Brito Neves B.B., & Fuck R.A. 1981. Brazilian structural provinces, an introduction. *Earth-Science Reviews*, **17**:1–29.

Almeida J., Dios F., Mohriak W.U., Valeriano C.D.M., Heilbron M., Eirado L.G., & Tomazzoli E. 2013. Pre-rift tectonic scenario of the Eo-Cretaceous Gondwana break-up along SE Brazil-SW Africa: insights from tholeiitic mafic dyke swarms. *Geological Society, London, Special Publications*, **369**(1):11–40.

Aslanian D., Moulin M., Olivet J.-L., Unternehr P., Matias L., Bache F., Rabineau M., Nouzé H., Klingelheofer F., Contrucci I., & Labails C. 2009. Brazilian and African passive margins of the Central Segment of the South Atlantic Ocean: Kinematic constraints. *Tectonophysics*, **468**(1–4):98–112.

Assumpção M., Bianchi M., Julià J., Dias F.L., Sand França G., Nascimento R., Drouet S., Pavão C.G., Albuquerque D.F., & Lopes A.E.V. 2013a. Crustal thickness map of Brazil: Data compilation and main features. *Journal of South American Earth Sciences*, **43**:74–85.

Assumpção M., Feng M., Tassara A., & Julià J. 2013b. Models of crustal thickness for South America from seismic refraction, receiver functions and surface wave tomography. *Tectonophysics*, **609**:82–96.

Audet P. & Bürgmann R. 2011. Dominant role of tectonic inheritance in supercontinent cycles. *Nature Geoscience*, **4**(3):184–187.

Augustin N., Devey C.W., van der Zwan F.M., Feldens P., Tominaga M., Bantan R.A., & Kwasnitschka T. 2014. The rifting to spreading transition in the Red Sea. *Earth and Planetary Science Letters*, **395**:217–230.

Autin J., Bellahsen N., Leroy S., Husson L., Beslier M.-O., & d'Acremont E. 2013. The role of structural inheritance in oblique rifting: Insights from analogue models and application to the Gulf of Aden. *Tectonophysics*, **607**:51–64.

Babinski M., Pedrosa-Soares a. C., Trindade R.I.F., Martins M., Noce C.M., & Liu D. 2012. Neoproterozoic glacial deposits from the Araçuaí orogen, Brazil: Age, provenance and correlations with the São Francisco craton and West Congo belt. *Gondwana Research*, **21**(2–3):451–465.

Barbosa J.S.. & Sabaté P. 2004. Archean and Paleoproterozoic crust of the São Francisco Craton, Bahia, Brazil: geodynamic features. *Precambrian Research*, **133**(1–2):1–27.

Beaumont C. & Ings S.J. 2012. Effect of depleted continental lithosphere counterflow and inherited crustal weakness on rifting of the continental lithosphere: General results. *Journal of Geophysical Research: Solid Earth*, **117**(8):1–25.

Becker T.W. & Kaus B.J.P. 2016. *Numerical Modeling of Earth Systems. An introduction to computational methods with focus on solid Earth applications of continuum mechanics*, 1.2. ed. University of Southern California.

Bento dos Santos T.M., Tassinari C.C.G., & Fonseca P.E. 2015. Diachronic collision, slab break-off and long-term high thermal flux in the Brasiliano–Pan-African orogeny: Implications for the geodynamic evolution of the Mantiqueira Province. *Precambrian Research*, **260**:1–22.

Blaich O.A., Faleide J.I., & Tsikalas F. 2011. Crustal breakup and continent-ocean transition at South Atlantic conjugate margins. *Journal of Geophysical Research*, **116**(B1):B01402.

Blaich O.A., Faleide J.I., Tsikalas F., Lilletveit R., Chiossi D., Brockbank P., & Cobbold P. 2010. Structural architecture and nature of the continent-ocean transitional domain at the Camamu and Almada Basins (NE Brazil) within a conjugate margin setting, *In*: *Petroleum Geology: From Mature Basins to New Frontiers—Proceedings of the 7th Petroleum Geology Conference*. Geological Society of London, pp. 867–883.

Blaich O.A., Tsikalas F., & Faleide J.I. 2008. Northeastern Brazilian margin: Regional tectonic evolution based on integrated analysis of seismic reflection and potential field data and modelling. *Tectonophysics*, **458**(1–4):51–67.

Braun J. & Beaumont C. 1989. Dynamical models of the role of crustal shear zones in

asymmetric continental extension. *Earth and Planetary Science Letters*, **93**(3–4):405–423.

Brownfield M.E. & Charpentier R.R. 2006. Geology and Total Petroleum Systems of the West-Central Coastal Province (7203), West Africa. *U.S. Geological Survey Bulletin*, **2207–B**:1–52.

Brune S., Heine C., Clift P.D., & Pérez-Gussinyé M. 2017. Rifted margin architecture and crustal rheology: Reviewing Iberia-Newfoundland, Central South Atlantic, and South China Sea. *Marine and Petroleum Geology*, **79**:257–281.

Brune S., Heine C., Pérez-Gussinyé M., & Sobolev S. V 2014. Rift migration explains continental margin asymmetry and crustal hyper-extension. *Nature communications*, **5**:4014.

Brune S., Popov A. a., & Sobolev S. V. 2012. Modeling suggests that oblique extension facilitates rifting and continental break-up. *Journal of Geophysical Research*, **117**(B8):B08402.

Brune S., Williams S.E., Butterworth N.P., & Müller R.D. 2016. Abrupt plate accelerations shape rifted continental margins. *Nature*, 1–4.

Buck W.R. 1991. Modes of continental lithospheric extension. *Journal of Geophysical Research*, **96**(B12):20161–20178.

Buck W.R. 1991. Modes of continental lithspheric extension. *Journal of Geophysical Research*, **96**:161–178.

Buiter S.J.H. & Torsvik T.H. 2014. A review of Wilson Cycle plate margins: A role for mantle plumes in continental break-up along sutures? *Gondwana Research*, **26**(2):627–653.

Cainelli C. & Mohriak W.U. 1999. Some remarks on the evolution of sedimentary basins along the eastern Brazilian continental margin. *Episodes*, **22**(3):206–216.

Caixeta J.M., Ferreira T.S., Lima F.D., Francisco C., & Dias A. 2009. Diachronous rift system along Bahia State coast: An example of extended crust and mantle exhumation in the South Atlantic Ocean, *In*: *APPG International Conference & Exhibition*. pp. 15–19.

Campos Neto M.C. & Figueiredo M.C.. 1995. The Rio Doce Orogeny, Southeastern Brazil. *Journal of South American Earth Sciences*, **8**(2):143–162.

Cappelletti a., Tsikalas F., Nestola Y., Cavozzi C., Argnani A., Meda M., & Salvi F. 2013. Impact of lithospheric heterogeneities on continental rifting evolution: Constraints from analogue modelling on South Atlantic margins. *Tectonophysics*, **608**:30–50.

Cavalcante G.C.G., Egydio-silva M., Vauchez A., & Camps P. 2013. Strain distribution

across a partially molten middle crust: Insights from the AMS mapping of the Carlos Chagas Anatexite, Araçuaí belt (East Brazil). *Journal of Structural Geology*, **55**:79–100.

Cavalcante G.C.G., Vauchez A., Merlet C., Egydio-Silva M., Bezerra de Holanda M.H., & Boyer B. 2014. Thermal conditions during deformation of partially molten crust from TitaniQ geothermometry: rheological implications for the anatectic domain of the Araçuaí belt, Eastern Brazil. *Solid Earth Discussions*, **6**(1):1299–1333.

Christiansson P., Faldeide J.I., & Berge A.M. 2000. Crustal structure in the northern North Sea : an integrated geophysical study. *Dynamics of the Norwegian Margin*, (McKenzie 1978):15–40.

Collins W.J. 2002. Hot orogens, tectonic switching and creation of continental crust. *Geology*, **30**(6):535–538.

Contrucci I., Matias L., Moulin M., Géli L., Klingelhofer F., Nouzé H., Aslanian D., Olivet J.-L., Réhault J.-P., & Sibuet J.-C. 2004. Deep structure of the West African continental margin (Congo, Zaïre, Angola), between 5°S and 8°S, from reflection/refraction seismics and gravity data. *Geophysical Journal International*, **158**(2):529–553.

Corti G. 2012. Evolution and characteristics of continental rifting: Analog modeling-inspired view and comparison with examples from the East African Rift System. *Tectonophysics*, **522–523**:1–33.

da Silva L.C., McNaughton N.J., Armstrong R., Hartmann L.A., & Fletcher I.R. 2005. The neoproterozoic Mantiqueira Province and its African connections: a zircon-based U–Pb geochronologic subdivision for the Brasiliano/Pan-African systems of orogens. *Precambrian Research*, **136**(3–4):203–240.

da Silva L.C., Pedrosa-Soares a. C., Teixeira L.R.., & Armstrong R. 2008. Tonian rift-related, A-type continental plutonism in the Araçuaí Orogen, eastern Brazil: New evidence for the breakup stage of the São Francisco–Congo Paleocontinent. *Gondwana Research*, **13**(4):527–537.

Davis M. & Kusznir N.J. 2004. Depth-dependent lithospheric stretching at rifted continental margins, *In*: Karner G.. (ed.), *Proceedings of National Science Foundation Rifted Margins Theoretical Institute*. Columbia University Press, New York, pp. 92–136.

Dupré S., Cloetingh S., & Bertotti G. 2011. Structure of the Gabon Margin from integrated seismic reflection and gravity data. *Tectonophysics*, **506**(1–4):31–45.

Ellis S., Schreurs G., & Panien M. 2004. Comparisons between analogue and numerical models of thrust wedge development. *Journal of Structural Geology*, **26**(9):1659–1675.

Erdős Z., Huismans R.S., van der Beek P., & Thieulot C. 2014. Extensional inheritance and

surface processes as controlling factors of mountain belt structure. *Journal of Geophysical Research: Solid Earth*, **119**(12):9042–9061.

Fernandez M. & Ranalli G. 1997. The role of rheology in extensional basin formation modelling. *Tectonophysics*, **282**:129–145.

Ferreira T.S., Caixeta J.M., & Lima F.D. 2009. Basement control in Camamu and Almada rift basins. *Boletim de Geociências da Petrobrás*, **17**(1):69–88.

Ferziger J.H. & Perić M. 2002. *Computational Methods for Fluid Dynamics*. Springer Berlin Heidelberg, Berlin, Heidelberg.

Fetter M. 2009. The role of basement tectonic reactivation on the structural evolution of Campos Basin, offshore Brazil: Evidence from 3D seismic analysis and section restoration. *Marine and Petroleum Geology*, **26**(6):873–886.

Fichler C., Odinsen T., Rueslåtten H., Olesen O., Vindstad J.E., & Wienecke S. 2011. Crustal inhomogeneities in the Northern North Sea from potential field modeling: Inherited structure and serpentinites? *Tectonophysics*, **510**(1–2):172–185.

Fillon C., Huismans R.S., & van der Beek P. 2012. Syntectonic sedimentation effects on the growth of fold-and-thrust belts. *Geology*, **41**(1):83–86.

Fletcher C.A.J. 1991. *Computational Techniques for Fluid Dynamics*. Springer-Verlag, Berlin, Heidelberg.

Fossen H. 2010. Extensional tectonics in the North Atlantic Caledonides: a regional view. *Geological Society, London, Special Publications*, **335**(1):767–793.

Fossen H., Gabrielsen R.H., Faleide J.I., & Hurich C. a. 2014. Crustal stretching in the Scandinavian Caledonides as revealed by deep seismic data. *Geology*, **42**(9):791–794.

Fossen H., Khani H.F., Faleide J.I., Ksienzyk A.K., & Dunlap W.J. 2016. Post-Caledonian extension in the West Norway-northern North Sea region: the role of structural inheritance. *Geological Society, London, Special Publications*, **439**.

Franke D. 2013. Rifting, lithosphere breakup and volcanism: Comparison of magma-poor and volcanic rifted margins. *Marine and Petroleum Geology*, **43**:63–87.

Fullsack P. 1995. An arbitrary Lagrangian-Eulerian formulation for creeping flows and its application in tectonic models. *Geophysical Journal International* , **120**(1):1–23.

Gerya T. 2010. *Introduction to Numerical Geodynamic Modelling*. Cambridge University Press, Cambridge.

Gerya T. V. 2013. Three-dimensional thermomechanical modeling of oceanic spreading initiation and evolution. *Physics of the Earth and Planetary Interiors*, **214**:35–52.

Gleason G.C. & Tullis J. 1995. A flow law for dislocation creep of quartz aggregates

determined with the molten salt cell. *Tectonophysics*, **247**(1–4):1–23.

Gonçalves L., Alkmim F.F., Pedrosa-Soares A.C., Dussin I. a., Valeriano C.D.M., Lana C., & Tedeschi M. 2015. Granites of the intracontinental termination of a magmatic arc: an example from the Ediacaran Araçuaí orogen, southeastern Brazil. *Gondwana Research*, **in press**.

Gonçalves L., Farina F., Lana C., Pedrosa-Soares A.C., Alkmim F., & Nalini H. a. 2014. New U–Pb ages and lithochemical attributes of the Ediacaran Rio Doce magmatic arc, Araçuaí confined orogen, southeastern Brazil. *Journal of South American Earth Sciences*, **52**:129–148.

Gordon A.C., Mohriak W.U., & Barbosa V.C.F. 2012. Crustal architecture of the Almada Basin, NE Brazil: an example of a non-volcanic rift segment of the South Atlantic passive margin, *In*: Mohriak W.U., Danforth A., Post P.J., Brown D.E., Tari G.C., Nemcok M., & Sinha S.T. (eds.), *Geological Society, London, Special Publications*. Geological Society, London, Special Publications, 369, pp. 215–234.

Gradim C., Roncato J., Pedrosa-Soares A.C., Cordani U., Dussin I., Alkmim F.F., Queiroga G., Jacobsohn T., Silva L.C. Da, & Babinski M. 2014. The hot back-arc zone of the Araçuaí orogen, Eastern Brazil: from sedimentation to granite generation. *Brazilian Journal of Geology*, **44**(1):155–180.

Guiraud M., Buta-Neto a., & Quesne D. 2010. Segmentation and differential post-rift uplift at the Angola margin as recorded by the transform-rifted Benguela and oblique-to-orthogonal-rifted Kwanza basins. *Marine and Petroleum Geology*, **27**(5):1040–1068.

Hacker B.R., Kelemen P.B., & Behn M.D. 2015. Continental Lower Crust. *Annual Review of Earth and Planetary Sciences*, **43**(1):167–205.

Hackspacher P.C., Ribeiro L.F.., Ribeiro M.C.., Fetter A.H., Hadler Neto J.C., Tello C.E.S., & Dantas E.L. 2004. Consolidation and Break-up of the South American Platform. *Gondwana Research*, **7**(I):91–101.

Heilbron M., Valeriano C.M., Tassinari C.C.G., Almeida J., Tupinamba M., Siga O., & Trouw R. 2008. Correlation of Neoproterozoic terranes between the Ribeira Belt, SE Brazil and its African counterpart: comparative tectonic evolution and open questions, *In*: Pankhurst R.J., Trouw R.A.J., Brito Neves B.., & de Witt M.. (eds.), *Geological Society, London, Special Publications*. pp. 211–237.

Heine C., Zoethout J., & Müller R.D. 2013. Kinematics of the South Atlantic rift. *Solid Earth*, **4**(2):215–253.

Heron P.J., Pysklywec R.N., & Stephenson R. 2016. Lasting mantle scars lead to perennial

plate tectonics. *Nature Communications*, **7**(May):11834.

Hiruma S.T., Riccomini C., Modenesi-Gauttieri M.C., Hackspacher P.C., Neto J.C.H., & Franco-Magalhães A.O.B. 2010. Denudation history of the Bocaina Plateau, Serra do Mar, southeastern Brazil: Relationships to Gondwana breakup and passive margin development. *Gondwana Research*, **18**(4):674–687.

Hubbert M.K. 1937. Theory of scaled models as applied to the study of geologic structures. *Bulletin of the Geological Society of America*, **48**:1459–1520.

Hudec M.R. & Jackson M.P. a 2004. Regional restoration across the Kwanza Basin, Angola: Salt tectonics triggered by repeated uplift of a metastable passive margin. *AAPG Bulletin*, **88**(7):971–990.

Huismans R. & Beaumont C. 2011. Depth-dependent extension, two-stage breakup and cratonic underplating at rifted margins. *Nature*, **473**(7345):74–8.

Huismans R.S. & Beaumont C. 2002. Asymmetric lithospheric extension: The role of frictional plastic strain softening inferred from numerical experiments. *Geology*, **30**(3):211–214.

Huismans R.S. & Beaumont C. 2003. Symmetric and asymmetric lithospheric extension: Relative effects of frictional-plastic and viscous strain softening. *Journal of Geophysical Research*, **108**(B10):1–22.

Huismans R.S. & Beaumont C. 2008. Complex rifted continental margins explained by dynamical models of depth-dependent lithospheric extension. *Geology*, **36**(2):163–166.

Huismans R.S. & Beaumont C. 2014. Rifted continental margins: The case for depth-dependent extension. *Earth and Planetary Science Letters*, **407**:148–162.

Ismail-Zaden A. & Tackley P. 2010. *Computational Methods for Geodynamics*. Cambridge University Press, Cambridge.

Jammes S. & Huismans R.S. 2012. Structural styles of mountain building: Controls of lithospheric rheologic stratification and extensional inheritance. *Journal of Geophysical Research: Solid Earth*, **117**(10):1–22.

Karato S. & Wu P. 1993. Rheology of the Upper Mantle: A Synthesis. *Science*, **260**(5109):771–778.

Kaus B.J.P., Gerya T. V., & Schmid D.W. 2008. Recent advances in computational geodynamics: Theory, numerics and applications. *Physics of the Earth and Planetary Interiors*, **171**(1–4):2–6.

Lentini M.R., Fraser S.I., Sumner H.S., & Davies R.J. 2010. Geodynamics of the central South Atlantic conjugate margins: implications for hydrocarbon potential. *Petroleum*

Geoscience, **16**(3):217–229.

Liao J. & Gerya T. 2014. Influence of lithospheric mantle stratification on craton extension: Insight from two-dimensional thermo-mechanical modeling. *Tectonophysics*, **631**:50–64.

Macdonald D., Gomez-Perez I., Franzese J., Spalletti L., Lawver L., Gahagan L., Dalziel I., Thomas C., Trewin N., Hole M., & Paton D. 2003. Mesozoic break-up of SW Gondwana: implications for regional hydrocarbon potential of the southern South Atlantic. *Marine and Petroleum Geology*, **20**(3–4):287–308.

Manatschal G., Lavier L., & Chenin P. 2015. The role of inheritance in structuring hyperextended rift systems: Some considerations based on observations and numerical modeling. *Gondwana Research*, **27**(1):140–164.

Matos R.M.D. De 2000. Tectonic Evolution of the Equatorial South Atlantic, *In*: Mohriak W.U., & Talwani M. (eds.), *Atlantic Rifts and Continental Margins - American Geophysical Union Vol. 115*. pp. 331–354.

McGee B., Collins A.S., & Trindade R.I.F. 2012. G'day Gondwana — the final accretion of a supercontinent: U–Pb ages from the post-orogenic São Vicente Granite, northern Paraguay Belt, Brazil. *Gondwana Research*, **21**(2–3):316–322.

Mckenzie D. 1978. Some remarks on the development of sedimentary basins. *Earth and Planetary Science Letters*, **40**(1):25–32.

Milani E.J., Hangel H.D., Bueno G.V., Stica J.M., Winter W.R., Caixeta J.M., & Neto O.C.. 2007. Brazilian sedimentary basins - stratigraphic charts. *Bulletin of Geosciences Petrobrás*, **15**(2):183–205.

Milani E.J. & Ramos V.A. 1998. Paleozoic orogenies in the southwestern domain of Gondwana and the subsidence cycles of the Paraná Basin. *Brazilian Journal of Geology*, **28**(4):473–484.

Misra A.A. & Mukherjee S. 2015. *Tectonic Inheritance in Continental Rifts and Passive Margins*, SpringerBriefs in Earth Sciences. Springer International Publishing, Cham.

Mohn G., Karner G., Manatschal G., & Johnson C. 2015. Structural and stratigraphic evolution of the Iberia and Newfoundland hyper-extended rifted margins: A quantitative modeling approach. *Geological Society, London, Special Publications*, **16**:9156.

Mohriak W., Nemcok M., & Enciso G. 2008. South Atlantic divergent margin evolution: rift-border uplift and salt tectonics in the basins of SE Brazil. *Geological Society, London, Special Publications*, **294**(1):365–398.

Monié P., Bosch D., Bruguier O., Vauchez A., Rolland Y., Nsungani P., & Buta Neto A. 2012. The Late Neoproterozoic/Early Palaeozoic evolution of the West Congo Belt of

NW Angola: geochronological (U-Pb and Ar-Ar) and petrostructural constraints. *Terra Nova*, **24**(3):238–247.

Mora C.A.S., Campanha G.A.D.C., & Wemmer K. 2013. Microstructures and K-Ar illite fine-fraction ages of the cataclastic rocks associated to the Camburu Shear Zone, Ribeira Belt, Southeastern Brazil. *Brazilian Journal of Geology*, **43**(4):607–622.

Morgan J. V., Hadwin M., Warner M.R., Barton P.J., & Morgan R.P.L. 1994. The polarity of deep seismic reflections from the lithospheric mantle: Evidence for a relict subduction zone. *Tectonophysics*, **232**(1–4):319–328.

Moulin M., Aslanian D., & Unternehr P. 2010. A new starting point for the South and Equatorial Atlantic Ocean. *Earth-Science Reviews*, **98**(1–2):1–37.

Naliboff J. & Buiter S.J.H. 2015. Rift reactivation and migration during multiphase extension. *Earth and Planetary Science Letters*, **421**:58–67.

Pasyanos M.E. & Nyblade A. a. 2007. A top to bottom lithospheric study of Africa and Arabia. *Tectonophysics*, **444**(1–4):27–44.

Pedrosa-Soares A.C., Alkmim F.F., Tack L., Noce C.M., Babinski M., Silva L.C., & MArtin-Neto M.A. 2008. Similarities and differences between the Brazilian and African counterparts of the Neoproterozoic Araçuaí-West Congo orogen. *Geological Society, London, Special Publications*, **294**(1):153–172.

Pedrosa-soares A.C., Noce C.M., Wiedemann C.M., & Pinto C.P. 2001. The Araçuaí -West-Congo Orogen in Brazil : an overview of a confined orogen formed during Gondwanaland assembly. *Precambrian Research*, **110**:307–323.

Pedrosa-Soares A.C., Vidal P., Leonardos O.H., & De Brito-Neves B.B. 1998. Neoproterozoic oceanic remnants in eastern Brazil: further evidence and refutation of an exclusively ensialic evolution for the Aracuai-west Congo orogen. *Geology*, **26**(6):519–522.

Peixoto E., Pedrosa-Soares A.C., Alkmim F.F., & Dussin I. a. 2015. A suture–related accretionary wedge formed in the Neoproterozoic Araçuaí orogen (SE Brazil) during Western Gondwanaland assembly. *Gondwana Research*, **27**(2):878–896.

Pérez-Díaz L. & Eagles G. 2014. Constraining South Atlantic growth with seafloor spreading data. *Tectonics*, **33**(9):1848–1873.

Pérez-Gussinyé M. 2013. A tectonic model for hyperextension at magma-poor rifted margins: an example from the West Iberia – Newfoundland conjugate margins. *Geological Society, London, Special Publications*, **369**:403–427.

Peron-Pinvidic G., Manatschal G., & Osmundsen P.T. 2013. Structural comparison of

archetypal Atlantic rifted margins: A review of observations and concepts. *Marine and Petroleum Geology*, **43**:21–47.

Peslier A.H., Woodland A.B., Bell D.R., & Lazarov M. 2010. Olivine water contents in the continental lithosphere and the longevity of cratons. *Nature*, **467**(7311):78–81.

Phillips T.B., Jackson C.A.L., Bell R.E., Duffy O.B., & Fossen H. 2016. Reactivation of intrabasement structures during rifting: A case study from offshore southern Norway. *Journal of Structural Geology*, **91**:54–73.

Piquè a. & Laville E. 1996. The Central Atlantic Rifting: reactivation of Paleozoic structures? *Journal of Geodynamics*, **21**(3):235–255.

Porada H. 1989. Pan-African rifting and orogenesis in southern to equatorial Africa and eastern Brazil. *Precambrian Research*, **44**(2):103–136.

Pysklywec R.N. 2002. Lithospheric deformation during the early stages of continental collision: Numerical experiments and comparison with South Island, New Zealand. *Journal of Geophysical Research*, **107**(B7).

Pysklywec R.N. & Beaumont C. 2004. Intraplate tectonics: Feedback between radioactive thermal weakening and crustal deformation driven by mantle lithosphere instabilities. *Earth and Planetary Science Letters*, **221**(1–4):275–292.

Ramos V.A. 2003. Paleozoic orogenies in the western margin of Gondwana, *In*: *International Symposium on Tectonics, 3*. Búzios, pp. 111–113.

Ranalli G. 1995. *Rheology of the Earth*. Chapman & Hall.

Reston T.J. 2010. The opening of the central segment of the South Atlantic: symmetry and the extension discrepancy. *Petroleum Geoscience*, **16**(3):199–206.

Schiffer C., Balling N., Jacobsen B.H., Stephenson R.A., & Nielsen S.B. 2014. Seismological evidence for a fossil subduction zone in the East Greenland Caledonides. *Geology*, **42**(4):311–314.

Schmitt R. da S., Trouw R. a. J., Van Schmus W.R., & Pimentel M.M. 2004. Late amalgamation in the central part of West Gondwana: new geochronological data and the characterization of a Cambrian collisional orogeny in the Ribeira Belt (SE Brazil). *Precambrian Research*, **133**(1–2):29–61.

Schmitt R.S., Trouw R. a. J., Van Schmus W.R., & Passchier C.W. 2008. Cambrian orogeny in the Ribeira Belt (SE Brazil) and correlations within West Gondwana: ties that bind underwater, *In*: Pankhurst R.J., Trouw R.A.., Brito Neves B.B., & de Witt M.J. (eds.), *Geological Society, London, Special Publications*. pp. 279–296.

Schreurs G., Buiter S.J.H., Boutelier D., Corti G., Costa E., Cruden a. R., Daniel J.-M., Hoth

S., Koyi H. a., Kukowski N., Lohrmann J., Ravaglia a., Schlische R.W., Withjack M.O., Yamada Y., Cavozzi C., Del Ventisette C., Brady J. a. E., Hoffmann-Rothe a., Mengus J.-M., Montanari D., & Nilforoushan F. 2006. Analogue benchmarks of shortening and extension experiments. *Geological Society, London, Special Publications*, **253**(1):1–27.

Schulmann K., Lexa O., Štípská P., Racek M., Tajčmanová L., Konopásek J., Edel J.-B., Peschler A., & Lehmann J. 2008. Vertical extrusion and horizontal channel flow of orogenic lower crust: key exhumation mechanisms in large hot orogens? *Journal of Metamorphic Geology*, **26**(2):273–297.

Sibuet J. & Tucholke B.E. 2013. The geodynamic province of transitional lithosphere adjacent to magma-poor continental margins. *Geological Society, London, Special Publications*, **369**(May):429–452.

Sleep N.H. 2003. Survival of Archean cratonal lithosphere. *Journal of Geophysical Research: Solid Earth*, **108**(B6):n/a--n/a.

Stüwe K. 2007. *Geodynamics of the Lithosphere*, 2nd ed. Springer Berlin Heidelberg.

Tack L., Wingate M.T.D., & Lie J. 2001. Early Neoproterozoic magmatism (1000 – 910 Ma) of the Zadinian and Mayumbian Groups (Bas-Congo): onset of Rodinia rifting at the western edge of the Congo craton. *Precambrian Research*, **110**:277–306.

Tedla G.E., Meijde M. van der, Nyblade A.A., & Meer F.D. van der 2011. A crustal thickness map of Africa derived from a global gravity field model using Euler deconvolution. *Geophysical Journal International*, **187**(1):1–9.

Thieulot C. 2011. FANTOM: Two- and three-dimensional numerical modelling of creeping flows for the solution of geological problems. *Physics of the Earth and Planetary Interiors*, **188**(1–2):47–68.

Thieulot C. 2014. ELEFANT: a user-friendly multipurpose geodynamic code. *Solid Earth Discussions*, **6**:1949–2096.

Thomas W.A. 2006. Tectonic inheritance at a continental margin. *GSA Today*, **16**(2):4–11.

Tommasi A. & Vauchez A. 2001. Continental rifting parallel to ancient collisional belts: An effect of the mechanical anisotropy of the lithospheric mantle. *Earth and Planetary Science Letters*, **185**:199–210.

Tommasi A. & Vauchez A. 2015. Heterogeneity and anisotropy in the lithospheric mantle. *Tectonophysics*, **661**:11–37.

Trompette R. 2000. Gondwana evolution; its assembly at around 600 Ma. *Comptes Rendus de l'Académie des Sciences - Series IIA - Earth and Planetary Science*, **330**(5):305–315.

Turcotte D.L. & Schubert G. 2002. *Geodynamics*. Cambridge University Press.

Unternehr P., Peron-Pinvidic G., Manatschal G., & Sutra E. 2010. Hyper-extended crust in the South Atlantic: in search of a model. *Petroleum Geoscience*, **16**(3):207–215.

van der Velden A.J. & Cook F.A. 2005. Relict subduction zones in Canada. *Journal of Geophysical Research B: Solid Earth*, **110**(8):1–17.

van Schmus W.R., Oliveira E.P., da Silva Filho a. F., Toteu S.F., Penaye J., & Guimaraes I.P. 2008. Proterozoic links between the Borborema Province, NE Brazil, and the Central African Fold Belt, *In*: Pankhurst R.J., Trouw R.A.J., Brito Neves B.B., & de Witt M.J. (eds.), *Geological Society, London, Special Publications*. pp. 69–99.

Vauchez a., Barruol G., & Tommasi a. 1997. Why do continents break-up parallel to ancient orogenic belts? *Terra Nova*, **9**(2):62–66.

von Nicolai C., Scheck-Wenderoth M., Warsitzka M., Schødt N., & Andersen J. 2013. The deep structure of the South Atlantic Kwanza Basin - Insights from 3D structural and gravimetric modelling. *Tectonophysics*, **604**:139–152.

Wiedemann C.M., Medeiros S.R. De, Ludka I.P., & Mendes J.C. 2002. Architecture of Late Orogenic Plutons in the Araçuai-Ribeira Fold Belt, Southeast Brazil. *Gondwana Research*, **5**(2):381–399.

Wilson J.T. 1966. Did the Atlantic Close and then Re-Open? *Nature*, **211**(5050):676–681.

Zalán P.V., Severino M.., Rigoti C.A., & Magnavita L.P. 2011. An entirely new 3-D view of the crustal and mantle structure of a South Atlantic Passive Margin, Santos, Campos and Espírito Santo Basins, Brazil, *In*: *AAPG Annual Conference and Exhibition*. pp. 1–3.